Doctoral   Science

2007-09-01

The Development of a Quantum Dot Solar Concentrator

Brenda Rowan
Technological University Dublin

Follow this and additional works at: https://arrow.tudublin.ie/sciendoc

Part of the Quantum Physics Commons

The Development of a Quantum Dot Solar

Concentrator

Brenda Rowan B.Sc.

PhD Thesis

Dublin Institute of Technology

Supervisors:

Dr. John Doran, Prof. Brian Norton, Dr. Sarah Mc Cormack

School of Physics

Submitted September 2007

ABSTRACT

The aim of this study was to investigate the feasibility of Quantum Dot Solar Concentrators (QDSCs). Quantum Dots offer the advantages of having broad absorption spectra, tunable emission and improved stability. A range of Cadmium Selenide/ Zinc Sulphide Quantum Dots were characterized in solution and composite form using time-resolved and steady state spectroscopic techniques and the stability of the composite samples was investigated over a 6-month period. A number of matrix materials were compared and the most suitable type for fabrication of QDSCs was identified. Techniques for fabrication and characterization of QDSCs were developed and a range of different QDSC types were produced and electrically characterised. The power output and concentration factors of QDSCs containing various QD concentrations, of different geometries and of varying sample thickness were measured and compared. The use of near infrared QDs and the mixing of different QD types were also investigated to extend the spectral range utilised by the QDSC. Results indicate that Quantum Dots with higher quantum yields and increased stability are required in order for QDSCs to become feasible.

DECLARATION

I certify that this thesis which I now submit for examination for the award of Doctor of Philosophy, is entirely my own work and has not been taken from the work of others save and to the extent that such work has been cited and acknowledged within the text of my work.

This thesis was prepared according to the regulations for postgraduate study by research of the Dublin Institute of Technology and has not been submitted in whole or in part for an award in any other Institute or University.

The work reported on in this thesis conforms to the principles and requirements of the Institute's guidelines for ethics in research.

The Institute has permission to keep, to lend or to copy this thesis in whole or in part, on condition that any such use of the material of the thesis be duly acknowledged.

Signature _____   Date _____
           Candidate

Acknowledgements:

My friends who encouraged me along the way and made weekends lots of fun -big love to you all; Kieran, Kathleen, Damhnait, Claire, Fiona, Eilis, Linda, Paul, Ruth, Mark, Nathan, Sean, Emma, Tucker, Linda C, Bob, Mick, Liv, Mary, Rory, Katie, Johnny.....etc.

Finally, to my lovely family; Mum, Dad, Paul and Dom- Thank you for all your encouragement, love, support and laughs. You're the best family a girl could ask for!

Abbreviations:

AM	Air Mass
A.U.	Arbitrary units
BIPV	Building integrated photovoltaics
CdSe	Cadmium Selenide
CdTe	Cadmium Telluride
CIGSS	Copper (Indium, Gallium)(Sulphur, Selemium)
CPC	Compound Parabolic Concentrator
FWHM	Full width at half maximum
HDA	Hexadecylamine
InP	Indium Phosphide
LSC	Luminescent Solar Concentrator
MEG	Multi Exciton Generation
NIR	Near Infrared
PbS	Lead Sulphide
PbSe	Lead Selenide
PFCB	Perfluorocyclobutane
PLMA	Polylaurylmethacrylate
PMMA	Polymethyl methacrylate
PV	Photovoltaic
QDs	Quantum Dots
QDSC	Quantum Dot Solar Concentrator
QW	Quantum Well
QY	Quantum Yield

TCSPC	Time correlated single photon counting
TFSi	Thin film silicon
TIR	Total Internal Reflection
TOPO	Tri-n-octylphosphine
UV	Ultraviolet
VIS	Visible
ZnS	Zinc Sulphide

Nomenclature:

η	Conversion efficiency	%
P_{max}	Power maximum	Watts
A_r	Area of PV cell	m^2
E_e	Incident Solar insolation	W/m^2
I_{sc}	Short circuit current	A
V_{oc}	Open circuit voltage	V
n	Refractive Index	
L	Amount of light totally internally reflected	
θc	Critical Angle	°
E_g	Band Gap	eV
D	Diameter	m
A	Absorbance	
I_0	Incident Intensity	W/m^2
I	Intensity of transmitted light	W/m^2
α	Absorption coefficient	cm^{-1}
x	Pathlength in sample	m
η_{opt}	Optical efficiency	%
P_{edge}	Power density of PV cell at edge of LSC	W
P_{ref}	Power density of reference PV cell	W
G	Geometric Gain	
A_{top}	Area of LSC illuminated by the light source	m^2
A_{edge}	Area of collecting edge	m^2

Contents

Page

Chapter 1 Introduction

Chapter 2 Background

Chapter 3 Spectroscopic Studies   Page

Chapter 4 Fabrication and Characterisation of Quantum Dot Solar Concentrators

Chapter 5 New Directions for Quantum Dot Solar Concentrator development

Chapter 6 Conclusions and Future Work

List of figures **Page**

List of tables

Chapter 1

Introduction

1.0 Introduction

It is becoming increasingly urgent to develop alternative energy sources due to both the effects of global warming and the increasing prices of fossil fuels. The looming oil crisis and its financial impact on world economies should provide the necessary incentive to advance new energy technologies in a way that a threat of global warming might not achieve. Non-oil producing nations like Ireland need to reduce their dependence on countries that provide them with fossil fuels at prices that are beyond their control. Fossil fuels accounted for 96% of all energy used in Ireland in 2005 leading to a total energy import dependency of 90% (*Howley et al 2006*). The 2007 white paper 'Delivering a sustainable energy future for Ireland' states that Ireland aims to achieve '...33% of electricity consumption from renewable sources by 2020 through support for research, development, commercialization, and technology transfer as well as grid connections and planning issues for off-shore wind, ocean technologies and biomass' (*DCMNR 2007*).

In Ireland in March 2007, planning exemptions were put in place for the installation of solar panels, heat pumps, wind turbines and wood pellet burners of a certain size. These changes along with government incentives like the Greener Homes Scheme help to encourage the development of renewable energy generation in Ireland. Since 1990,

renewable energy has grown 133% in absolute terms, wind energy being the largest contributor (*Howley et al 2006*).

The EU is keen to develop renewable energy technologies in order to decrease import dependency and to contribute to sustainable development. As well as reducing carbon emissions, this will provide increased employment opportunities and diversify sources of energy production. A EU directive (RES E directive) has set a target to increase the share of renewable energy to 21% by 2010 for 25 member states and has also set individual targets for each country. Projected figures indicate that this can be achieved with the major increases resulting from wind, biomass, solar and tidal energy developments. The solar energy aspect includes both solar thermal electricity and photovoltaic (PV) cells (*Ragwitz et al 2005*).

1.1 Solar Energy

Solar energy technologies convert a percentage of solar radiation that reach the earth's surface into heat and electricity for use in domestic and commercial buildings (*Norton 1992*). In one hour, enough solar energy reaches earth to power the whole world for one year (*Markvart 1997*). Solar energy resources are abundant and free, the difficulty is developing technologies that will utilise this energy in an efficient and economic manner. It has been calculated that 25,000 square miles of solar arrays could supply the entire planet with electricity (*Leckie 2002*). Although, due to high expenses and limitations of efficiencies of solar cells such a large-scale solution is not realistic at this point. This thesis

is concerned with concentration of sunlight onto PV cells to produce electricity while keeping costs to a minimum.

1.1.1 Photovoltaics

PV cells have developed rapidly in the past 50 years and continue to do so. Crystalline silicon dominates the PV manufacturing industry accounting for over 90% of the total volume of the PV market (*PV Technology Platform 2007*). Multi-crystalline silicon is cheaper and is therefore used more than mono-crystalline silicon. Amorphous silicon is even cheaper but produces less efficient PV cells. Wafer based PV cells such as these have become known as 'first generation' solar cells and their efficiency to date is typically 13%, reaching a maximum of 17% at best (*PV Technology Platform 2007*).

Further development has led to a second generation of cells which includes thin-film technologies with low cost potential due to the small amount of high cost materials required. There are three main types of inorganic thin film technologies; amorphous/microcrystalline silicon (TFSi-13% efficiency), polycrystalline semiconductors CdTe (16.5% efficiency) and $Cu(In,Ga)(S,Se)_2$ (CIGSS-19.5% efficiency). Thin-film technologies currently have a market share below 10% but this is expected to rise in the future (*PV Technology Platform 2007*). It is predicted that a third generation cell will outperform the previous generations with high efficiency cells such as tandem cells (*Green 2002*). Tandem cells involve stacking PV cells with different band gaps allowing conversion of different parts of the solar spectrum at maximum efficiency (*Goetzberger and Heibling 2000*). A description of PV technology is provided in chapter 2.

1.1.2 Solar Concentrators

Solar Concentration is used to reduce PV costs by reducing the amount of material required by concentrating sunlight using, lenses or mirrors (imaging concentrators) or using optical systems (non-imaging optics), onto a small PV cell area. The Luminescent Solar Concentrator (LSC) is a type of non-imaging solar concentrator that has been studied since the 1970s (*Weber and Lambe 1976, Goetzberger and Greubel 1977, Rapp and Boling 1978*). LSCs have advantages over other concentrator systems that make it attractive for building integration, an increasingly popular feature due to the high cost of land space and issues of planning permission. A description of LSCs and their advantages is provided in chapter 2.

LSCs absorb both direct and diffuse radiation making tracking of the sun unnecessary. As well as reducing system costs and allowing for building integration, the absorption of diffuse radiation increases the amount of light harvested, especially in Northern European climates where diffuse radiation makes up ~60% of incoming light (*Goetzberger 1978*). They are highly versatile systems that could be incorporated into other types of solar collectors to produce hybrid systems (*Zastrow et al 1984*). Problems arose during their development due to dye instability and the limited absorption spectra of luminescent dyes. Improved dyes and novel ideas to minimise system losses are bringing the commercialization of LSCs closer to realization.

BASF® lumogen dyes were improved in the 1990s for use in LSCs and they are estimated to have a ten-year lifetime with the presence of an ultraviolet (UV) absorbing layer (*Richards et al 2004*). This layer limits the amount of incoming light absorbed by the LSC. One possible solution to long-term stability is the use of liquid LSCs, allowing for easy

replacement of the dye solution upon degradation. However, the use of solutions limits the index of refraction of the matrix material thereby affecting the amount of light internally reflected (*Sholin et al 2007*). Another solution is to protect the sensitive dye layer with a UV absorbing layer that can utilize the incident UV light e.g. cerium doped glass (*Richards et al 2004*). If this layer is connected to a PV cell, the UV light can also be utilized to produce electricity. Stacking LSC plates with different absorption wavelengths is a promising way of utilising the full solar spectrum (*Goetzberger and Wittwer 1981*).

Recent innovations include the use of photonic layers that act as band stop filters on the top surface of LSCs. It is claimed that they can increase the amount of light trapped in a LSC and suppress re-emission (*Rau et al 2005*). High cost and varied performance with angles of incidence introduce problems but improvements of up to 25% have been predicted (*Richards et al 2004*). Other novel ideas being investigated currently include cylindrical LSCs (*McIntosh et al 2007*), the use of semiconducting polymers (*Sholin et al 2007*), bent LSCs (*El-Shaarawy et al 2007*) and nanocomposite thin films (*Schuler et al 2007*).

1.2 Quantum Dot Solar Concentrators

This thesis investigates the feasibility of using Quantum Dots (QDs) instead of luminescent dyes in LSC systems, creating a Quantum Dot Solar Concentrator (QDSC)(*Barnham et al 2000*). QDs are novel, man-made, semiconductor nanocrystals. They are developing rapidly due to their unique properties that make them suitable for a range of optical, biological and electronic applications. Their broad absorption spectrum, size tunability, high quantum yield (QY) (the ratio of absorbed to emitted photons) and increased stability make them

18

potential replacements for luminescent dyes. Their broad absorption spectrum utilizes a larger amount of the solar spectrum and size tunability grants flexibility and control over the emission wavelength of the QDSC plate. Greater stability is expected from QDs due to surface passivation of QD cores with higher band gap material (*Alivisatos 1997*). QDSCs and QDs are described in chapter 2.

1.2.1 Spectroscopic Studies

A range of commercial core-shell QDs were characterised using steady state spectroscopy. The efficiency of the various QD types was quantified by the intensity of their emission spectra. Concentration dependence studies were also necessary to find the optimum concentration for different QD samples. Transient spectroscopy was used to investigate the fluorescence lifetime of QDs and the effects that re-absorption of light has on emission spectra was studied. QD characterisation was continuous throughout this study and the results are discussed in chapter 3.

It was necessary to identify a suitable host material for the QDs before QDSC fabrication commenced. A material with high transparency, minimal effect on QD efficiency and the ability to retain this efficiency over time was required. Seven different polymer materials were compared and the material with the lowest absorption coefficient was identified. The effect that encapsulation into each polymer had on QD efficiency and the efficiency over time was investigated. The results are discussed in chapter 3 and the most suitable material was identified.

1.2.2 Quantum Dot Solar Concentrator Fabrication and Characterisation

The techniques for QDSC fabrication and characterisation are described in chapter 4. Small-scale QDSCs containing a range of QD concentrations were fabricated using different QD types. Electrical characterization showed the effect that QDs and the QD concentration had on the electrical output of the systems.

In chapter 5, certain aspects of QDSC development were investigated with the aim of optimizing QDSC efficiency. A number of reflective materials and the benefit of air gaps were investigated and the optimum configuration was identified. Different QDSC geometries were fabricated and their power outputs and concentration ratios were compared. The results were compared with those predicted by a ray trace model.

To increase the percentage of the solar spectrum that is absorbed by a QDSC, near infrared (NIR) QDs were examined over a range of concentrations and the feasibility of mixing QDs with different absorption features was investigated.

Finally, a comprehensive overview of the findings of this study is given in chapter 6, followed by recommendations for future work.

References:

Alivisatos, A.P. (1997), Nanocrystals: building blocks for modern materials design, *Endeavour*, Vol. 21, No. 2, pp. 56-60.

Barnham, K.W.J., Marques, J.L., Hassard, J., O'Brien, P. (2000) Quantum-dot concentrator and thermodynamic model for the global redshift, *Applied Physics Letters*, Vol. 76, No. 9, pp. 1197-1199.

El-Shaarawy, M.G., El-Bashir, S.M., Hammam, M., El-Mansy, M.K., (2007), Bent Fluorescent solar concentrators: Spectroscopy, Stability and outdoor performance, *Current Applied Physics*, Vol.7, No.6, pp. 643-649.

Goetzberger, A., Greubel, W., (1977), Solar energy conversion with fluorescent concentrators, *Applied Physics*, Vol. 14, pp. 123-139.

Goetzberger, A., (1978), Fluorescent Solar Energy Collectors: Operating conditions with diffuse light, *Applied Physics*, Vol. 16, pp. 399-404.

Goetzberger, A., Heibling, C., (2000), Photovoltaic material, past,present,future, *Solar energy materials and solar cells*, Vol. 62, pp. 1-19.

Goetzberger, A. Wittwer, V., (1981), Fluorescent planar collector-concentrators:a review, *Solar Cells,* Vol. 4, pp. 2-23.

DCMNR, (2007), Delivering a Sustainable Energy future for Ireland, *The Energy policy framework, Government White Paper* pp. 29. Department of communications, marine and natural resources (DCMNR) Ireland.

Green, M.A., (2002), Third generation photovoltaics: Solar cells for 2020 and beyond, *Physica E: Low dimensional systems and nanostructures*, Vol. 14, No. 1-2, pp 65-70.

Howley, M., O'Leary, F., O Gallachoir, B., (2006) Energy In Ireland 1990-2005 Trends, issues, forecasts and indicators *SEI Report*.

Leckie, J. (2002), The urgent need for clean energy, *Proceedings of WREC VII, Cologne, Germany 29 June-5 July 2002* pp. 758.

Markvart, T., (1997), *Solar Electricity*, John Wiley and Sons, London.

McIntosh, K.R., Yamada, N., Richards, B.S., (2007), Theoretical comparison of cylindrical and square-planar luminescent solar concentrators, *Applied Physics B*, Lasers and optics, Vol.88, No. 2, pp. 285-290.

Norton, B., (1992), *Solar Energy Thermal Technology*, Springer Verlag, New York, USA.

PV Technology Platform, (2007), A Strategic Research Agenda for Photovoltaic Solar Energy Technology, Working group 3.

Ragwitz, M., Schleich, J., Huber, C., Resch, G., Faber, T., Voogt, M., Coenraads, R., Cleijne, H., Bodo,P., (2005), FORRES 2020: Analysis of the renewable energy sources' evolution up to 2020. *DG Tren Report, E.U. Brussels.*

Rapp, C.F. and Boling, N.L., (1978), Luminescent Solar Concentrators, *Proceedings of the 13th IEEE Photovoltaics Specialists Conference*, pp. 690-693.

Rau, U., Einsele, F., Glaeser, G.C., (2005), Efficiency limits of photovoltaic fluorescent collectors, *Applied Physics Letters*, Vol. 87, No. 17, pp 171101.

Richards, B.S., Shavlav, A., Corkish, P., (2004), A low escape cone loss luminescent solar concentrator, *19th E.C. Photovoltaic Solar Energy Conference, Paris, France, June 7-11*[th] *2004*, pp 113-116.

Schuler, A., Python, M., Valle del Olmo, M., de Chambrier, E., (2007), Quantum dot containing nanocomposite thin films for photoluminescent solar concentrators, *Solar Energy, In Press.*

Sholin, V., Olson, J.D., Carter, S.A., (2007), Semiconducting polymers and quantum dots in luminescent solar concentrators for solar energy harvesting, *Journal of Applied Physics*, Vol.101, No. 12, pp. 123114.

Weber, W.H., and Lambe, J., (1976), Luminescent greenhouse collector for solar radiation, *Applied Optics* Vol. 15, No. 10, pp. 2299-2300.

Zastrow, A., Wilson, H.R., Heidler, K., Wittwer, V., Goetzberger, A., (1983), Improvement of efficiency and stability of fluorescent planar concentrators (FPCs). First results from a $1m^2$ test collector system, *Proceedings of the Fifth International Conference, Athens, Greece, October 17-21*, pp. 202-206.

Chapter 2

Background

2.0 Introduction

This chapter provides a detailed description of PV technology as this thesis is concerned with the concentration of sunlight onto PV cells. Solar concentration is discussed with particular attention to non-imaging Luminescent Solar Concentrators (LSCs), followed by an introduction to Quantum Dot Solar Concentrators (QDSCs). Quantum Dots (QDs) are described in detail as they play a vital role in the development of QDSCs. A description of QDs, their structure, synthesis and properties is included.

2.1 Photovoltaics

The power output of PV cells can be enhanced by concentrating sunlight onto a small area of PV material. PV cells convert incident sunlight into electricity by a process known as the photovoltaic effect. The photovoltaic effect was first discovered in 1839 by Alexandre-Edmund Becquerel, who noticed that an electric current was produced when sunlight struck certain materials. His discovery was not further developed until 1876 when Adams and Day observed the same effect in selenium. A better understanding of the photovoltaic effect

came with the development of quantum theory of solids in 1930 and in 1954 the first usable solar cell was produced with 6% efficiency by Chaplin et al (*Partain 1995*).

2.1.1 The Photovoltaic effect

The photovoltaic effect occurs when incident photons of light create mobile charged particles within a semiconductor that lead to the production of an electric current. To explain the photovoltaic effect it is necessary to outline the energy band model. The energy band model states that the energy of an electron in a crystal falls within well-defined bands. The valence band is the lower band of states and in a semiconductor is almost full since electrons tend to fill lower energy states. The conduction band is the next higher band of states and it is separated from the valence band by an energy band gap (E_g). The band gap represents the amount of energy required to move an electron from the valence band into the conduction band. When an electron is excited into the conduction band it leaves a hole in the valence band and an electron-hole pair is created (see figure 2.1).
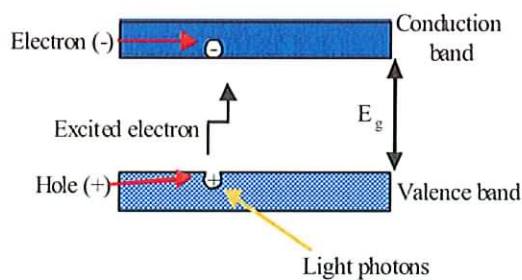
Figure 2.1: The energy band model

The hole in the valence band is mobile and behaves like a positively charged particle. At the same time the electron in the conduction band behaves like a negatively charged

26

particle and it is the movement of the electrons and holes that give rise to currents in semiconductors (*Neaman 2003*). The ability of a material to conduct electricity depends on the material's band structure and based on this, solids can be classified into three categories: conductors, insulators and semiconductors, illustrated in figure 2.2.
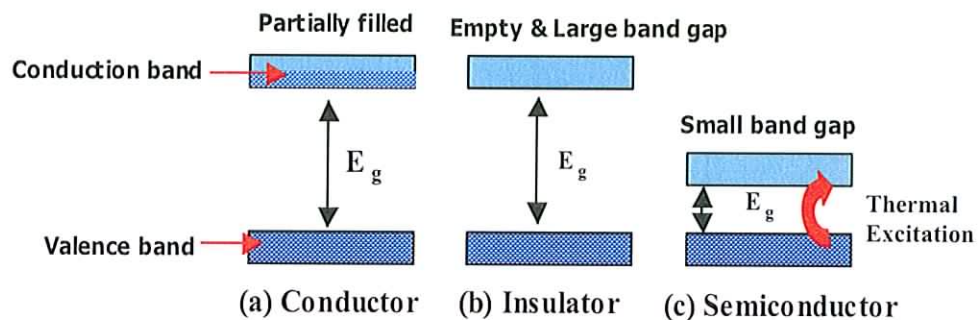
Figure 2.2 Band structure of (a) a conductor (b) an insulator and (c)a semiconductor

A conductor has a partially filled conduction band so when an electrical field is applied these electrons are free to move about *e.g.* copper, gold and most metallic materials (figure 2.2 a). An insulator consists of a full valence band and empty conduction band separated by a large band gap (see figure 2.2 b). The electrons in this material cannot move and therefore there are no free electrons to allow a flow of electricity e.g. polyethylene and most polymers. Semiconductors have a completely full valence band separated from an empty conduction band at T= 0 K (see figure 2.2 c). At temperatures above 0 K a number of electrons in the valence band gain enough energy to move into the conduction band thereby allowing current to be generated *e.g.* silicon and germanium and compound semiconductors such as gallium arsenide or indium phosphide.

2.1.2 P-N Junctions

A pure semiconductor containing no impurity atoms or defects is known as an *intrinsic* semiconductor. In order to make intrinsic semiconductors better conductors, electrons either need to be removed from the valence band or added to the conduction band. This is achieved by a process known as *doping i.e.* the addition of impurities to semiconductor materials. After doping the semiconductor is then known as an *extrinsic* semiconductor.

Silicon is a group IV semiconductor so it requires 4 electrons to fill the valence band. If a material with 5 valence electrons is added to the silicon mix *e.g.* phosphorous, four of the five electrons will be used to fill the valence bands and the fifth electron will be promoted to the conduction band. The silicon is now a conductor and since the current is carried by negatively charged carriers it is known as an *n-type* semiconductor.

If a group III element e.g. boron with 3 valence electrons is added to silicon, the dopant atoms accept electrons from the valence band without generating electrons on the conduction band. In this way holes are created in the valence band that act as positively charged electrons. Therefore they are known as *p-type* semiconductors. The n-type impurities are often referred to as donors and the p-type impurities as acceptors.

When a p-type and an n-type semiconductor are brought into contact with each other a p-n junction is created. Such junctions consist of a crystal that is doped in one region with donor atoms to create the n region and the other region is doped with acceptor atoms to create the p region. The area between both regions is known as the depletion region (see figure 2.3)(*Markvart 1997*).

28
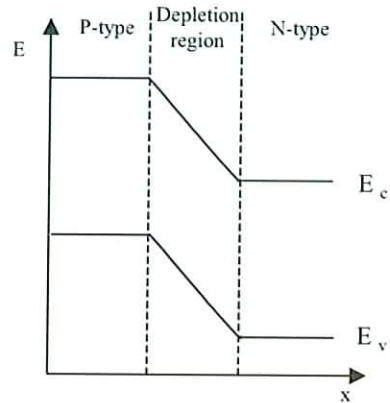
Figure 2.3 Band diagram of a PV cell

This junction contains a strong electric field due to the opposing charges of the ions. When a p-n junction is illuminated light photons are absorbed and they excite electrons from the valence band to the conduction band. These electrons flow from the n-type region to the p-type region while the holes flow in the opposite direction (see figure 2.4).
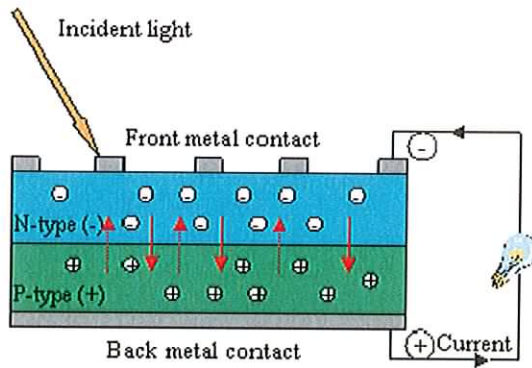
Figure 2.4: A photovoltaic cell showing movement of electrons and holes

These generated charge carriers are swept from the junction by the electric field producing a current across the device. Any current generated by the device is extracted by metal contacts in the form of thin strips on the front surface and a larger bus bar at the rear of the cell (*Neaman 2003*). This principle is the basis of a photovoltaic cell.

The efficiency of a PV cell is defined as the maximum power produced by the cell under standard test conditions. These conditions are usually 1000 W/m^2, Air Mass 1.5 spectrum and 25°C (*Markvart 1997*). PV cells are rated by their conversion efficiency (η) given by:

$$\eta = \frac{P_m}{E \times A_r}$$

(*Eqn. 2.1) (Partain 1995*)

P_m= Power maximum (W)

E= Incident solar irradiation (W/m^2)

A_r= Area of PV cell (m^2)

2.1.3 Limitations of Photovoltaic cells

In 1961 Shockley and Queisser calculated the maximum efficiency of a PV cell, regardless of improvements in materials, to be 30% (*Shockley and Queisser 1961*). To date the highest efficiency achieved in a laboratory is 18.1% for a large area multi-crystalline silicon solar cell and it is predicted that 17.6% is achievable in industry with existing techniques or 18% with innovation (*McCann et al 2006*). These limitations are due to the absorption capabilities of semiconductor materials. A semiconductor will only convert light with energy in excess of its band gap into electricity. Any light below the band gap energy will not be absorbed and is therefore wasted. Energy in excess of the band gap is also lost in the form of heat after an electron-hole pair has been generated. Crystalline silicon has a band gap of 1.12 eV corresponding to a spectral range of 400-1200 nm (*Goetzberger and Hoffman 2005*). Silicon PV cells can therefore only convert about two thirds of the solar spectrum (*Markvart 1997*). This is why new materials with different band gaps are being investigated *e.g.* GaAs with a band gap of 1.42 eV. The concept of stacking PV cells of

30

different band gap materials allows the maximum efficiency of 30% to be surpassed. Such cells are known as multi-junction cells and the highest efficiency achieved to date is 32.5% (*Dimroth et al 2007*).

2.2 Optical Solar Concentrators

Due to the high cost of PV materials, it is desirable to concentrate solar radiation onto small areas of PV cells. In order to be worthwhile, the concentrator needs to be cheaper and more efficient than the equivalent area of PV cells (*Markvart 1997*). Optical Solar concentrators can be divided into imaging and non-imaging devices.

2.2.1 Imaging Concentrators

Imaging concentrators use lenses or mirrors to focus parallel rays onto a point or a line. Since they only focus direct sunlight they require tracking systems to follow the path of the sun throughout the day and frequent direct sunlight conditions. Fresnel lenses, as illustrated in figure 2.5, and parabolic mirrors are good examples of non-imaging concentrators. They present problems of non-uniform illumination of the PV cells and, in the case of mirrors, cooling systems are required due to heat generation (*Markvart 1997, Ryu et al 2006*).
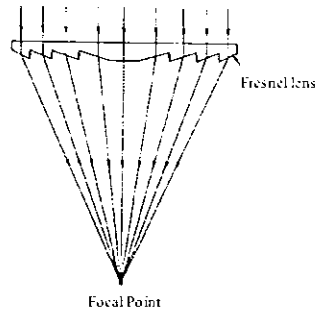
Figure 2.5: Example of an imaging concentrator using a fresnel lens

2.2.2 Non-imaging Concentrators

In the case of non-imaging concentrators the suns rays are focused onto the PV cell but no

image of the sun is produced. They have the advantage of using both direct and diffuse

radiation and no expensive tracking systems are required. The compound parabolic

concentrator (CPC) is an important type of non-imaging concentrator. It consists of two

reflective parabolic surfaces each having its focus point at opposite ends of the PV cell.

Rays entering the system within a range of critical angles are focused onto the PV cell area

(see figure 2.6)
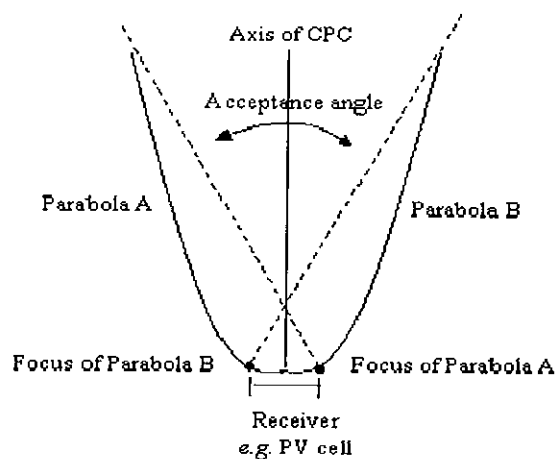
Figure 2.6: Schematic of a compound parabolic concentrator

2.3 Luminescent Solar Concentrators (LSCs)

LSCs are non-imaging devices that were first proposed in the 1970s (*Weber and Lambe 1976, Goetzberger and Greubel 1977*). Originally designed for use as greenhouse glazing, they have not been fully developed due to a number of limitations that will be discussed in this section.

A LSC consists of a flat plate of glass, plastic or liquid doped with a luminescent dye (*Mansour 1998*). Reflective material is situated on three of the plate edges and the back surface of the plate and a PV cell is placed on the fourth edge as illustrated in figure 2.7.
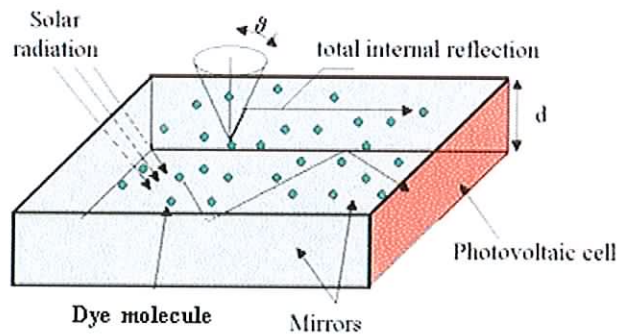
Figure 2.7: Schematic of a LSC

Incident solar radiation enters the system through the exposed upper surface and light of particular wavelengths is absorbed by the luminescent dye and re-emitted isotropically. A percentage of this emitted light will be trapped inside the plate by total internal reflection (TIR). TIR occurs as light passes from a medium with a high refractive index (*n*) (e.g. plastic/glass) into a medium with a low *n* (e.g. air). If the light strikes the plastic-air interface at an angle greater than the critical angle, it will be refracted into the plastic

33

medium, while if the angle is smaller than the critical angle it will be lost. The amount of emitted light that will be totally internally reflected (L) is determined by the n of the matrix material by:

$$L = \frac{\left(n^2 - 1\right)^{1/2}}{n}$$
(Equation 2.2)

For a material with $n = 1.5$, 74.5% of emitted light would be trapped inside the plate (*Goetzberger and Wittwer 1979*). The critical angle (θ_c) is determined by:

$$\theta_c = \sin^{-1}\left(\frac{1}{n}\right)$$
(Equation 2.3)

For a plastic material with $n = 1.5$, $\theta_c = 42°$.

LSCs potentially have many significant advantages over alternative concentrating systems. These advantages are:

1- LSCs absorb both direct and diffuse radiation. This means that no expensive tracking system is required thus reducing system costs. These systems are suitable for the typical northern European climate where there are limited periods of high intensity illumination and diffuse radiation comprises 60% of global radiation on a flat surface (*Goetzberger 1978*).

2- The narrow band of luminescence produced by the luminescent dye can be matched to the maximum spectral response of the PV cell.

3- Infrared light and heat energy lost by red-shifting incident radiation is dispersed throughout the LSC plate and therefore does not reduce the PV cell efficiency (*Rapp and Boling 1978*). PV cells only absorb above band gap light so the PV cells

34

operate cooler and more efficiently than a standard PV module (*Richards et al 2004*).

4- LSCs also offer many possibilities for incorporation into hybrid systems with solar thermal collectors. For example, a LSC plate could be used as a second cover on a thermal flat plate collector and its electrical output could power the water circulation pump (*Zastrow et al 1983*). This could be used as a stand-alone system in a remote area with no power supply.

5- LSCs offer the possibility of separating the solar spectrum and concentrating different parts simultaneously. This can be achieved by stacking plates containing dyes with different absorption characteristics.

6- Due to their static nature, LSCs are well suited for building integrated photovoltaics (BIPV). They could be incorporated into buildings as skylights, shading devices or attractive building facades.

LSCs have not yet been fully developed due to a number of problems. Luminescent dyes suffer from photo-degradation and so have a limited lifetime (*Hermann 1982*). Re-absorption is also a major problem with LSCs- many dyes have a small Stokes shift i.e. the difference between the absorption peak and the emission peak as shown in figure 2.8.
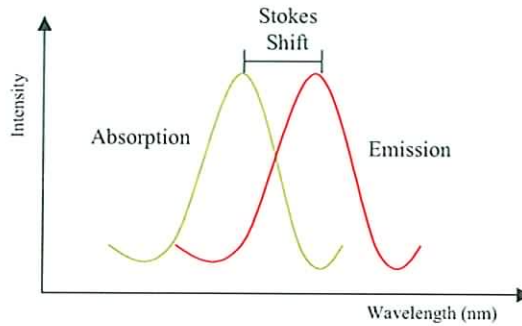
Figure 2.8: Stokes shift between absorption and emission peaks

Overlap of the absorption and emission spectra leads to emitted light being re-absorbed by the dye molecules. In addition, the narrow absorption band of dyes limits the percentage of the solar spectrum that can be utilized by a LSC.

2.4 Quantum Dot Solar Concentrators

A QDSC is based on the LSC concept but the luminescent dyes are replaced with QDs in an attempt to solve the problems presented by dyes (*Barnham et al 2000*). QDs offer the advantages of having tunable emission, broad absorption spectra, high emission intensity and increased stability. These characteristics are discussed in detail in the following section. Figure 2.9 shows a diagram of a QDSC. Air gaps are included in this diagram as they were found to increase the efficiency of QDSC plates. This will be discussed in more detail in chapter 5.
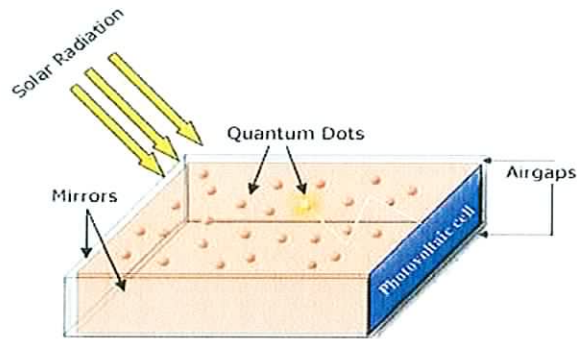
Figure 2.9: Schematic of a QDSC

2.4.1 Quantum Dots

Quantum Dots (QDs), also known as nanocrystals are semiconductor nanocrystals that range from two to tens of nanometers in diameter. They are man-made structures often composed of compound semiconductors e.g. Cadmium Selenide (CdSe) or Lead Sulphide (PbS) that possess unique properties compared to their bulk form.

QDs are often characterised by their emission wavelength, which is determined by their size. Their size dependence is a result of the quantum confinement of electrons in QDs in all 3 dimensions. When an electron hole pair is formed in a QD, the electron and hole are attracted by Coulomb force to form an exciton *(Weisbuch and Vinter 1991)*. The average distance between an electron and hole in an exciton is known as the Bohr radius, as shown in figure 2.10. As the dimensions of the QD approaches the size of the Bohr radius, quantum confinement effects alter the bandgap of the material.
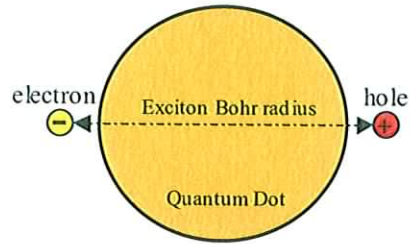
Figure 2.10: Exciton Bohr Radius of a QD

The result of quantum confinement is the formation of discrete energy levels rather than the quasi-continuous valence and conduction bands found in bulk materials. The band gap (E_g) of QDs is inversely proportional to the square of the diameter (d) of the QD;

$$E_g \alpha \frac{1}{d^2}$$ *(Equation 2.4)*

As the diameter of a QD decreases the band gap increases. This means that smaller QDs will emit photons with higher energy at shorter wavelengths and larger QDs will emit photons with lower energy at longer wavelengths. Figure 2.11 shows simplified band energy diagrams of two different sized QDs, where E_1^h= valence band containing holes and E_1^e=conduction band containing electrons. It can be seen that the QD with the larger diameter has a smaller band gap.
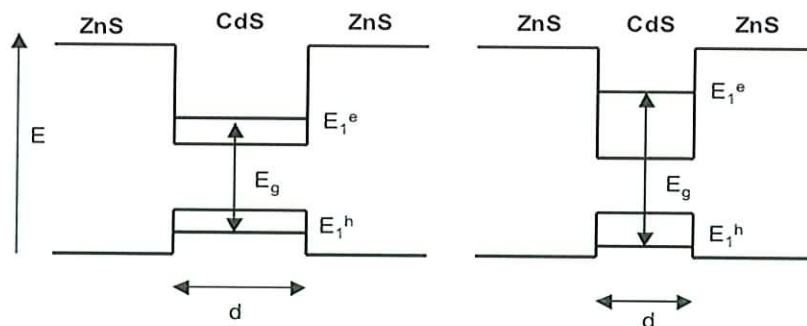
Figure 2.11: Band energy diagrams of two different sized QDs

38

The correlation between band gap and quantum dot size is depicted in figure 2.12 with the band structure of a bulk semiconductor and an indication of the spacing of energy levels in the valence and conduction bands included.
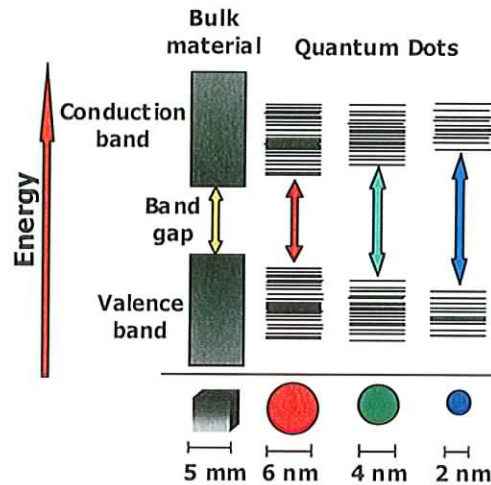
Figure 2.12: Size dependency of QDs

There are two main types of QDs: core QDs and core-shell QDs. Core QDs consists only of a core of semiconductor material *e.g.* Cadmium Telluride (CdTe) or Indium Phosphide (InP). Due to their high surface to volume ratio, QDs are sensitive to surface defects or impurities that can act as traps for electrons and holes. These traps can lead to non-radiative recombination of the electron hole pairs and therefore degrade the optical and electrical properties of the QD.

In order to produce more efficient QDs it is necessary to passivate the QD core with a shell of higher band gap material (see figure 2.13). Passivation of a core QD increases the quantum yield (QY) (the ratio of absorbed to emitted photons), by reducing the effects of

39

defects on the core surface that can lead to non-radiative recombination and by terminating loose bonds on the core surface (*Alivisatos 1996*).
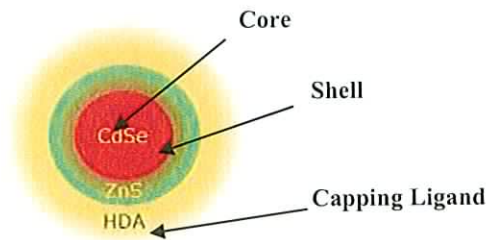
Figure 2.13: A Core-shell Quantum Dot

The surface atoms of QDs are highly reactive and can lead to agglomeration. For this reason, and for increased stability, the QDs are passivated or capped with organic ligands (*Pickett 2001*). The capping ligands also provide increased solubility in organic solvents. The most commonly used capping ligands are hexadecylamine (HDA) and tri-n-octylphosphine (TOPO).

2.4.2 Quantum Dot Synthesis

There are numerous methods available for QD synthesis including epitaxy and chemical (colloidal) methods. Epitaxially grown QDs are suited to electronic applications that require connections to be attached while colloidal synthesis is better suited for large-scale QD production *(Ouellette 2003)*. The main techniques for QD synthesis are described in the following section.

- **Epitaxial Growth**

Epitaxial growth is a process of depositing a thin layer of single-crystal material onto a substrate of another or the same single-crystal material There are several well-known methods of epitaxy including, molecular beam epitaxy, chemical vapour deposition and metal-organic chemical vapour deposition.

Self-assembled QDs grow when a thin layer of material is deposited onto a substrate that is lattice mismatched (see figure 2.14 (1) and (2)). The strain that this creates causes islands to form on top of a 'wetting layer' and these island can then be buried to form quantum dots (see figure 2.14 (3)).This method is known as Stranski-Krastanov growth.
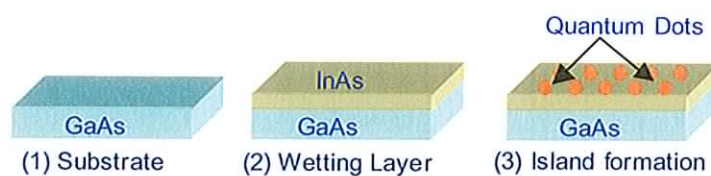
Figure 2.14: Stranski-Krastanov growth of QDs

QDs can also be formed by growing a two dimensional structure (quantum well)(QW) and then by using ion or electron beam techniques. The quantum wells are confined in the third dimension to produce QDs *(Woggan 1996)*. Overall, epitaxial growth is an expensive technique that is not suitable for mass production of QDs, it is better suited to single particle analysis.

- **Colloidal Methods**

Colloidal synthesis is a chemical preparation method that involves the mixing of two compounds, one containing metal ions (e.g. Cd^{2+}, Zn^{2+}) and the second containing

41

chalcogenide ions (e.g. S^{2-}, Se^{2-}). Covalent bonding creates the semiconductor compounds e.g. CdSe or ZnS *(Woggan 1996)*.

Organometallic reagents are very efficient carriers of the chalcogenide ions and they are also able to carry capping molecules that can terminate the growth of the QDs. Synthesis was initially a two-step process but in recent years one-step procedures have been developed using single source precursors. A typical reaction involves the injection of precursors into a vigorously stirred flask containing a hot coordinating solvent where thermolysis occurs (see figure 2.15).
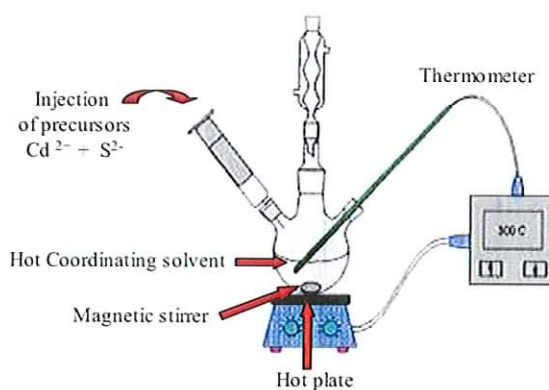
Figure 2.15: Colloidal synthesis of Quantum Dots

Once the precursor and solvent are mixed, nucleation occurs and QD growth begins. The solvent stabilises the QD surface as it grows and prevents aggregation. The size of the QDs is determined by the growth time *(Knight et al 2004)*. Another common colloidal method involves aqueous solutions using thiols as stabilizers *(Talapin 2001)*.

Once the QDs are grown it is then necessary to carry out size fractionation of the colloidal solution to enhance monodispersity. A broad range of QD sizes result in inhomogenous

broadening of the absorption and emission spectra and thus increased re-absorption problems *(Weller 1993)*.

- **Electron Beam Lithography**

The first lithographic QDs were made in 1987 using a semiconductor containing a buried layer of Quantum well (QW) material *(Reed 1993)*. Pillars of quantum well material were created using advanced lithographic techniques and the surrounding material was etched away except for a part that is covered in metal. The remaining part is a QD created by confining a QW in three dimensions.

2.4.3 Quantum Dot Properties

QDs exhibit unique properties that make them versatile and efficient and thus an attractive replacement for traditional semiconductors and luminescent dyes in numerous applications. These properties are:

- **Broad Absorption Spectrum**

QD optical absorption spectra consist of a series of peaks. Each peak corresponds to an energy transition between the discrete energy levels. Photons with a longer wavelength than the first absorption peak (the absorption peak at the longest wavelength) are not absorbed. The wavelength of the first absorption peak is determined by the size of the QD and in this way it is tunable *e.g.* a smaller QD will have a first absorption peak at a shorter wavelength *(Norris and Bawendi 1995, 1996)*. The absorption spectrum of an ideal single QD would appear as a series of narrow lines at separate wavelengths representing different energy levels. An ensemble of QDs generally has a degree of size distribution and this

causes broadening of the absorption spectrum. Figure 2.16 shows the absorption spectra of (a) an idealized single QD, (b) a QD ensemble with a small size distribution and (c) a QD ensemble with a typical size distribution.

E_1=Energy transition at energy level 1 $i.e.$ $E_1^h \rightarrow E_1^e$

E_2=Energy transition at energy level 2 $i.e.$ $E_2^h \rightarrow E_2^e$

E_3=Energy transition at energy level 3 $i.e.$ $E_3^h \rightarrow E_3^e$
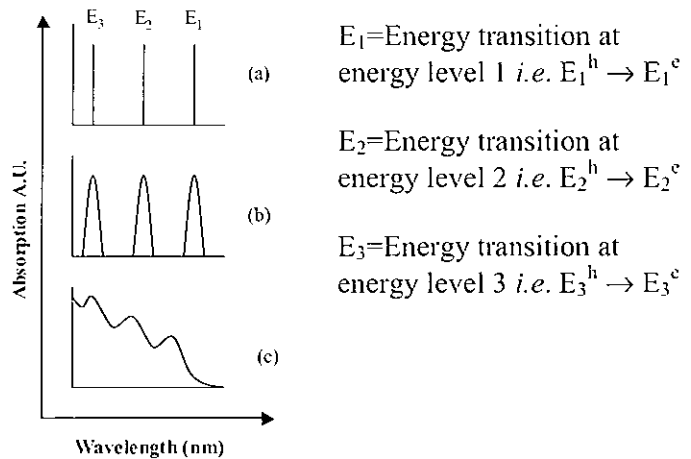
Figure 2.16: Absorption spectra of (a) an idealised QD (b) a QD ensemble with a small size distribution (c) a typical QD absorption spectrum

The broad absorption spectrum of QDs offers the advantage that the QDs can be excited by broadband light e.g. daylight and several different sized QDs can be excited simultaneously by a single light source.

- **Tunable Emission**

The emission spectrum of a QD ensemble is a Gaussian lineshape that occurs at a longer wavelength than the first absorption peak. The difference between the absorption peak wavelength and the emission wavelength is known as the Stokes Shift. Smaller QDs have a larger band gap and therefore absorb higher energy photons, resulting in a shorter emission

44

wavelength. Larger QDs have more energy levels, packed closely together and so they can absorb lower energy photons, leading to emission spectra at longer wavelengths. Emission tunability is an attractive feature for applications that require narrow band emission for example light-emitting diodes or lasers.

- **High Quantum Yield**

QD efficiency is characterised by the quantum yield (QY). QY is defined as the percentage of absorbed photons that result in a photon being emitted (*Lakowicz 1999*). QY is a function of the relative influences of radiative and non-radiative recombination. The surface of a QD plays an important role in determining the QY-defects and free electrons can create hole traps that lead to non-radiative transitions. The addition of a higher band gap shell minimises these problems and leads to an increase in QY (*Alivisatos 1998*).

It is desirable for a QD to have a large Stokes Shift (see figure 2.8) *i.e.* for the emission peak to be as far from the absorption peak as possible. In the region where the absorption and emission overlap, re-absorption occurs *i.e.* emitted photons are re-absorbed by the QD ensemble thereby reducing the overall emission intensity. QDs are said to have high QYs comparable to those of luminescent dyes (*Knight et al, 2004*).

- **Stability**

QDs are expected to be able to retain their QY over time. Passivation of core QDs with higher band gap shells make the QDs more resistant to chemical and photochemical degradation (*Alivisatos 1997*). There have been reports on spectral diffusion (blueshift of emission) and bleaching (decrease in emission) of QDs after exposure to oxygen (Van Sark et al 2002), these effects are caused by etching of the QD shell. Oxidation rates are reduced

with thicker shells by slowing down the diffusion of oxygen to the QD core (*Van Sark 2002, Knight et al 2004, Gallagher et al 2007*). Generally, a core-shell QD with a higher band offset between the core and shell material will display higher efficiency and stability (*Xie et al 2004*). Recent developments in QD fabrication have led to core-multishell QDs whereby the composition of the shell is gradually changed from the core to shell material e.g. a core of CdS is passivated with $Zn_{0.5} Cd_{0.5} S$ followed by an outermost shell of ZnS (*Xie et al 2004*). This reduces the strain caused by lattice mismatches therefore preventing the formation of defect sites. Such QDs were found to be highly luminescent and display superior stability.

- **Fluorescence Lifetime**

QDs typically have fluorescence lifetimes of tens of nanoseconds (ns), which is long compared to luminescent dyes or cellular autofluorescence -so QDs are easily distinguished from other fluorescent bodies in lifetime measurements (*Evident Technologies 2007*). QDs with high QYs display longer fluorescent lifetimes due to a reduction of non-radiative decay, which is known to have faster decay time (*Wuister 2003*).

- **Molecular Coupling**

QDs can be attached to a broad range of capping ligands e.g. thiols, amines, phosphines making them soluble in a large number of solvents. They can be capped in siloxane to make them water-soluble and therefore suitable for biological applications.

2.5 Conclusions

This 'Background' chapter has provided a description of photovoltaics including the band structure of different materials, the photovoltaic effect and p-n junctions. The inherent limitations of PV cells and the highest efficiencies achieved to date were outlined. Imaging and non-imaging concentrators were briefly described followed by a description of LSCs. The advantages of LSCs and the problems that hindered their development were discussed and this led to the introduction of the QDSC. The band structure and various types of QD were described followed by an overview of prevailing QD synthesis techniques. Finally, a description of the unique properties of QDs that make them suitable for application in solar concentration was given.

References:

Alivisatos, A.P., (1996), Perspectives on the physical chemistry of semiconductor nanocrystals, *Journal of Physical Chemistry*, Vol. 100, pp.13226-13239.

Alivisatos, A.P. (1997), Nanocrystals: building blocks for modern materials design, *Endeavour*, Vol. 21, No. 2, pp. 56-60.

Alivisatos, A.P., (1998), Electrical studies of semiconductor nanocrystal colloids, *MRS Bulletin*, February 1998, pp. 18-23.

Barnham, K.W.J., Marques, J.L., Hassard, J., O'Brien, P., (2000), Quantum-dot concentrator and thermodynamic model for the global redshift, *Applied Physics Letters*, Vol. 76 No. 9, pp. 1197-1199.

Dimroth, F. Baur, C., Bett, A.W., Meusel, M., Strobl, G., (2005), 3-6 junction photovoltaic cells for space and terrestrial concentrator applications, Proceedings of Photovoltaic Specialist Conference, Conference record of the 31st IEEE, pp. 525-529.

Evident technologies, (2007), www.evidenttech.com/applications/quantum-dot-fluor-label.php

Gallagher, S. J., Rowan, B. C., Doran, J. D., Norton, B., (2007), Quantum Dot Solar Concentrator: Device characterisation using spectroscopic techniques, *Solar Energy*, 81 pp. 540-547.

Goetzberger, A., Greubel, W., (1977), Solar energy conversion with fluorescent concentrators, *Applied Physics*, Vol. 14, pp. 123-139.

Goetzberger, A., (1978), Fluorescent Solar Energy Collectors:Operating conditions with diffuse light, *Applied Physics*, Vol. 16, pp. 399-404

Goetzberger, A., Witter, V., (1979), Fluorescent planar collector-concentrator for solar energy conversion, *Festkorperprobleme*, Vol XIX, pp. 427-450.

Goetzberger, A. Hoffman, V.U., (2005), *Photovoltaic solar energy generation*, 1st edition, Springer, New York.

Hermann, A.M., (1982), Luminescent Solar concentrators-a review, *Solar Energy*, Vol. 29, No. 4, pp.323-329.

Knight, A., Gaunt, J., Davidson, T., Chechik, V., Windsor, S., (2004), Evaluation of the Suitability of Quantum Dots as Fluorescence Standards, *NPL Report DQL-AS 007*.

Lakowicz, J.R., (1999), *Principles of Fluorescent Spectroscopy*, 2nd edition, Springer, New York.

Mansour, A.F., (1998), Outdoor testing of luminescent solar concentrators in a liquid polymer and bulk plate of PMMA, *Polymer Testing*, Vol.17, pp. 153-162.

Markvart, T., (1997), *Solar Electricity*, John Wiley and Sons, London, England.

Mc Cann, M., Raabe, B., Jooss, W., Kopecek, R., Fath, P., (2006), 18.1% efficiency for a large area, multicrystalline silicon solar cell, *Photovoltaic Energy Conversion, Conference Record of the 2006 IEEE 4th World Conference* Vol. 1, pp. 894-899.

Neaman, D.A, (2003), *Semiconductor Physics and Devices Basic Principles*, 3rd Edition, Mc Graw Hill, New York.

Norris, D.J., Bawendi, M.G., (1995), Structure in the lowest absorption feature of CdSe quantum dots, *Journal of Chemical Physics*, Vol. 103, No. 13, pp. 5260-5268.

Norris, D.J., Bawendi, M.G., (1996), Measurement and assignment of the size dependant optical spectrum in CdSe quantum dots, *Physical Review B*, Vol. 53, No. 24, pp. 16338-16346.

Ouellette, J., (2003), Quantum Dots for Sale, *The Industrial Physicist*, Feb/March 2003 pp. 14-17.

Partain, L.D., (1995), *Solar cells and their applications*, Wiley Interscience, New York.

Pickett, N.L., O'Brien, P., (2001), Syntheses of Semiconductor Nanoparticles Using single-molecular Precursors, *The Chemical Record*, Vol. 1, pp. 467-479.

Rapp, C.F. and Boling, N.L. (1978), Luminescent Solar Concentrators, *Proceedings of the 13th IEEE Photovoltaics Specialists Conference*, pp. 690-693.

Reed, M.A., (1993), Quantum Dots, *Scientific American 268*, No. 1, pp. 118-123.

Richards, B.S., Shavlav, A., Corkish, P., (2004), A low escape cone loss luminescent solar concentrator, *19th E.C. Photovoltaic Solar Energy Conference*, Paris, France, June 7-11th 2004, pp 113-116.

Ryu, K, Rhee, J-G.,Park, K-M.,Kim, J., (2006), Concept and design of modular fresnel lenses for concentration solar PV system, *Solar Energy*, Vol. 80, pp. 1580-1587.

Shockley, W., Queisser, H.J., (1961), Detailed Balance Limit of Efficiency of p-n Junction Solar Cells, *Journal of Applied Physics*, Vol.32, pp. 510519.

Talapin, D.V., Haubold, S., Rogach, A.L., Kornowski, A., Haase, M., Weller, H., (2001), A Novel Organometallic Synthesis of Highly Luminescent CdTe Nanocrystals, *Journal of Physical Chemistry B*, Vol. 105, pp. 2260-2263.

Van Sark, W.G.J.H.M, Frederix, P.L.T.M, Bol, A.A., Gerritsen, H.C., Meijerink, A. (2002), Photooxidation and photobleaching of single CdSe/ZnS qds probed by room temperature time resolved spectroscopy, *Journal of Physical Chemistry B*, Vol. 105, pp. 8281-8284.

Weber, W.H., and Lambe, J., (1976), Luminescent greenhouse collector for solar radiation, *Applied Optics*, Vol. 15., No. 10, pp. 2299-2300.

Weisbuch, C., Vinter, B., (1991), *Quantum Semiconductor structures, Fundamentals and applications*, Academic Press, Inc. Harcourt Brace & company, California, USA.

Weller, H., (1993), Quantized Semiconductor Particles: A Novel State of Matter for Materials Science, *Advanced Materials*, Vol. 5, No. 2, pp. 88.

Woggan, U., (1996), *Optical Properties of Semiconductor Quantum Dots*, Springer, New York.

Wuister, S.F., Van Driel, F., Meijerink, A., (2003), Luminescence of CdTe nanocrystals, *Journal of Luminescence*, Vol. 102, pp. 327-332.

Xie, R., Kolb, U., Li, J., Basche, T., Mews, A., (2004), Synthesis and characteristaion of highly luminescent CdSe-Core CdS/Zn 0.5Cd0.5S/ZnS multishell nanocrystals, *Journal of the American Chemical Society*, Vol.127 (20), 7480 –7488.

Zastrow, A., Wilson, H.R., Heidler, K., Wittwer, V., Goetzberger, A., (1983), Improvement of efficiency and stability of fluorescent planar concentrators (FPCs). First results from a 1m^2 test collector system, *Proceedings of the Fifth International Conference, Athens, Greece*, October 17th-21st 1983, pp. 202-206.

Chapter 3

Spectroscopic Studies

3.0 Introduction

The steady state spectroscopic techniques used to characterise QDs, matrix materials and QD composites throughout this study are described in this chapter. The results of the characterisation of various QDSC components are then described as follows:

- Quantum Dots

    o **Quantum Yield:** It was necessary to identify the QD type with the highest QY. A number of commercially available QDs were characterized spectroscopically and the most efficient type was identified.

    o **Fluorescent Lifetimes:** The fluorescent lifetime of two QD samples were compared over a range of temperatures. The effect that low temperature and QY has on fluorescent lifetimes was investigated.

    o **Re-absorbance:** The effect that re-absorption has on emission spectra was studied and the results were compared to those predicted by a ray trace

model. It was also seen that high QD concentrations lead to increased re-absorption.

- **Matrix Absorption**

In a QDSC system it is important to employ a matrix material with a low absorption coefficient in order to minimise the absorption of light by the QD host material. Various casting resins were investigated and the material with the lowest absorption coefficient was identified.

- **QD Composites**

The host material must have minimal effect on the efficiency of QDs following encapsulation. QDs composites were produced using seven types of host material and the emission intensity of each sample was measured. The sample with the least detrimental effect on QD efficiency was identified.

- **Stability**

It is imperative that QD composites retain their efficiency over time and under illumination. The stability of QDs in the host materials was studied by comparing the samples emission spectra over time. The host material that provided the most stable sample was identified.

3.1 Spectroscopic Techniques for Quantum Dot Characterisation

QDs are available commercially from a growing number of companies with many founded in the last 10 years e.g. Applied Nanoworks (2004), Evident Technologies (2000) and Qdot Corporation (1998). This recent surge of nanotechnology corporations highlights the potential that QD development holds for the future. The majority of these companies offer QDs for biomolecular detection, where QDs have special coatings and conjugates that are used to bind the QDs to target cells and tissues. This makes them unsuitable for the application of this thesis.

Nanoco Technologies Ltd. in Manchester (UK) supplied the majority of the QD types used throughout this study. Several different QD types were also purchased from Evident Technologies Inc., (New York, USA). Water soluble CdTe QDs were purchased from PlasmaChem (Germany) and ZnS QDs were purchased from Applied Nanoworks (New York, USA). All QDs characterised in this study will be discussed in the next section.

The QDs were characterised using steady-state spectroscopic techniques to measure their absorption and emission spectra. The efficiency of the QDs was interpreted from this data. Firstly, the absorption and emission processes within QDs will be discussed. When light is absorbed by a QD, electrons are excited from the ground state up to an excited state. Recombination can be radiative with light emitted by the QD or non-radiative with no light being emitted. Non-radiative emission is generally caused by imperfections on the surface of the QD acting as traps for the charge carriers. Figure 3.1 shows both recombination processes in a QD.
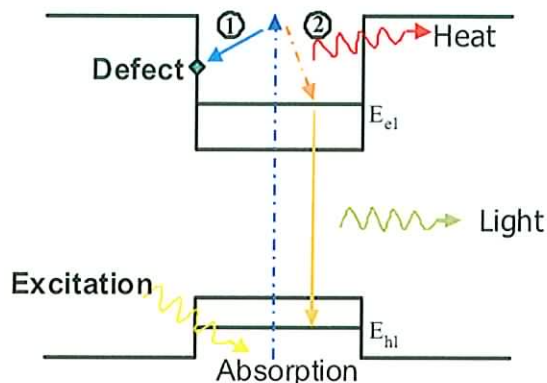
Figure 3.1: Non-radiative (1) and radiative (2) recombination in a QD

When emission does occur it is always at a longer wavelength than the absorbed light, this is due to rapid decay of the carriers to lower levels with the loss of excitation energy generating heat (*Lackowicz 1999*).

3.1.1 UV-VIS Spectroscopy

UV-VIS Spectroscopy was used to measure the absorption characteristics of the QDs investigated in this study. Matched optical glass cuvettes were used and toluene, water or chloroform were used as solvents depending on the QD type. Background measurements were taken with two reference samples of the solvent only in glass cuvettes.

The UV/VIS/NIR Spectrometer used throughout this study was a Perkin Elmer Lambda 900, shown in figure 3.2 and figure 3.3.
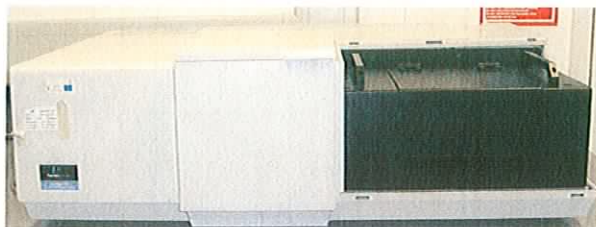
Figure 3.2: Perkin Elmer Lambda 900 UV/VIS/NIR Spectrometer

Reference channel

Sample channel

Integrating Sphere
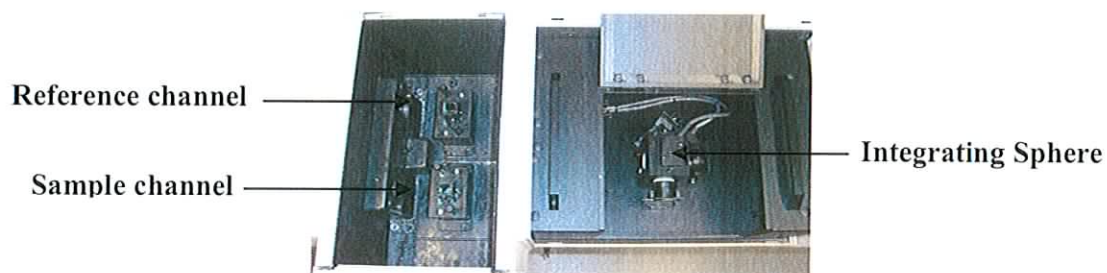
Figure 3.3: Sample holders and the integrating sphere in a Perkin Elmer Lambda 900

The Perkin Elmer Lambda 900 is a double beam, double monochromator ratio recording spectrometer which uses tungsten halogen and deuterium lamps as sources that cover a range of wavelengths from 175 to 3300 nm. The broadband light source is first passed through a grating monochromator, producing narrow band radiation that is divided by a beam-splitter. The beams travel through the sample and reference channel as shown in figure 3.4. The spectrometer measures the amount of light transmitted by the sample relative to that transmitted by the reference sample (*Focas 2005*).
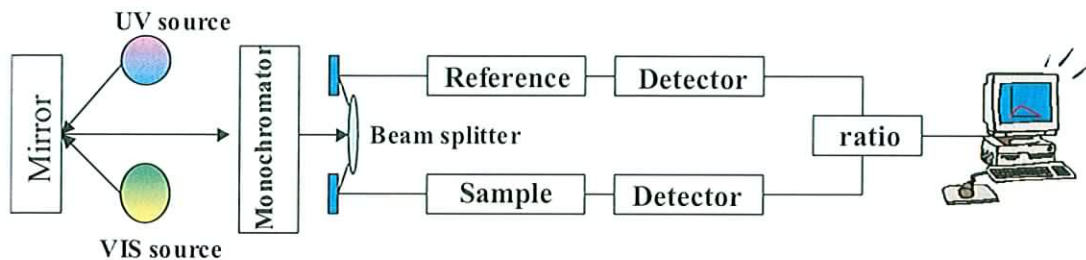
Figure 3.4: Schematic of a UV/VIS Spectrometer

The UV/VIS Spectrometer determines the absorbance of a sample from:

$$A = -\log_{10}\left(\frac{I}{I_0}\right) \qquad \text{(Equation 3.1)}$$

A= absorbance of a sample

I_0 = incident intensity

I = intensity of the transmitted light

In some cases it was necessary to calculate the absorption coefficient of samples. The absorption coefficient (α) of a material is a measure of light absorbed per unit distance in a material (*Duffie and Beckman 1991*):

$$I = I_0 e^{-\alpha x} \qquad \text{(Equation 3.2)}$$

x = pathlength in sample

Some of the experimental work required a different setup for absorption measurements, one that reduced scattering effects. Scattering is the redirection of light photons by inhomogeneties within a sample. Scattering can have no effect on light energy (elastic scattering) or it can reduce the light energy (inelastic scattering). Light can be scattered by

59

random changes in refractive index or by tiny molecules of dust, air bubbles or impurities. Scattering effects can be distinguished from QD absorption in an absorption spectrum by their characteristic wavelength dependence.

It was possible to take absorption measurements with samples placed directly in front of the integrating sphere of the UV/VIS spectrometer to minimise the measurement of scattered light. Figure 3.5 shows the normal sample arrangement and figure 3.6 shows the sample positioned in front of the integrating sphere.
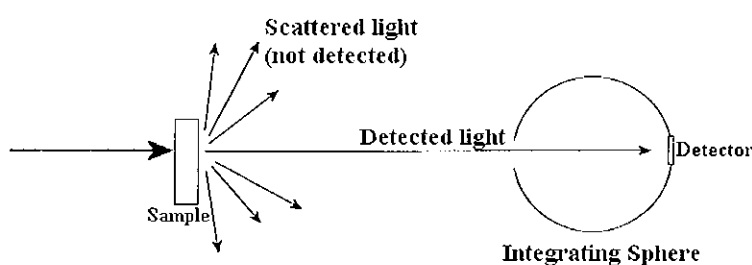
Figure 3.5: Schematic of normal absorbance measurement
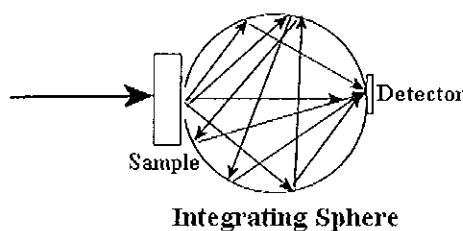
Figure 3.6: Schematic of absorbance measurement using integrating sphere

As explained in chapter 2, QD absorption spectra consist of a series of overlapping peaks. The most important one is the longest wavelength peak. A QD sample will not absorb any light at longer wavelengths than this peak. Figure 3.7 shows a typical absorption spectrum.

This particular QD (Nan550) has an absorption peak of 524 nm and higher energy peaks can be seen at 450 nm and 390 nm.
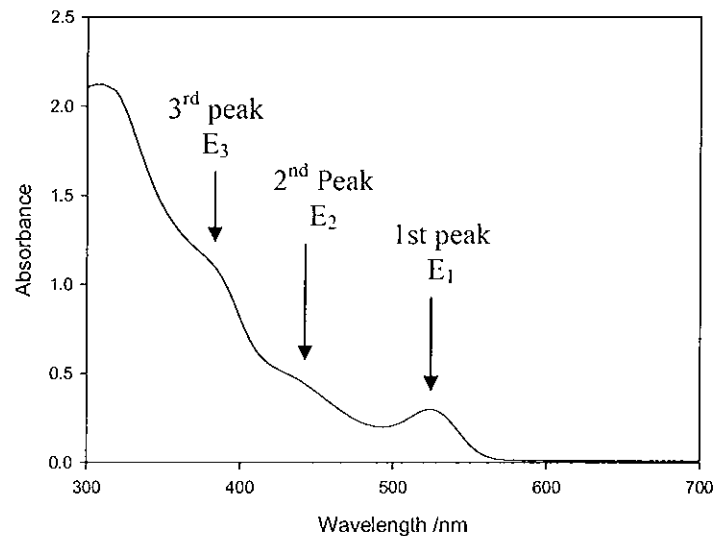
Figure 3.7: Absorption spectrum of Nan 550 QDs showing 3 energy levels

3.1.2 Fluorescence Spectroscopy

A Perkin Elmer LS55B Luminescence spectrometer was used to measure emission spectra by optically pumping samples using a high intensity light source. The LS55B uses a pulsed Xenon discharge lamp to provide its light source, passing through a Monk-Gilleson type monochromator before exciting the sample. The monochromator has a range of 200-800 nm. Light emitted by samples passes through an emission monochromator with a range of 200-900 nm (*Focas 2005*). Filtering of the emission controls the wavelengths reaching the detector and eliminates scatter and background radiation. A schematic of the operational setup of a luminescence spectrometer is shown in figure 3.8.

61
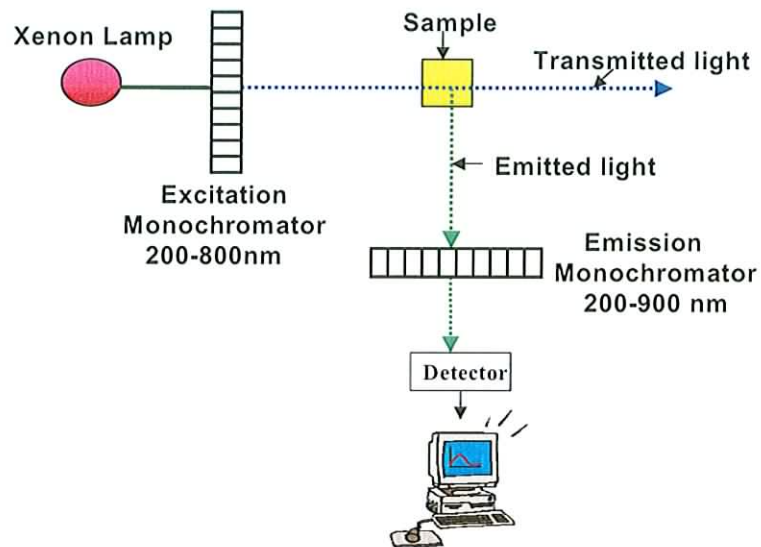
Figure 3.8: Schematic diagram of a luminescence spectrometer

The two basic types of fluorescence measurements were carried out using the luminescence spectrometer: (1) emission measurement and (2) excitation measurement.

(1) Emission measurement: the excitation wavelength was fixed and a range of emission wavelengths was scanned. The resultant emission spectrum showed the wavelength distribution of the emission, measured at a single constant excitation wavelength. Figure 3.9 shows an emission spectrum of Nan550 QDs excited at 450 nm.
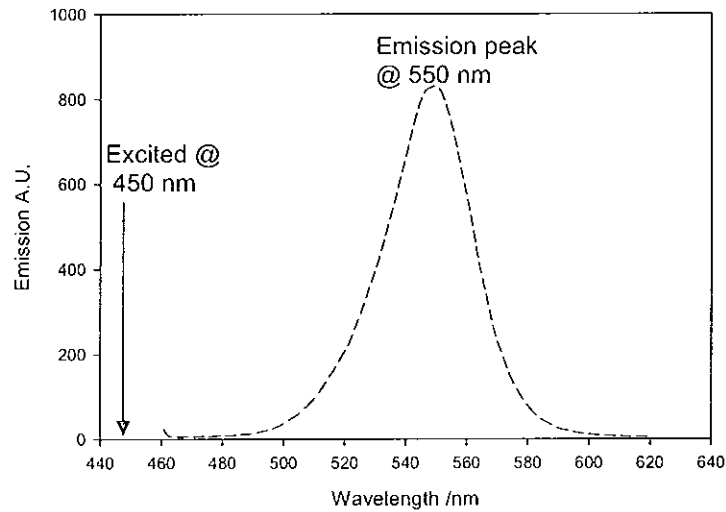
Figure 3.9: Emission spectrum of Nan550 QDs

(2) Excitation measurement: one emission wavelength was monitored while the sample was excited by light of a range of wavelengths. The spectrum displays the dependence of the emission intensity upon the excitation wavelength (*Lakowicz, 1999*). The highest peak on an excitation spectrum indicates the optimum excitation wavelength for that sample and corresponds closely to the absorption peaks of that QD. Figure 3.10 shows an excitation scan of the Nan550 QDs, it can be seen that the peaks seen in the excitation spectrum match the absorption peaks of figure 3.7.
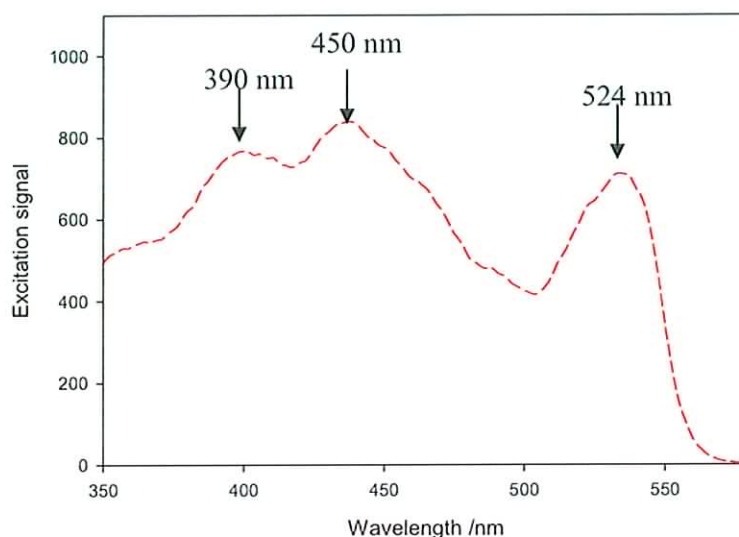
Figure 3.10: Excitation spectrum of Nan550 QDs

Excitation scans can also be used to confirm if a feature in a QD absorption spectrum is QD related. If excitation at the wavelength of that feature does not produce a signal in an excitation scan, this would indicate that the absorption feature was not related to the QD. The intensity of an emission spectrum is determined by the efficiency of the QD. Low QY indicates that non-radiative recombination is occurring possibly due to surface defects or other traps. An emission spectrum is also characterized by its full-width at half maximum (FWHM). It gives an indication of the size distribution of QDs within a sample. A FWHM of ~30 nm indicates a size distribution of approximately 5% (*Evident 2006*). Broadening of an emission spectrum due to size distribution is known as inhomogenous broadening (*Redigolo et al 2003*).

64

3.2 Quantum Dot Characterisation

The aim of this study was to identify the QD type with the highest QY. This was achieved by finding the QD type that produced the highest emission intensity. Eighteen different QDs were characterised throughout this study. Nanoco Technologies Ltd. and Evident Technologies were the main suppliers and two CdTe QD samples were purchased from PlasmaChem GmBh. Table 3.1 shows the details of all QDs characterised in this study.

Table 3.1: Description of QDs characterised in this study including label, supplier, QD type and emission peak.

QD label	Supplier	QD Type	Emission Maximum (nm)
Nan 488A	Nanoco Technologies Ltd.	CdSe/ZnS	490.5
Nan 488B	Nanoco Technologies Ltd.	CdSe/ZnS	481.0
Nan 488C	Nanoco Technologies Ltd.	CdSe/ZnS	487.5
Evi 520	Evident Technologies	CdSe/ZnS	522.5
Plas 520	PlasmaChem GmbH	CdTe	566.5
Nan 540	Nanoco Technologies Ltd.	CdSe/ZnS	543.5
Evi 540	Evident Technologies	CdSe/ZnS	556.0
Evi 540B	Evident Technologies	CdSe/ZnS	551.5
Nan 550	Nanoco Technologies Ltd.	CdSe/ZnS	550.5
Nan 556	Nanoco Technologies Ltd.	CdSe/ZnS	561.5
Nan 560	Nanoco Technologies Ltd.	CdSe/ZnS	560.0
Evi 580	Evident Technologies	CdSe/ZnS	587.5
Evi 600	Evident Technologies	CdSe/ZnS	606.5
Evi 600B	Evident Technologies	CdSe/ZnS	606.5
Plas 610	PlasmaChem GmbH	CdTe	624.5
Nan 620	Nanoco Technologies Ltd.	CdSe/ZnS	629.5
Evi 620	Evident Technologies	CdSe/ZnS	623.0
Evi900	Evident Technologies	PbS	906.5

3.2.1 Comparison of Quantum Dot Solutions of equal concentration

QD quantum yield is the ratio of the number of photons absorbed to the number of photons emitted and high QY values result in bright emission spectra. The emission intensity of the individual QD solutions was used as a marker of QD efficiency.

Initially QDs were compared in equal mass/volume concentrations. A 0.5 mg/ml toluene solution was prepared and measured for each QD type. The absorbance and emission spectra for 8 QD samples purchased from Nanoco Technologies Ltd. are shown in figures 3.11 and 3.12.
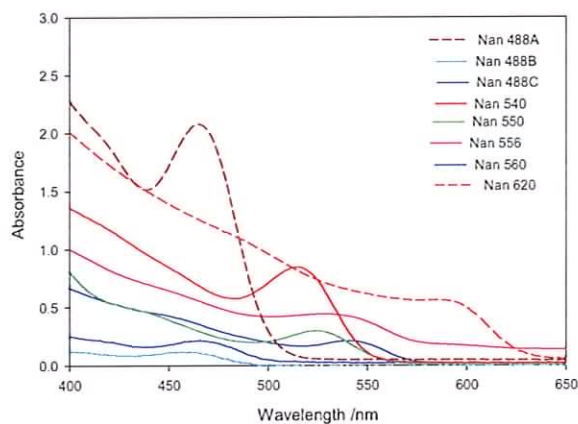
Figure 3.11: Absorbance spectra of Nanoco QDs
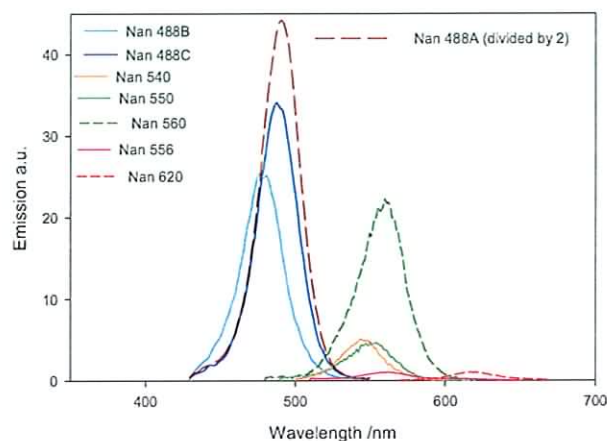
Figure 3.12: Emission Spectra of Nanoco QDs

Due to its high emission intensity, the emission spectrum of Nan488A was halved for display purposes (figure 3.12). It was clearly the most efficient QD sample provided by Nanoco. It was not possible to purchase additional Nan488A QDs from Nanoco- instead Nan488B and Nan488C were sent as alternatives. It can be seen in figure 3.12 that Nan488C were the next most efficient QDs when compared in equal concentrations.

The absorbance and emission spectra of the 0.5mg/ml solutions of Evident QDs are shown in figures 3.13 and 3.14.
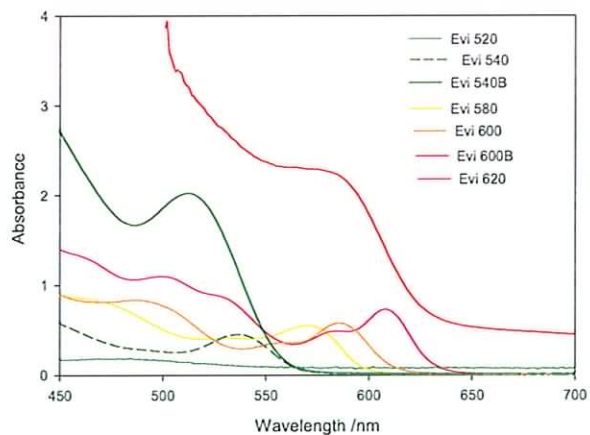
Figure 3.13: Absorbance spectra of Evident QDs

67

Evi540B and Evi600B were second versions of the original Evi540 and Evi600. It is clear in figure 3.13 that the second versions displayed much higher absorbance values. In the case of Evi540B, higher emission intensity accompanied this increased absorption (see figure 3.14). The emission spectra for Evi540 and Evi540B have been reduced by a factor of ten to fit the scale of the other QD samples. Evi540B displayed the highest emission intensity of the evident samples, followed by Evi540.
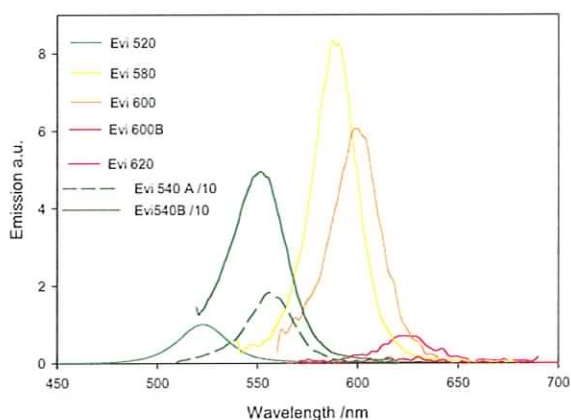
Figure 3.14: Emission Spectra of Evident QDs

The emission wavelength of the NIR QDs from Evident was outside the range of the luminescence spectrometer and therefore had to be characterised using a different instrument (Raman spectrometer). The results are shown in chapter 5 section 5.5 where the NIR QDs are encapsulated into QDSC systems.

The QDs from PlasmaChem GmbH were water-soluble CdTe core QDs. There was difficulty in dissolving the QDs properly in water however and settling occurred rapidly. The absorbance and emission spectra for the Plas520 and Plas610 QDs are shown in figure 3.15. The emission intensity was extremely low making these QDs unsuitable for this application.

68
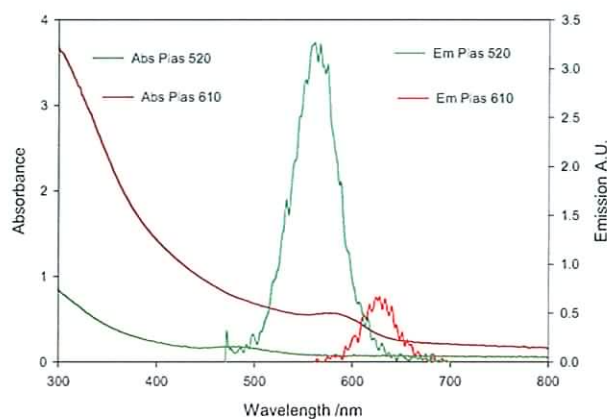
Figure 3.15: Absorbance and emission spectra of CdTe QDs from PlasmaChem

Of all the QD samples characterised in this comparison the Nan488A QDs appeared to be the most efficient. Following this, the Evi540B QDs displayed the second highest efficiency. This characterisation of the QDs was not comprehensive because a 0.5 mg/ml solution of one QD type will not contain the same number of QDs as another type, due to the different QD sizes. This means it is not sufficient to compare QDs based on equal mass/volume concentration alone.

3.2.2 Absorbance matching of Quantum Dot solutions

The quantum efficiency or quantum yield of a QD ensemble is defined as the ratio of the number of emitted photons to the number of absorbed photons. It is usually measured by comparing the emission of the QD sample to that of a substance with a known QY *e.g.* a luminescent dye with a similar emission wavelength to the QD being measured. Accurate characterisation requires the QD and dye solution to have equal absorbance values at their excitation wavelength, so that both samples absorb an equal amount of light when the emission is being measured. In this case, QD types with a range of absorption

69

characteristics were to be compared and it proved to be difficult to chose an excitation wavelength that would suit all the QD types. Difficulty also arose in matching their absorbance values at a single wavelength. The approach taken was to measure the relative emission intensities of the different QD types with their absorbance values matched at their respective peak excitation wavelengths. This eliminated the need to match individual dyes to the emission wavelength of each individual QD type. The next section describes this QD characterisation that was carried out on six QD types.

QDs that displayed the highest emission intensity in the previous study were characterised in this study, Nan488B, Nan488C, Nan550, Nan560, Evi 540B and Evi 600B. Excitation scans were carried out to identify the optimum excitation wavelength for each QD type and the concentration was adjusted until all solutions had an absorbance value of 0.25 at their excitation wavelength. The concentrations that produced the required absorbance value at their respective excitation wavelengths are shown in table 3.2.

Table 3.2: Description of the six QD types characterised by absorbance matching

QD label	Excitation λ (nm)	Emission λ (nm)	Conc. (mg/ml)
Nan488B	395	476	0.50
Nan488C	392	490	0.38
Nan550	440	545	0.11
Nan560	395	561	0.17
Evi540B	476	555	0.06
Evi600B	500	605	0.03

Figure 3.16 shows the emission spectra for each of the six QDs. It can be seen that the Nan488B QDs produced the highest emission intensity, indicating that they were most efficient QD type characterised in this study. The Nan488C QDs displayed similar emission intensity.
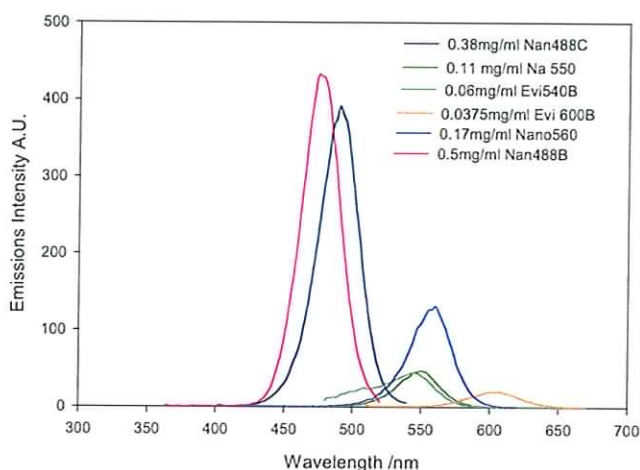
Figure 3.16: Emission Spectra of 6 QDs with absorbance values matched at excitation wavelengths

It appeared that the larger QDs with longer emission wavelengths were less efficient. This has been observed before and was attributed to the longer exposure to high temperatures required for fabrication of larger QDs, this was found to lead to increased surface degradation and lower QY (*Knight et al 2005*).

3.2.3 Fluorescent Lifetime Spectroscopy

Time-resolved (transient) fluorescence spectroscopy is a technique used to measure the distribution of times between the electronic excitation of a fluorescent body and the radiative decay of the electrons from the excited state. It was used in this study to assess the

71

balance between radiative and non-radiative processes and provide further information on the efficiency of QDs. The lifetime (τ) of a QD is the average amount of time it remains in an excited state following excitation (*Lakowicz 1999*). Fluorescence lifetimes were measured using a computer controlled Time Correlated Single Photon Counting (TCSPC) Spectrometer FL900 from Edinburgh Instruments. A nanosecond nF900 flashlamp excitation source using deuterium gas at a pressure of ~0.40 bar provided the fluorescence excitation pulses at 300 nm. Two QD samples with different QYs (Nan550 and Nan 560) were measured at a range of temperatures. Since it is expected that non-radiative effects may be reduced at low temperatures (*Weisbuch and Vinter 1991*), comparing the QD lifetimes at different temperatures provided an insight into the amount of non-radiative recombination that occurred at room temperature. Measurements were taken at the following temperatures; 290 K, 250K, 211K, 125K and 77K. Due to the low temperatures it was necessary to prepare QD composite samples in epoxy (described in section 3.3) since toluene has a freezing point of 178.5 K. QD composite samples of the concentrations used in the previous characterisation were prepared in PMMA cuvettes. Based on the results of the QD efficiency characterisation, these two QD samples would facilitate an investigation of the correlation between QY and lifetime and the effect of temperature on QDs of higher and lower efficiency. The emission spectra of the Nan 550 and Nan560 composites measured using the Perkin Elmer LS55B Luminescence spectrometer described in section 3.1.2 are shown in figure 3.17.
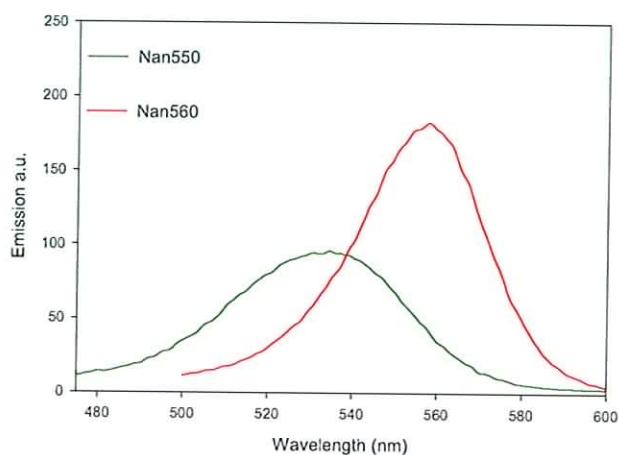
Figure 3.17: Emission spectra of QD composites characterised using TCSPC

The decay profiles of each sample at 77K can be seen in figures 3.18 & 3.19. Both samples produced decay curves that showed a non-exponential character. This is evidence of the presence of multiple decay times and a double exponential decay function was used as a best fit. This tail fitting technique allowed the calculation of both lifetimes present in the sample.
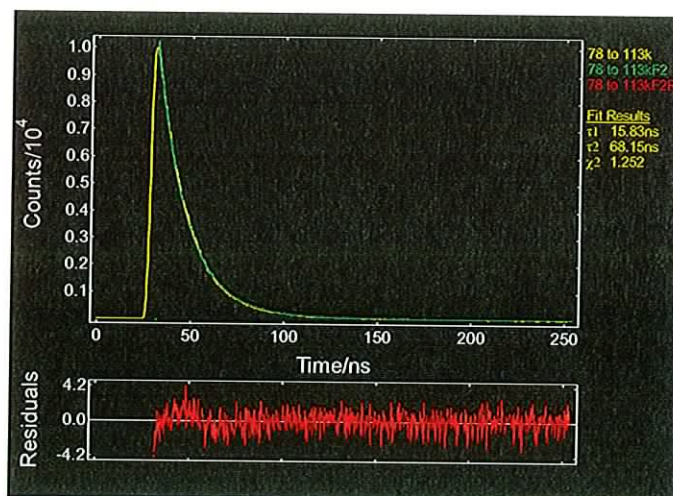
Figure 3.18: Decay profile for 0.017 mg/ml Nan560 composite at 77K
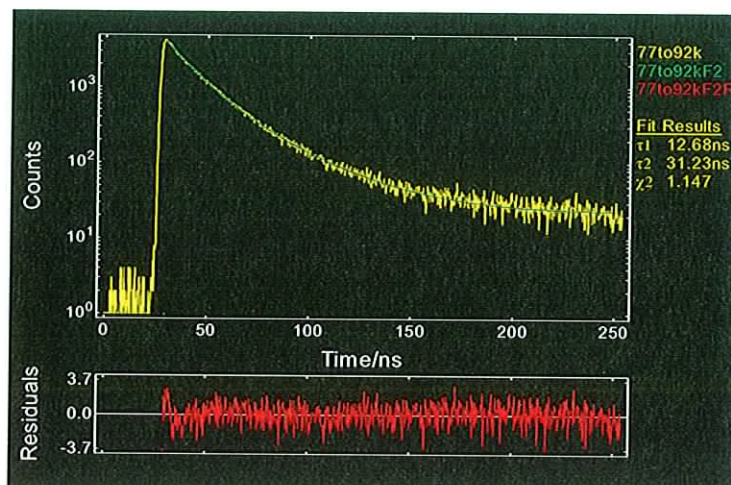
Figure 3.19: Decay profile for 0.11 mg/ml Nan550 composite at 77K

In both cases it was found that both a short (τ_1) and a long (τ_2) fluorescence lifetime existed. It has been documented that fluctuations in the environment surrounding the quantum dots induce a broad distribution of non-radiative decay channels, hence explaining the non-single exponential decay (*Lodahl et al 2004*).

The Nan560 and Nan550 composites were found to have room temperature fluorescence lifetimes of 13.4 ns and 8.45 ns respectively, when considered over the shorter window of ~20ns. The fluorescence lifetimes of Nan560 and Nan550 at each temperature are shown in figures 3.20 and 3.21 respectively.
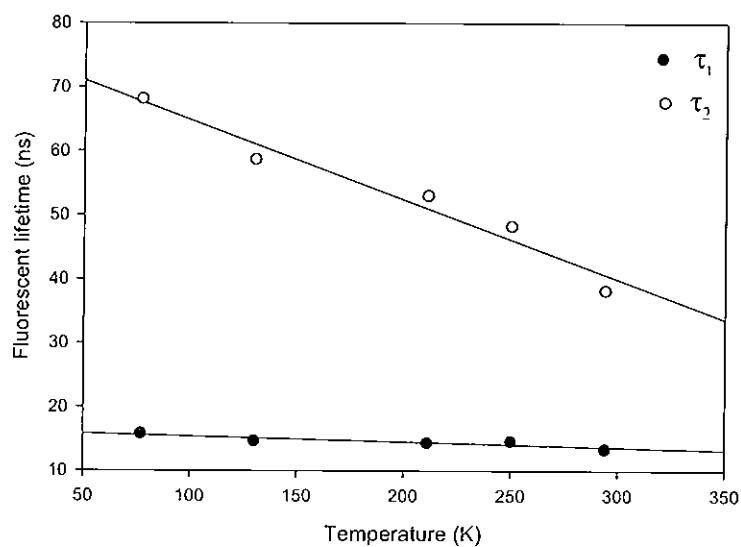
Figure 3.20: Lifetimes of 0.017mg/ml Nan560 composite
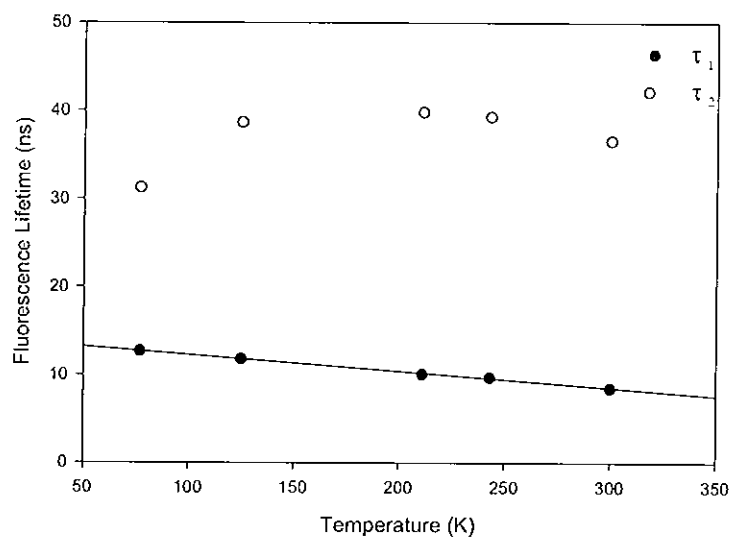
Figure 3.21: Lifetimes of 0.11mg/ml Nan550 composite

Long lifetimes are correlated with high QY (*Van Sark et al 2002*) and shorter lifetimes indicate rapid non-radiative decay. It is apparent that as the temperature is increased a

systemic decrease in the shorter fluorescence lifetime is observed in both quantum dot samples. This is caused by an increase in non-radiative processes at higher temperatures (*Weisbuch and Vinter 1991*). The values for both exponential decay components can be found in table 3.3.

Table 3.3: Lifetimes of Nan560 and Nan550 composites

Temp. (K)	Nan 560		Nan 550	
	τ_1 (ns)	τ_2(ns)	τ_1(ns)	τ_2(ns)
77	15.83	68.15	12.68	31.23
125	14.70	58.72	11.76	38.63
211	14.39	53.04	10.05	39.80
250	14.64	48.29	9.68	39.26
300	13.40	38.22	8.45	36.55

The shorter lifetime (τ_1) of Nan560 is longer than that of Nan550 at every temperature. This is expected due to the higher QY of the Nan560 QDs. This longer lifetime is explained by a reduction of fast non-radiative decay (*Wuister et al 2003*).

The lifetime of Nan560 was 15% longer at lower temperatures (77K) and the lifetime of Nan550 was 33% longer at 77K. If the QY at room temperature was very low due to thermally activated non-radiative effects then a significant change in lifetime would be expected at lower temperatures. The greater change in lifetime (33%) for Nan550 represents the lower QY of this sample relative to Nan560.

3.2.4 Re-absorbance Study and Ray Trace Model

As noted previously, a large Stokes shift is desirable since overlap of the absorption and emission spectra leads to a decrease in emission intensity. Re-absorption of light emitted in

the overlap region causes emission spectra to shift to longer wavelengths. Therefore it is difficult to quantify the overlap of QD samples because the measured emission spectra have already been reshaped by re-absorption. An emission spectrum that has been red-shifted by re-absorption could appear to have a larger Stokes shift.

An investigation into the effects of re-absorption was carried out, by measuring the light emitted from the edge of a QD composite plate. The front of the plate was excited by a laser and emission measurements were taken as the laser was placed at increasing distances from the edge. A schematic diagram of the experimental setup is shown in figure 3.22.
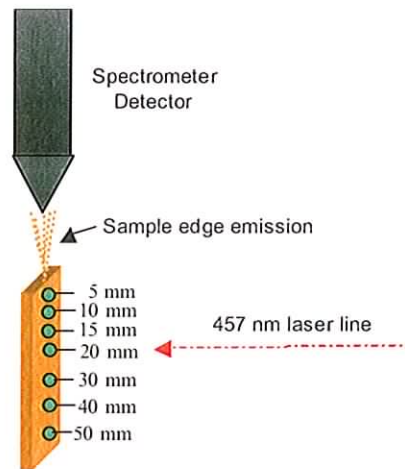
Figure 3.22: Schematic of edge emission measurements

A 6 x 6 x 0.3 cm QD composite plate containing a 0.05% (m/v) concentration of Nan 550 QDs was used, the fabrication methods used will be described in sections 3.3 and 4.1. The sample was excited at seven positions ranging from 5 mm to 50 mm from the edge of the sample using the 457 nm line of an argon ion laser. The edge emission was measured using an Instruments S.A. Labram 1B Raman spectrometer, a confocal Raman imaging

microscope system. A decrease in emission intensity with increasing distance from the sample edge was expected, accompanied by a red-shift of the emission peak due to re-absorption effects (*Chattan 2004*).

The results are compared to those predicted by a ray trace model, which uses Monte Carlo ray trace modeling to predict the efficiency of QDSC devices (*Kennedy 2007*). Photons entering the device perpendicular to the top surface of the plate are represented by ray vectors that travel through the device until they are lost from the system or transmitted to the PV cell.

The loss mechanisms included in the model are escape-cone losses, matrix attenuation losses, quantum dot (QD) quantum efficiency (QE) losses, side mirror reflection losses, and losses due to initial reflection from the top surface (*Kennedy 2007*).

As expected, a reduction in emission intensity and a red-shift of the emission peak was observed. The measured emission spectra are shown in figure 3.23a and the spectra predicted by the model are shown in figure 3.23b.
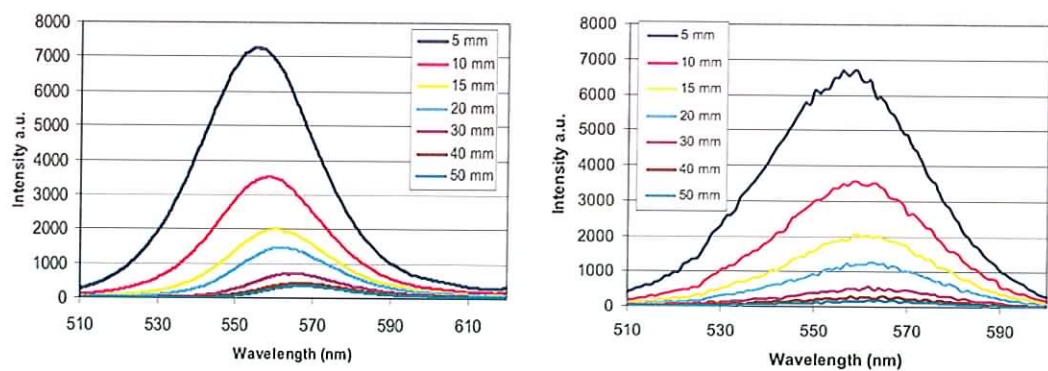
Figure 3.23: (a) Measured edge emission spectra of 0.05% (m/v) QD plate (b) Predicted edge emission spectra of 0.05% (m/v) QD plate (*Kennedy 2007*)

The agreement between the measured and predicted spectra is depicted in figures 3.24 and 3.25. The peak wavelength values for each measurement are shown in figure 3.24 and the relative integrated intensity values are shown in figure 3.25. The results are close in each case indicating good agreement between the experimental and the ray trace model.
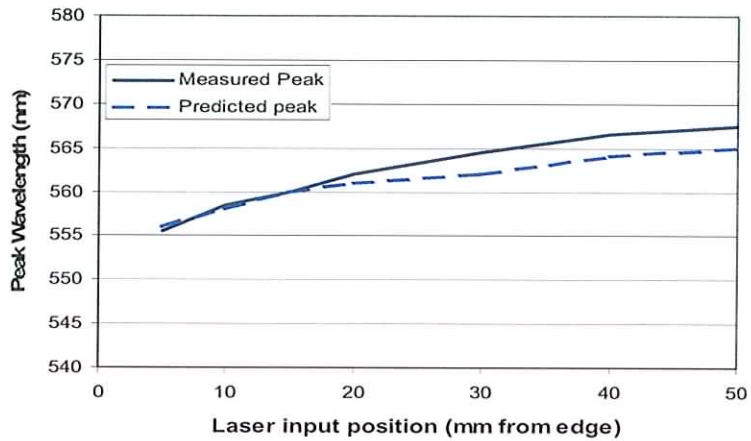
Figure 3.24: Agreement between predicted and measured emission in peak wavelength values
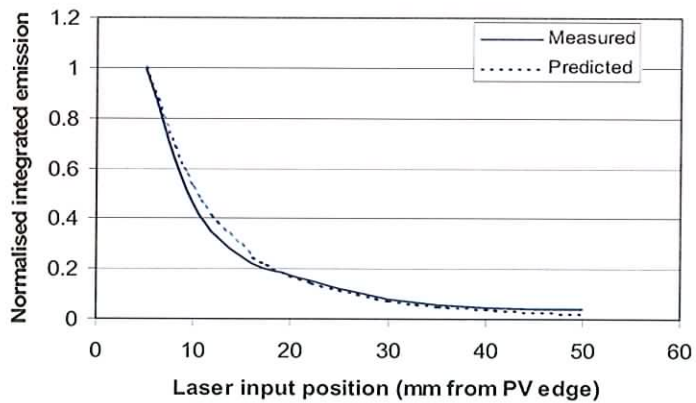
Figure 3.25: Agreement between predicted and measured emission in relative integrated intensities (*Kennedy 2007*)

These results elucidate that re-absorption occurs as light traverses QD composite samples. Nan 550 QD composite plate was also measured at a range of distances from the PV edge to investigate how QD concentration influences re-absorption effects. Figure 3.15 shows the edge emission spectra of the 0.0125% (m/v) QD plate.
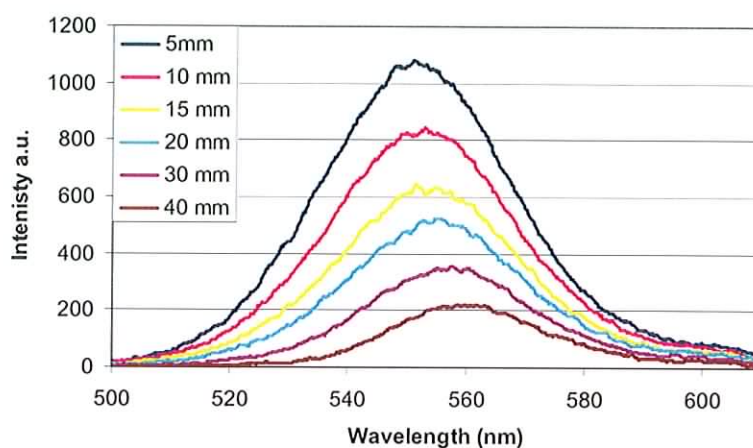
Figure 3.26: Measured edge emission spectra of 0.0125% (m/v) QD plate

The spectra shown in figure 3.26 did not appear to decrease or red-shift as dramatically as those for the 0.05% (m/v) QD composite plate (in figure 3.23). Figure 3.27 shows the peak wavelengths for each distance measured for the 0.05% and 0.0125% samples.
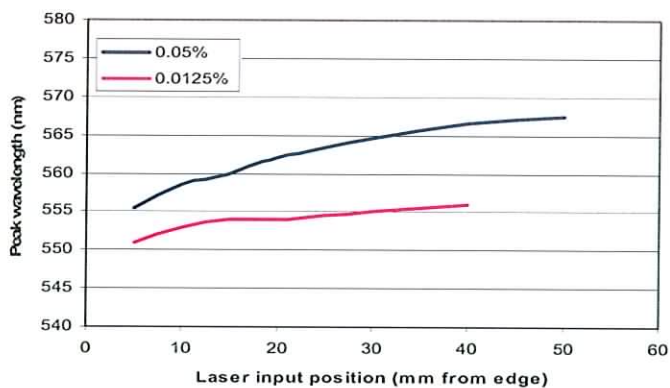
Figure 3.27: Peak wavelengths for 0.05% (m/v) and 0.0125% (m/v) QD samples

It is clear that the 0.05% (m/v) sample has red-shifted to longer wavelengths than the 0.0125% (m/v) sample and continues to red-shift further at increasing distances from the PV edge. These results confirm that re-absorption effects are enhanced in samples of higher QD concentration. This effect can also be observed in QD concentration dependence studies, where solutions of higher concentrations have emission peaks at longer wavelengths due to re-absorption by other QDs within the sample.

3.3 Quantum Dot Composites

QD composites are produced by encapsulating QDs into a polymer matrix (PMMA, Polystyrene etc.) to form a solid material. QD composites are being widely investigated as they broaden the application range of QDs into solid-state devices e.g. LEDs, PV cells. Past attempts to incorporate QDs into monomers such as styrene and methylmethacrylate, which were subsequently polymerized, have shown limited success due to the effects of polymerization (*Knight et al 2004,Pang et al 2005*). Large blue-shifts and the appearance of broad peaks at shorter wavelengths indicated damage to the QDs. The possible causes included thermal damage, oxidation and damage from radicals produced during polymerisation (*Knight et al 2004*). Aggregation of the QDs was also found to cause luminescence quenching. When QDs are situated close together in a highly concentrated sample, the likelihood of energy transfer to a non-luminescing QD is increased (*Chang et al 2005*). In this application, QD encapsulation was central to the development of a QDSC and it was essential to find the most suitable polymer material. The characteristics that were considered when choosing a suitable resin for QDSC development are outlined in the next section.

81

3.3.1 Details and comparison of matrix materials

It is essential that the carrier material is highly transparent. The transparency of each resin is determined by their absorption coefficients. The absorption coefficient of a material is defined as the fraction of light absorbed per unit distance in a material. A resin should be free of structural defects e.g. air bubbles or tiny particles because collision of light photons with such particles quenches the photons energy. In a QDSC system this effect would decrease the amount of light reaching the PV cell and therefore the electrical output of the system.

A suitable resin should be able to combine with QDs and have a minimal effect on their efficiency *i.e.* the QDs should retain high emission intensity after encapsulation. The efficiency of a QDSC is affected greatly by the emission intensity of the QDs, therefore this factor is considered most important when choosing a host matrix.

Once the QDs are incorporated into a resin, it is vital that they retain their efficiency over time. When a large-scale system is produced, it must be a long-term device that does not degrade. The stability of the emission intensity of QD composites is investigated in this study. Seven different casting resins were compared, the details of each are shown in table 3.4.

Table 3.4: Details of casting resins investigated

Number	Name	Composition	Supplier
1	Biothan	Clear casting resin	Canonbury Arts. U.K.
2	Alumilite	Urethane	Alumilite Corp. U.S.A.
3	Clear Cast Epoxy Resin	Epoxy	ABL Stevens, U.K.
4	Plexit 55	PMMA	Carl Roth GmbH & Co KG
5	Crystal Clear 200	Polyurethane	RPM Supplies, Dublin
6	Water Clear 781	Polyurethane	BJB Enterprises Inc. U.S.A.
7	Water Clear 782	Polyurethane	BJB Enterprises Inc. U.S.A.

The casting procedure was carried out in a fume cupboard and PMMA cuvettes were used as moulds in each case as they provided samples suitable for spectroscopic measurements. The setup is pictured in figure 3.28.
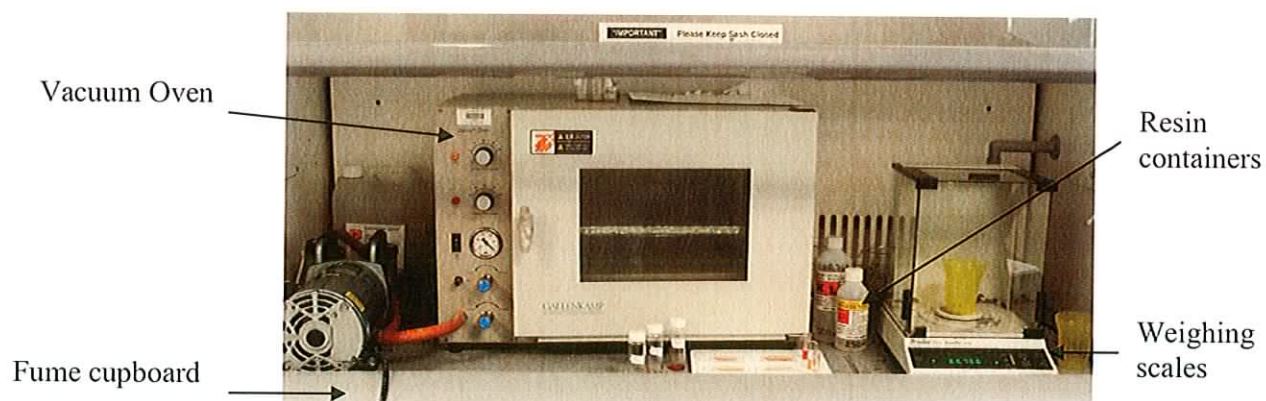
Figure 3.28: Setup for casting procedure

All resins had two parts that were combined at a ratio specified by the manufacturer. Most of the resins' manufacturers recommend placement in a vacuum chamber for various lengths of time in order to degas the sample and prevent the formation of bubbles during curing. When left in the vacuum chamber for periods of 10 minutes or more some samples hardened or became too sticky to pour into a cuvette e.g Alumilite. If not degassed sufficiently some resins bubbled up while curing overnight (see figure 3.29).

Biothan   Alumilite   Plexit 55   Crystal Clear

Figure 3.29: Resin samples containing bubbles

The following resins were characterised:

(1) Biothan is a casting resin composed of sugar-, Caprolacton- and OLEO- polyols with several proprietary natural additives. It has no safety labeling requirements, a long pot life and is toxicologically harmless to use (*Canonbury Arts 2004*).

(2) Alumilite is a water clear, urethane casting system that produces a high impact rigid material with good weatherability and exceptional clarity (*Alumilite 2004*).

(3) Epoxy resin is a clear rigid epoxy resin that is totally clear and UV stabilised giving excellent optical properties (*ABL Stevens, 2004*). Longer curing time than was recommended was necessary because the samples were still in a liquid state after 24 hours. Samples were fully hardened after 48 hours.

(4) Plexit 55 is a Methylmethacrylate (MMA) that requires exposure to UV light to induce polymerisation (*Forjahn,B.*, *2004*). Problems encountered include the mixture hardening inside the vacuum chamber and cuvettes cracking during the curing process due to 14% shrinkage of the resin.

(5) Crystal Clear 200 is one of a range of rigid urethane casting compounds that differ only in working and de-mould times. The cured castings are UV resistant and are not brittle (*Smooth-On 2004*).

(6/7) Water Clear 781/782 are both polyurethane resins, which boast exceptional clarity, good impact resistance and good weatherability. WC782 has a 15-minute working time, while WC 781 has a longer working time of 30 minutes (*BJB Enterprises Inc.*, *2004*). Table 3.5 shows the toxicity, pot life and cost/kg of each resin.

Table 3.5: Toxicity, pot life and cost per kg of each casting resin

Resin	Toxicity	Pot Life (mins)	Cost per kg(€)
Biothan	Non-Toxic	40-180	29.3
Alumilite	Toxic	6	22.5
Epoxy resin	Toxic	600	24.6
Plexit 55	Toxic	4	24.3
CC200	Toxic	20	47.3
WC781	Toxic	30	37.5
WC782	Toxic	15	37.5

Table 3.5 shows that Biothan is the only resin that was toxicologically harmless. The Epoxy resin has the longest pot life (the amount of time available for handling the resin

before curing begins). UV light was required to cure Plexit however it was found that curing began after degassing and the material became difficult to work with. With regards to cost, Alumilite was the cheapest followed by the epoxy resin.

A cuvette sample of each resin type was cast into a PMMA cuvette. Once resin samples were cured, they were placed in a UV-VIS Spectrometer to measure their absorbance. No reference samples were used. The reflection losses were subtracted from the absorbance values and absorption coefficient values were calculated.
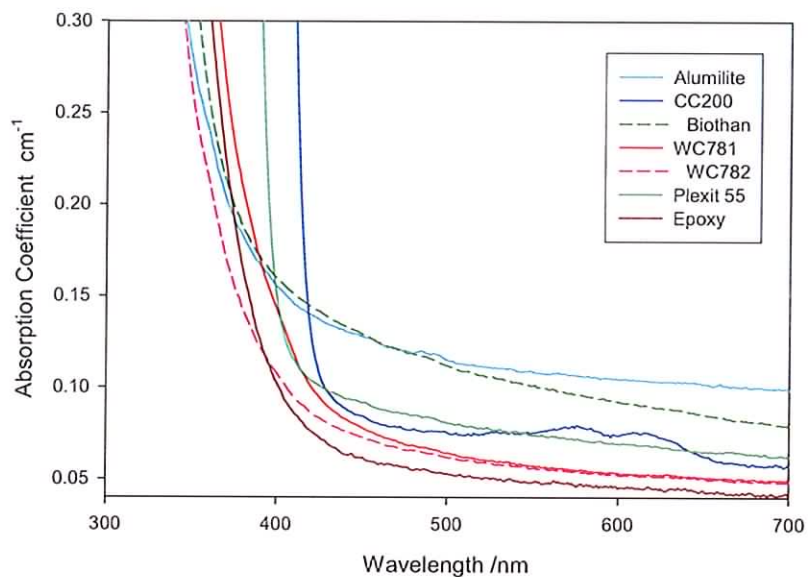
Figure 3.30: Absorption coefficient of each resin

Figure 3.30 shows the absorption spectra of each resin. CC200 begins to absorb at approximately 425 nm, if this resin was used in a QDSC it would limit the amount of light entering the device below 425 nm and would lead to a decrease in overall efficiency. WC782 begins absorbing at the shortest wavelength. The Alumilite sample has the highest absorption coefficient and the Epoxy resin has the lowest, followed by WC782. From the

absorption measurements, it appeared that WC782 and the Epoxy resin would be the most suitable carrier materials for a QDSC (*Gallagher et al 2005*).

3.3.2 Quantum Dot composite comparison

The effect of each resin on the efficiency of QDs was the most important factor to consider in this evaluation. It was crucial that the QDs maintained their high emission characteristics after incorporation into a QD composite.

QD composites containing an equal concentration of Nan488A QDs were prepared (0.02%, mass/volume %). A solution of the same concentration was prepared on the day of casting for comparison with the QD performance after casting. A photograph of the samples is shown in figure 3.31.
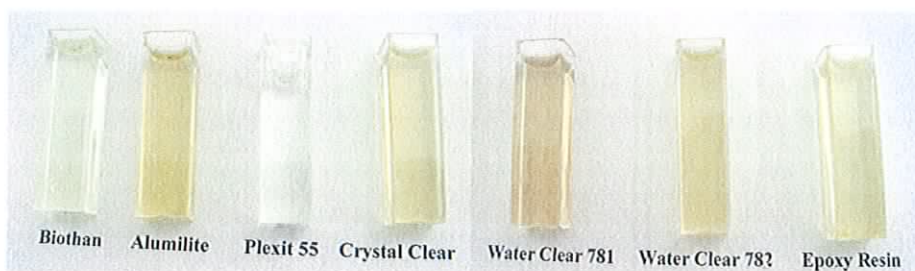
Figure 3.31: All resins containing 0.02% of 488A QDs
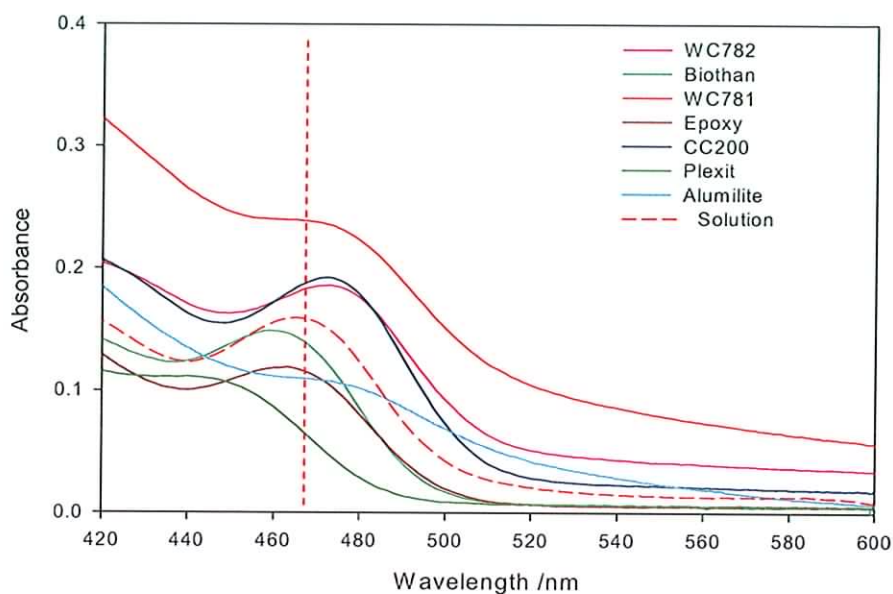
Figure 3.32: Absorbance of 0.02% QD composites taken using an integrating sphere

The absorbance spectra of the 0.02% QD composites are shown in figure 3.32. It is clear from this graph and from the photographs in figure 3.31 that the casting procedure affected the QDs differently in each case. A QD composite with an absorption curve similar to that of the solution is desirable, where the peak is well defined and the absorption curve falls to zero at the longer wavelength side of the peak. Tails of absorption following the absorption curve lead to increased re-absorption and are therefore undesirable. The graph shows that the Biothan and Epoxy samples appeared to be the most suitable for use in a QDSC.

QD absorption peaks of the Plexit, Epoxy and Biothan samples blue-shifted with respect to the 0.02% QD solution, the absorption peaks with respect to the solution peak are shown clearly in table 3.5. A possible explanation of these blue-shifts is that they were caused by the QDs decreasing in size, causing them to absorb and emit at shorter wavelengths. This shrinking has been previously observed in CdSe QDs in solution and was attributed to

88

etching of the QD surface by photo-oxidation (*Knight et al 2004*). Plexit was the only resin that required photo-polymerisation and it showed the greatest blue-shift. It could be the exposure of the QDs to UV light that caused increased degradation leading to a larger blue-shift.

Another possible explanation for the blue-shifts is that the larger QDs were ceasing to function. If smaller QDs had larger protective shells they would be more resistant to oxidisation, while larger QDs would degrade faster due to their thinner shell. At this point, information on the likelihood of this situation was not available and it requires further analysis.

The shifts observed in absorption could also be caused by scattering losses. It was evident that there were scattering losses occurring in the resin samples as some of them had a cloudy appearance. When compared to the absorption spectrum of the solution, most QD composites showed a clear background absorption that appeared to be wavelength dependant. This background absorption may have caused a shift in the QD absorption peak. Increased scattering would cause a blue-shift of the absorption peak and decreased scattering would cause a red-shift. It was not possible at this point to say what was responsible for the shifts in absorption, although scattering seemed to be the most likely explanation.

Red-shifts of the absorption peak have been observed and attributed to agglomeration of QDs within the matrix, the QD clusters could behave like larger QDs and absorb at longer wavelengths (*Knight et al 2004*). In this case there was no evidence for agglomeration. Future investigation in this area would be of benefit.
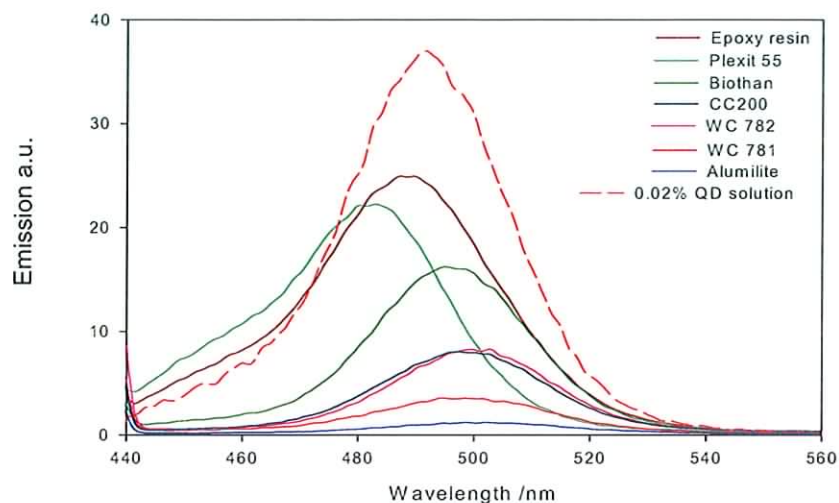
Figure 3.33: Emission spectra of 0.02% (m/v) Quantum Dot composites.

The emission spectra of all samples are shown in figure 3.33. The error in the emission intensity is +/- 0.3.

The emission intensity decreased in all samples when compared with the solution. In some cases it reduced significantly, *e.g.* Alumilite and WC781 emission intensity reduced by ~95%, while the two samples with the highest emission intensities, Epoxy and Plexit reduced by 22.5% and 35% respectively.

The values for the emission peaks and their change with respect to the solution emission can be seen in Table 3.6, a minus sign indicating a blue-shift while a plus sign indicates a red-shift.

90

Table 3.6: Absorption and emission shifts of the 0.02% QD composites, Stokes

shift and integrated emission values

Sample	Absorption (nm)	Emission (nm)	Stokes Shift (nm)	Integ. Emission
Solution	467	491.5	24	2825
Biothan	-1	+3	29	1240
Alumilite	+1	+7.5	25	115
Epoxy	-1	-4.5	24	2189
Plexit	-10	-8.5	27	1852
CC200	+2	+6	27	656
WC781	-4	+3	29.5	322
WC782	-1	+11	35	652

Most of the samples showed a red-shift of the emission wavelength relative to the solutions' emission wavelength. The two resins with the highest emission intensity (Epoxy and Plexit) showed a blue-shift of the emission curve relative to the solution.

Alumilite had the lowest emission intensity of all the samples and it did not show a clear absorption peak (see figure 3.32), this indicated that the Alumilite resin had an extremely negative effect on the QDs and was not suitable for this application. Table 3.6 includes integrated emission values for each sample. It shows that the epoxy sample exhibited the highest emission intensity followed by Plexit and Biothan (*Gallagher et al 2006*).

3.3.3 Stability of QD composites

It is important for this application that the QD composites retain their efficiency following encapsulation. Absorption and emission spectra of the QD solution during week 1 and after 23 weeks are show in figure 3.34.
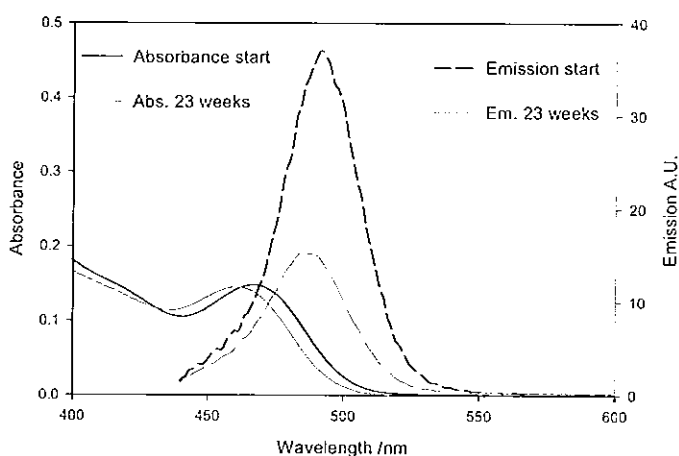
Figure 3.34: Absorbance and emission spectra of 0.02% (m/v) QD solution at week 1 and week 23.

A blue-shift of both spectra and a 70% decrease in emission intensity was observed, this was due to degradation of the QDs efficiency by oxygen and light (*Van Sark et al 2002*). This indicated that QDs were not displaying the stability that was expected from their core-shell structures and inorganic composition. Absorbance and emission measurements were carried out on the 0.02% (m/v) QD composites after 6, 12, 14 and 23 weeks. The spectra for the QD composite samples over 23 weeks are shown in the figures 3.35 to 3.41.
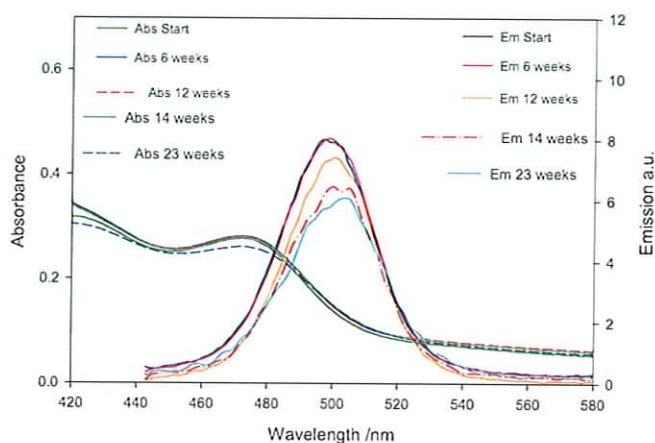
Figure 3.35: Absorbance and emission spectra of CC200 over 23 weeks

The CC200 sample (figure 3.35) showed ~20% reduction in emission intensity after 23 weeks. The Alumilite QD composite (figure 3.36) displayed a clear drop in emission over time. The absorption spectrum became less defined indicating that the QDs had ceased to function as emitters. It was clear that significant degradation had occurred in this sample and therefore it was not a suitable carrier material for a QDSC.
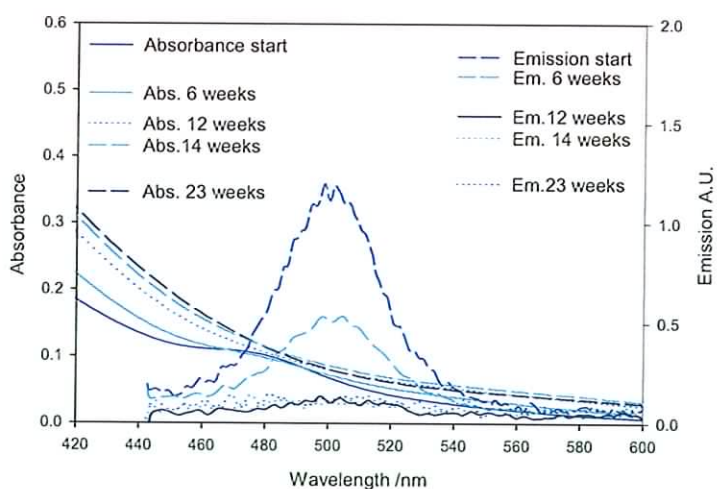
Figure 3.36: Absorbance and emission spectra of Alumilite over 23 weeks
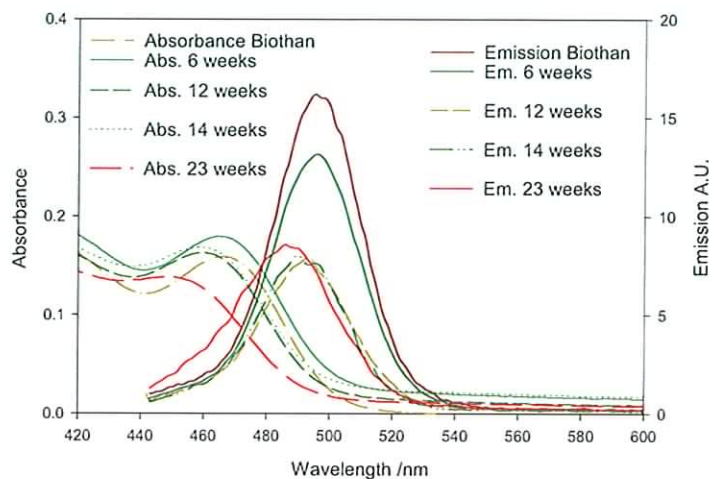
Figure 3.37: Absorbance and emission spectra of Biothan over 23 weeks

Figure 3.37 shows that after 23 weeks the Biothan sample displayed a decrease in absorbance and emission intensity over time and blue-shifted in each case. It was clearly degrading over time.
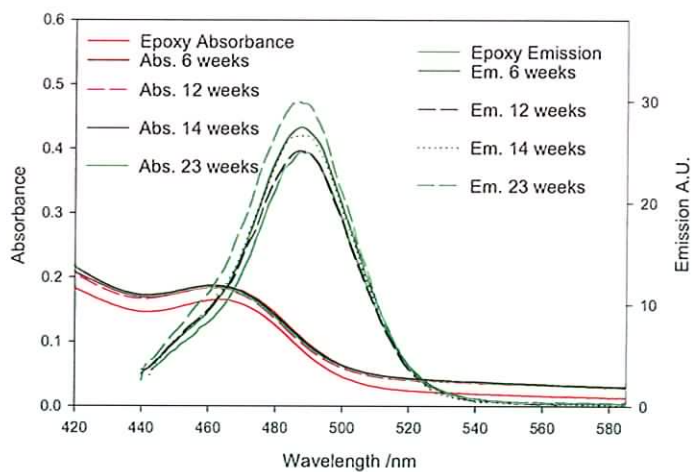
Figure 3.38: Absorbance and emission spectra of Epoxy over 23 weeks

After 6 weeks the Epoxy resin (figure 3.38) showed an increase in absorption and emission intensity. After this time the absorption remains stable and the emission intensity fluctuated to a small extent but retained high emission intensity.
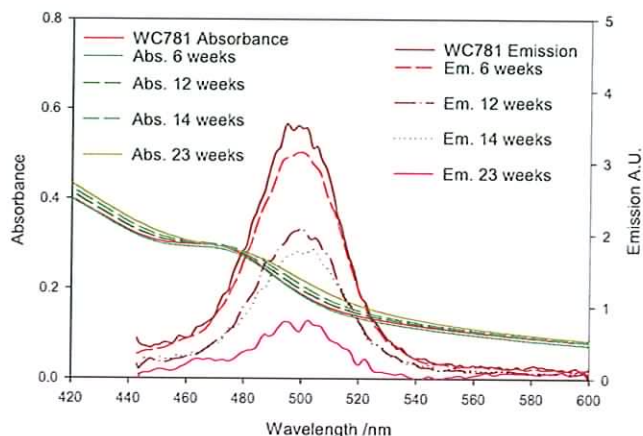
Figure 3.39: Absorbance and emission spectra of WC781 over 23 weeks

Figure 3.39 shows the spectra for WC781, it can be seen that the absorption peak became less defined while the emission degraded gradually over 23 weeks. This indicates significant degradation had occurred.
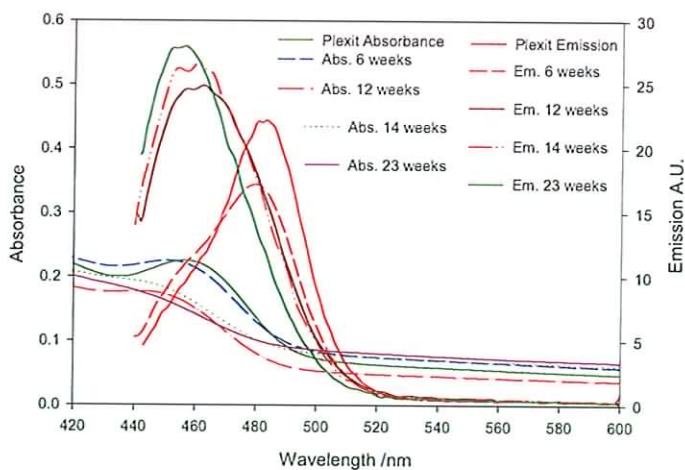
Figure 3.40: Absorbance and emission spectra of Plexit over 23 weeks

The Plexit sample (figure 3.40) showed the most dramatic changes, there was an overall blue-shift and decrease in absorbance after 14 weeks and after 23 weeks the absorption peak had diminished. The emission intensity decreased initially but after 12 weeks it showed a blue-shift, a broadening of the peak and an increase in emission intensity. These effects have been observed by others and were attributed to photo-annealing, the re-arrangement of surface atoms upon exposure to light (*Knight et al 2004*). If photo-annealing was responsible it would have occurred earlier in the experiment. The blue-shifting of the absorption spectrum over time could be caused by the larger QDs ceasing to function as discussed in section 3.3.2. This could have led to a decrease in re-absorption effects leading to an increase in emission intensity.
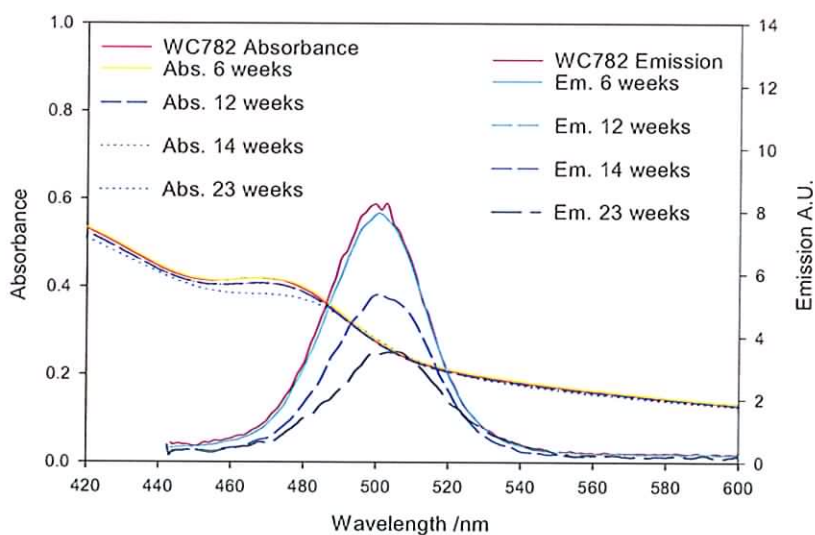
Figure 3.41: Absorbance and emission spectra of WC782 over 23 weeks

The WC782 sample (figure 3.41) showed the same changes as WC781, the absorption peak diminished and the emission intensity decreased gradually.

In summary, the behaviour of the QDs after incorporation into the casting resins was variable. It was seen that the QDs did not maintain their efficiency in Alumilite, Biothan, WC781 and WC782. The Epoxy resin and CC200 could maintain sufficient QD efficiency for the work intended in this project. Due to the low emission intensity of the CC200 sample, the epoxy sample was considered the most suitable.

The most important factors to consider when comparing the QDs performance in resin materials are the emission intensity and sample stability. It is clear in Table 3.6 and figure 3.38, that the Epoxy resin had the highest emission intensity, with an integrated emission 77.5% the intensity of the solution. Plexit had the second highest emission intensity with 65% the intensity of the solution, followed by Biothan with 43.9%. Of the three resins with the highest emission intensities, the Epoxy resin was the most stable.

3.3.4 Investigation of the Photo-stability of QD composites

In order to observe the effects of light exposure on the stability of the QD composites, 0.02% (m/v) QD composites were prepared using the three resins that displayed the highest emission intensities in the previous experiment (Epoxy, Plexit and Biothan). Nan488A QDs were incorporated into the resins and two cuvette samples were prepared in each case. One of each sample was stored in darkness and the second was exposed to daylight. Absorption and emission measurements were taken after 2, 4 and 12 weeks. Figure 3.42 shows the absorbance and emission of the 0.02% (m/v) Biothan sample that was exposed to light. It can be seen that both the absorption and emission curves blue-shifted after 12 weeks and there was a decrease in intensity.
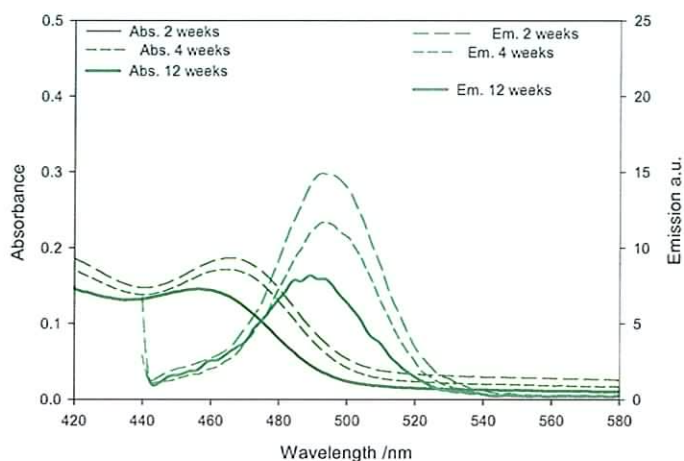
Figure 3.42: Absorbance and emission of Biothan sample exposed to light

The absorption and emission of the Biothan sample stored in darkness are shown in figure 3.43. After 12 weeks there was no shift in the absorption or emission peaks only a small decrease in emission intensity. This indicated that photo-oxidation was responsible for degradation in the Biothan sample.
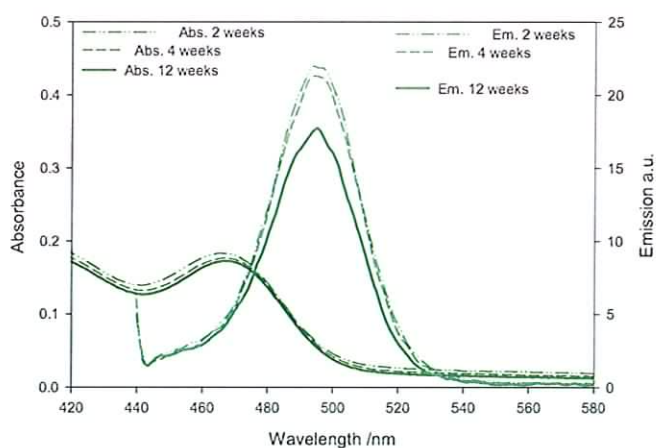
Figure 3.43: Absorbance and emission of Biothan sample stored in darkness

98

In figure 3.44 it can be seen that the Plexit sample exposed to light showed an overall rise in absorption and the peak became difficult to identify. The emission showed a large blue-shift accompanied by a rise in intensity.
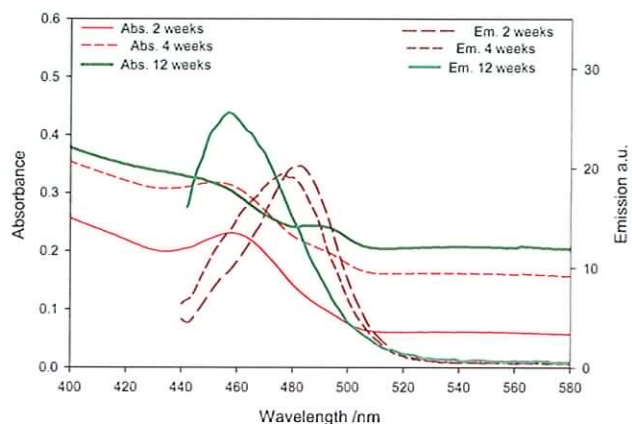
Figure 3.44: Absorbance and emission of Plexit sample exposed to light

The Plexit sample stored in darkness (figure 3.45) showed a reduction and a blue-shift in absorption and emission after 2 weeks and remained stable after this time. This was further evidence for photo-degradation.
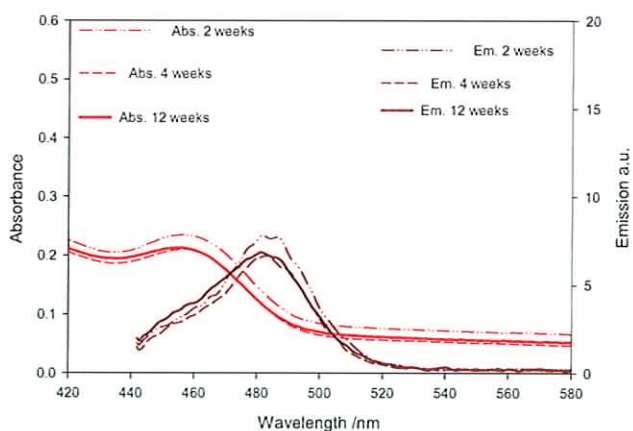
Figure 3.45: Absorbance and emission of Plexit sample stored in darkness

A similar trend can be seen with the epoxy sample in figure 3.46. It can be seen that the emission intensity of the sample exposed to light decreased dramatically after 12 weeks, while in figure 3.47 it can be seen that the sample stored in darkness remained stable. The emission intensity of the sample exposed to light after 2 weeks is higher than the sample stored in darkness, this could be due to photo-annealing of the QDs whereby a re-arrangement of the surface structure due to light exposure leads to a temporary improvement in QD efficiency (*Van Sark et al 2002*).
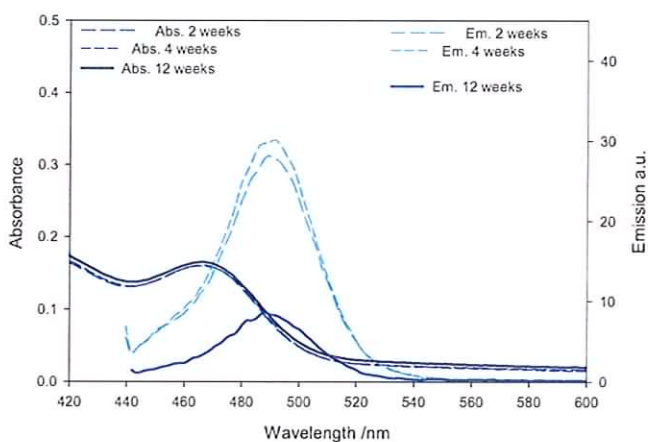
Figure 3.46: Absorbance and emission of Epoxy sample exposed to light
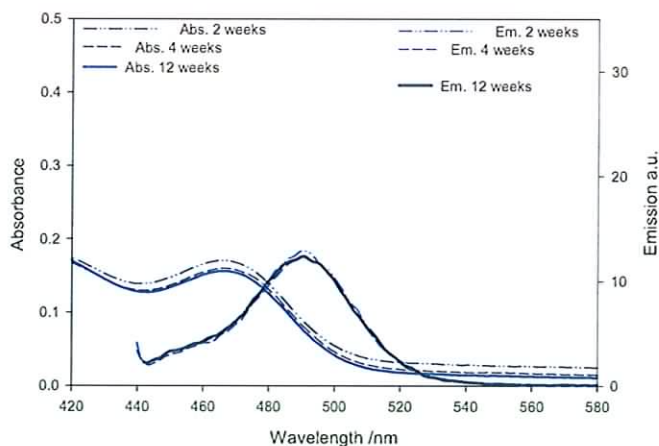
Figure 3.47: Absorbance and emission of Epoxy sample stored in darkness

3.4 Conclusions

The aims of this chapter were to determine:

(1) The Quantum Dot with the highest Quantum Yield

The initial comparison of QD efficiencies in solutions of equal concentrations found Nan488A and Evi540B to be the most efficient QD types. As this type of comparison was not comprehensive, a further characterisation was carried out on six QD types by matching the absorbance values of each sample at their respective excitation wavelengths. This comparison found Nan488B to be the most efficient QD followed by Nan488C.

(2) Fluorescent Lifetimes of Quantum Dots

An investigation of the fluorescent lifetime of two QD types showed that QDs with higher QYs had longer lifetimes due to reduced effects of non-radiative decay. It was also concluded that lifetimes increased at lower temperatures due to a reduction in non-radiative processes. The improvement was minimal which suggests that non-radiative processes do not increase significantly at room temperature.

(3) Re-absorption effects

The effect that re-absorption of emitted light has on emission spectra was established using experimental results and those predicted by a ray trace model. Red-shifting of the emission peak and decreases in emission intensity were observed. It was also shown that increased path length through a QDSC plate and high QD concentrations caused increased re-absorption effects.

(3) Matrix Material with lowest absorption coefficient

Seven different matrix materials for QD encapsulation were selected with the aim to identify the material with the highest transparency. This was established by measuring the absorption coefficient of each material and it was found that the epoxy resin had the lowest absorption coefficient followed by WC782.

(4) Matrix Material with least effect on Quantum Dot efficiency

It was necessary to find the matrix material that had the least detrimental effect on QD efficiency following QD encapsulation. QD composite samples of equal concentration were fabricated and their emission characteristics were examined. The QD composite made using the epoxy resin produced the highest emission intensity.

(5) Most stable Quantum Dot composite

A stability study carried out over 23 weeks showed that the epoxy resin retained its emission intensity while other samples changed significantly. These results clearly indicated that the epoxy resin was the most suitable matrix material for use in QDSC systems. An investigation into the effects of light exposure on sample stability showed that photo-oxidation played a major role in sample degradation.

References:

ABL Stevens, (2004), 8 Zan Industrial Park, Wheelock, Sandbach, Chesire, CW11 4PR, U.K., www.resin-supplies.co.uk.

Alumilite, (2004), *Alumilite Corporation Casting Manual*, www.alumilite.com

BJB Enterprises Inc., (2004), BJB enterprises Inc., California, U.S.A., www.bjbenterprises.com

Canonbury Arts, (2004), www.canonburyarts.co.uk/materials/resins/775N.html

Chang, T-W.F., Maria, A., Cyr, P.W., Sukhovatkin, V., Levina, L., Sargent, E.H., (2005), High near-infrared photoluminescence quantum efficiency from PbS nanocrystals in polymer films, *Synthetic Metals*, Vol. 148, pp. 257-261.

Chatten, A.J., Barnham, K.W.J, Buxton, B.F., Ekins-Daukes, N.J., Malik M.A., (2004), Quantum Dot Solar Concentrators, *Proceedings Symposium on the Efficient Use of Solar Radiation in Photovoltaic Power Engineering, St. Petersburg*, pp. 949-957.

Duffie, J.A., Beckman, W.A., (1991), *Solar engineering of thermal processes*, John Wiley and sons, Inc. New York, USA.

Evident, (2006), http://www.evidenttech.com/qdot-definition/quantum-dot-features.php

Focas, (2005), http://www.focas.dit.ie/core/index.html

Forjahn, B., (2004), Personal communication, Carl Roth GmbH. & Co. KG Germany, Schoemperlenstrabe 1-5, 76185 Karlsruhe.

Gallagher, S. J., Rowan, B. C., Doran, J. D., Norton, B., (2005), Quantum Dot Solar Concentrator device characterisation using spectroscopic techniques, *Proceedings of ISES 2005 Solar World Congress, Orlando, Florida, USA, August. CD ROM.*

Gallagher, S. J., Rowan, B. C., Doran, J. D., Norton, B., (2006), Quantum Dot Solar Concentrator: Device characterisation using spectroscopic techniques, *Solar Energy*, 81, pp. 540-547.

Kennedy, M., Rowan, B., McCormack, S.J., Doran, J., Norton, B., (2007), Modelling of a Quantum Dot Solar Concentrator and comparison with fabricated devices, *Proceedings of 3rd Photovoltaic Science Application and Technology (PVSAT) Conference and Exhibition 28 – 30 March 2007, Durham University, Durham.*

Knight, A.,Gaunt, J., Davidson, T., Chechik, V., Windsor, S., (2004), Evaluation of the Suitability of Quantum Dots as Fluorescence Standards, *NPL Report DQL-AS 007.*

104

Knight, A.,Gaunt, J., Davidson, T., Chechik, V., Windsor, S., (2005), Stability and quantum yield effects of small molecule additives on solutions of semiconductor nanoparticles, *Journal of Colloid and Interface Science*, Vol. 290, Issue 2 .

Lakowicz, J.R., (1999), *Principles of Fluorescent Spectroscopy*, 2nd edition, Springer, New York.

Lodahl, P., Floris van Driel, A., Nikolaev, I.S., Irman,A., Overgaag,K., Vanmaekelbergh,D., Vos, W.L., (2004), Controlling the dynamics of spontaneous emission from quantum dots by photonic crystals, *Nature*, Vol. 430, pp. 654-657.

Pang, L.,Shen, Y., Tetz, K., Fainman, Y., (2005), PMMA quantum dots composites fabricated via use of pre-polymerisation, *Optics Express*, Vol. 13, No. 1, pp. 44-49.

Redigolo, L.M., Barbosa, L.C., De Paula, A.M., Brito Cruz, C.H., (2003), Optical absorption and transmission electron microscopy analysis of CdTe quantum dots size distribution, *Proceeding of Microscopy and microanalysis in San Antonio , Texas, USA, August 3-7 2003*.

Sholin, V., Olson, J.D., Carter, S.A., (2007), Semiconducting polymers and quantum dots in luminescent solar concentrators for solar energy harvesting, *Journal of Applied Physics*, Vol.101, No. 12, pp. 123114.

Smooth-On, (2004), 2000 Saint John Street Easton, PA 18042, U.S.A. www.smooth-on.com

Van Sark, W.G.J.H.M, Frederix, P.L.T.M, Bol, A.A., Gerritsen, H.C., Meijerink, A., (2002), Photooxidation and photobleaching of single CdSe/ZnS qds probed by room temperature time resolved spectroscopy, *Journal of Physical Chemistry B,* Vol. 105, pp. 8281-8284.

Weisbuch, C., Vinter, B., (1991), *Quantum semiconductor structures, Fundamentals and applications,* Academic Press Inc., Harcourt brace and company publishers, CA 92101, USA.

Wuister, S.F., Van Driel, F., Meijerink, A., (2003), Luminescence of CdTe nanocrystals, *Journal of Luminescence,* Vol. 102-103, pp. 327-332.

Chapter 4

Fabrication and Characterisation of Quantum Dot

Solar Concentrators

4.0 Introduction

Efficiencies achieved by LSCs containing luminescent dyes are most often determined by their optical efficiency (η_{opt}) defined as the ratio of the total emitted optical power to the total incident optical power (*Kondepudi and Srinivasan 1990*) usually expressed as;

$$\eta_{opt} = \frac{P_{edge}}{P_{ref}} \frac{1}{G} \qquad (Eqn\ 4.1)\ (Salem\ et\ al\ 2000)$$

P_{edge}=Power density of PV cell at edge of LSC

P_{ref}= Power density of reference PV cell

G= Geometric Gain

Geometric gain (G) is defined as the ratio of the surface area of a LSC plate to the area of the PV edge:

$$G = \frac{A_{top}}{A_{edge}} \qquad (Eqn\ 4.2)$$

A_{top}= Surface area of LSC

A_{edge}=Area of collecting edge

To date optical efficiencies for single sheet LSCs of various geometries have ranged from 1.8-18.8% (*Friedman 1981, Wittwer et al 1981, Roncali and Garnier 1984, Kondepudi et al 1990, Resifeld et al 1994, Mansour et al 1998, Salem et al 2000)*. For stacked LSCs, optical efficiencies up to 15.8% have been recorded *(Wittwer et al 1981, Wittwer et al 1984, Zastrow et al 1984)*.

A recent study compared the optical efficiency of liquid LSCs containing different types of dye, semiconducting polymers and CdSe/ZnS QDs. The maximum optical efficiency (3.4%) was achieved with a semiconducting polymer (red polyfluorene) and the CdSe/ZnS QDs had an optical efficiency of 0.3% *(Sholin et al 2007)*. These efficiencies will be compared with those achieved in this study in section 6.6.

In this chapter the techniques used to fabricate Quantum Dot Solar Concentrator plates, mould construction, casting procedure and polishing of the QDSC plate edges are described. The electrical characteristics are defined and the experimental setup for electrical measurements is described. Following this, the results of fabrication and characterisation of five sets of QDSCs are shown.

The first three sets were not electrically characterised but led to improvements in the fabrication technique. The fourth set of QDSCs containing a range of concentrations of Nan488C QDs were electrically characterised and the results are shown. The fifth set of QDSCs was removed from the moulds due to problems with flaking of reflective material from the mirrored acrylic sheets and to eliminate absorption of light by the top mould plates. This set of QDSCs contained a range of concentrations of Evi540b QDs.

4.1 Fabrication of Small Scale Quantum Dot Solar Concentrators

This section describes the techniques used to fabricate small-scale QDSCs. Throughout the study these techniques are adjusted in order to improve the electrical output of systems.

4.1.1 Mould construction

QDSC moulds were constructed by securing an acrylic plate cut to the required QDSC plate dimensions between two solid acrylic sheets (see figure 4.1). The lower plate consisted of mirrored acrylic which provided the reflective backing for the QDSC and self-adhesive reflective material placed around the inner surface of the middle sheet provided the mirrored edges. The middle and top plates were both cut to the required dimensions from 0.3cm clear extruded acrylic sheets and the lower plates were cut from 0.3 cm mirrored acrylic sheets.

The moulds were made with an extra 0.5 cm in length to allow for cutting and polishing which was necessary to provide a clear and smooth edge for PV cell attachment. Tensol 70 adhesive was used to attach the plates together. Tensol 70 is a two-component system that provides a good structural bond for acrylics for external applications. The ratio of Part A:B was 20:1 and once combined the mixture was used immediately as it cured rapidly. The middle plate was attached to the lower mirrored plate first and was left to harden for at least 1 hour to ensure a strong airtight bond. The top plate was then attached and the mould was left to harden overnight. Care was required to avoid excess glue seeping into the mould cavity.
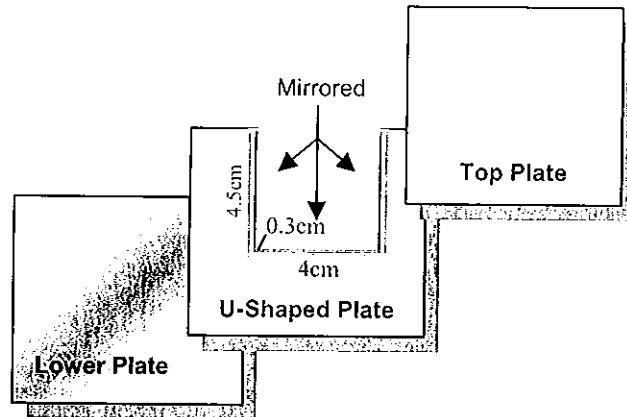
Figure 4.1: Three acrylic plates used to construct a QDSC mould

4.1.2 Casting Procedure

Based on the results discussed in section 3.3, a clear cast epoxy resin was used for QD encapsulation. The required mass of QD material was diluted in 0.5 ml toluene before being added to the epoxy mixture. It was necessary to use as little solvent as possible during encapsulation as it is known to have a detrimental effect on plastic materials. A 10ml disposable plastic syringe was used to transfer the QD/epoxy mixture into the moulds to minimise the introduction of bubbles to the mixture.

4.1.3 Post-cure treatment of QDSCs

In order to produce samples of the desired dimensions with smooth edges for PV cell attachment, approximately 0.4 cm was cut from the top of the QDSC plates and the exposed surface underwent a grinding treatment followed by polishing. Six different grades of silicon carbide abrasive paper pads ranging from 80-1200μm were rotated on a Struers

grinding machine (see figure 4.2 a). Following this treatment, 3μm and 1μm water based diamond suspensions were used on the rotating plates of a Struers Diamond Paste polishing machine (see figure 4.2 b). It was important to keep the sample edge flat on the rotating polishing pads as any tilting of the sample led to an uneven finish.
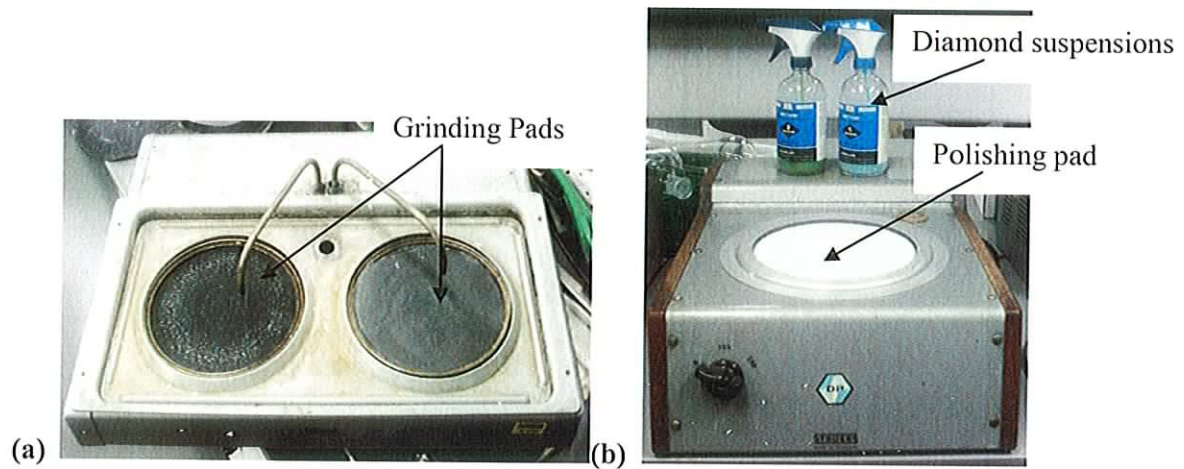
Figure 4.2 (a) Struers grinding machine (b) Struers polishing machine

4.2 Electrical characterisation of QDSCs

To electrically characterise the QDSCs, a range of Current (I) and Voltage (V) values were measured. These measurements were taken manually using a voltmeter, an ammeter and a variable resistor while the samples were illuminated by a suitable light source. A circuit diagram of the setup is shown in figure 4.3.

Should probably give details of the instruments
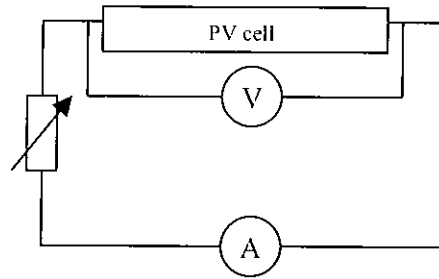
Figure 4.3: Circuit diagram of experimental setup for electrical measurements

4.2.1 Current and Voltage Measurements

The I-V data was then used to determine the following characteristics:

- Short-circuit current (I_{sc}) – the current produced when the positive and negative terminals of the cell are short-circuited, the voltage between the terminals is zero. This corresponds to a load resistance of zero.

- Open-circuit voltage (V_{oc}) – the voltage across the positive and negative terminals under open circuit conditions, the current is zero. This corresponds to a load resistance of infinity.

- Maximum power point (P_{max}) the point where current-voltage product is a maximum.

- Conversion Efficiency (η) - Ratio of the optimal electric power, P_{max}, delivered by the PV cell to the area of the cell, A_r, and solar irradiation E_e received. (*Partain 1995*)

$$\eta = \frac{P_{max}}{A_r E_e}$$ (*Eqn.4.4)(Partain*

1995)

The conversion efficiency of a solar cell is the amount of the solar energy incident on the PV device that is converted into electricity.

- Concentration Factor- Ratio of the power maximum achieved by the PV cell to that achieved with by the PV cell attached the QDSC plate

4.2.2 Experimental setup for electrical characterisation

A 1200W high efficiency metal halide discharge lamp (illustrated in figure 4.4a) was used as the radiation source for electrical measurements.
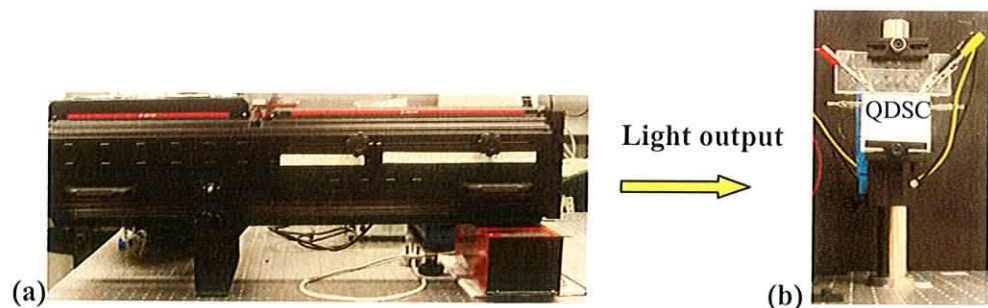
Figure 4.4: (a) 1200W Metal halide discharge lamp (b) PV mount and QDSCs position during I-V testing with discharge lamp

The lamp was mounted on an optical bench and it required vertical mounting of the QDSCs. This was undertaken using optical equipment to hold the samples in position. A photograph of the arrangement is shown in figure 4.4b. The spectral power distribution of this lamp is shown in figure 4.5.
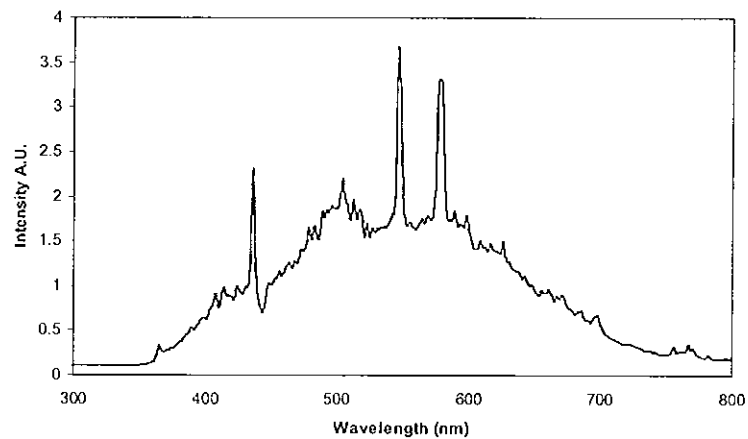
Figure 4.5: Spectral power distribution of the discharge lamp

Integrated radiation intensity measurements were taken using a Kipp and Zonen pyranometer. While certain pyranometers are intended for outdoor use, it was sufficient to provide relative intensity values prior to each electrical measurement. The intensity was approximately 1000 W/m^2 in each case, normalisation of the electrical data eliminated the effects of intensity variation.

PV cells were not permanently attached to each concentrator. Instead, one PV cell was attached to a mount comprised of three rectangular sheets of acrylic glued together. The back of the PV cell was affixed to the middle plate of this stack keeping the PV cell in a position that corresponded to the QD matrix layer when a QDSC was placed against it (see

figure 4.6). The pyranometer was placed in the same position as the QDSCs and enabled radiation intensity readings to be taken before each set of I-V measurements.

Figure 4.6: Mount used to hold PV cell in position for electrical measurements

4.3 Characterisation of Quantum Dot Solar Concentrators

The first four sets of QDSCs produced were made using the mould type described in section 4.1.1. With each QDSC that was produced, a PMMA cuvette was filled with the same QD resin mixture to provide a suitable sample for spectroscopic measurements. The following section includes details and results of the different QDSC systems produced.

4.3.1 Fabrication of two 6 cm^2 QDSCs (QDSC1)

In order to establish a reliable encapsulation procedure, two practice QDSC samples were produced, one containing epoxy only (QDSC1.1) and the other containing a 0.02% (m/v) concentration of the Nan488A QDs. (QDSC 1.2).

Due to improper adhesion of the mould plates QDSC 1.1 leaked and cured only half-full. Following this, all moulds were checked before use by filling them with water. QDSC 1.2 was used to practice the grinding and polishing process. This caused a size reduction of the sample to 6 x 5.3 cm. Photographs of samples 1.1 and 1.2 are shown in figure 4.7.

115

(a)   (b)
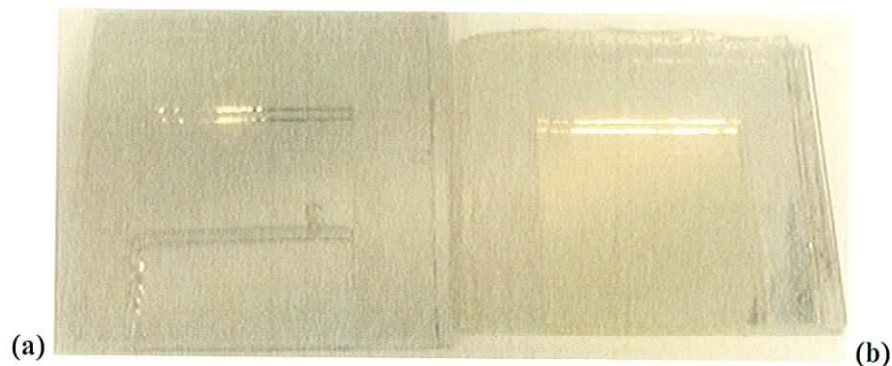
Figure 4.7: (a) QDSC 1.1 Epoxy only (leaked) (b) QDSC1.2 0.2% (m/v) 488A

4.3.2 Fabrication of four 6 cm² QDSCs containing Nan 550 QDs (QDSC2)

The second set of QDSCs produced included a range of QD concentrations of the Nan 550 QDs; 0.012% (m/v) (QDSC2.2), 0.025% (m/v) (QDSC2.3), 0.050% (m/v) (QDSC2.4) and a reference sample of epoxy only (QDSC2.1).

It was not possible to purchase the Nan488A QDs from Nanoco as they had not succeeded in reproducing these QDs with quantum efficiency equal to their first batch. Therefore it was necessary to identify the QDs with the next highest emission intensity. Figure 4.8a and 4.8b show the emission spectra of the 5 QD types that were available at the time. A solution containing 0.5 mg/ml of each QD type was prepared. They include Evi 560, Nan 550 and Nan 488B and two QD samples that were given by Imperial College London Nan 620 and Nan 540. It was necessary to display the emission curves on two separate graphs because the low emission intensity of the Nan 540 and Nan 620. It can be seen in figure 4.8b that the Nan 550 QDs display the highest emission intensity.

116
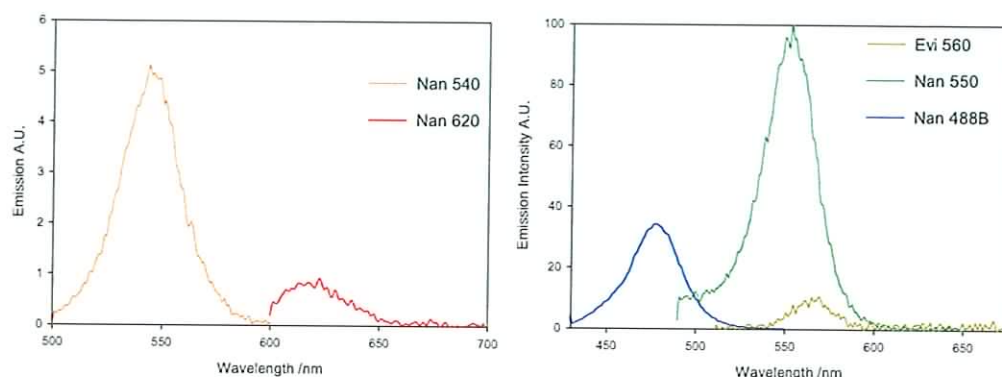
Figure 4.8: (a) Emission of 0.5mg/ml solutions of Nan540 and Nan620 QDs and (b)Emission of 0.5 mg/ml solutions of Nan550, Evi 560 and Nan488B QDs.

Once filled with the QD and resin mixture, the QDSC moulds and cuvettes were placed in an oven at 60 ° C for 15 hours as recommended by the Epoxy resin manufacturer. This "quick cure" would allow for electrical measurements to be taken as soon after casting as possible.

The QDSC and cuvette samples had an opaque appearance once they were cured, this was thought to be due to the oven curing procedure as it had not occurred with previous QD composite samples cured at room temperature. Although the cuvette samples are not of the same dimensions as the QDSC samples, they do provide an indication as to how the QD efficiency has been affected by the casting procedure. Figure 4.9 shows the absorption and emission spectra for the QDSC 2 cuvette samples.
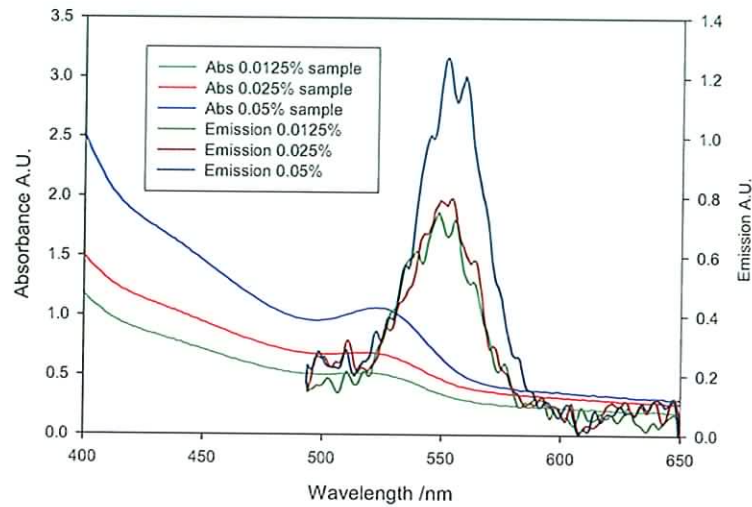
Figure 4.9: Absorption and emission spectra of QDSC2 cuvette samples

It can be seen in figure 4.9 that the emission from each of the QDSC 2 cuvette samples is very low due to the cloudiness of the samples due to scattering effects.

Another problem encountered with these samples was flaking of the reflective material on the back of the moulds. As this did not occur with QDSC 1.2, it was possible that the oven curing process might also be responsible for weakening of the bond between the acrylic sheet and the mirrored backing. This was investigated in the next batch of concentrators, QDSC 3 (see section 4.2.3) where samples with different curing techniques were compared. Details and photographs of the QDSC 2 samples are shown in table 4.1.

Table 4.1: Details and photographs of QDSC2

Sample Number	QD Concentration Mass-Volume %	Photograph
2.1	0	
2.2	0.012	
2.3	0.025	
2.4	0.050	

4.3.3 Investigation of the effects of oven curing using two 6cm^2 epoxy plates (QDSC3)

To investigate whether the oven curing process caused the cloudy appearance of the samples or not, two QDSCs were cast containing epoxy resin only. One sample was cured in a fume cupboard at room temperature for 24 hours (QDSC 3.1) and the other was cured in the oven at 60 $^{\circ}$C for 15 hours (QSDC 3.2). The following day it was clearly visible that the oven curing procedure was responsible for clouding of the epoxy resin (see figure 4.10). Both samples showed flaking of the reflective material as a result of the grinding treatment. This indicated that a different technique was required or an alternative type of reflective backing.
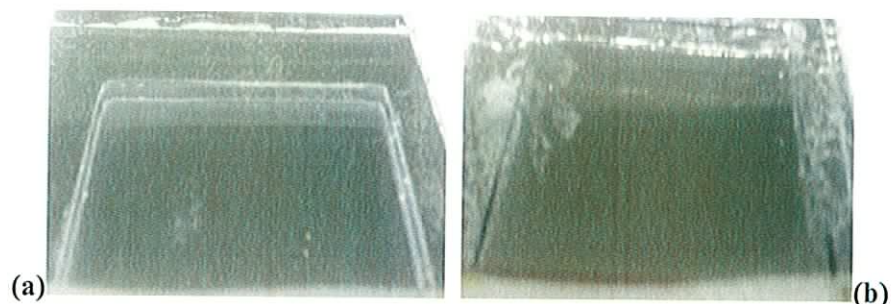
Figure 4.10: QDSC 3 (a) oven cured (b) cured at room temperature

4.3.4 Characterisation of seven 4 cm² QDSCs containing a range of quantum dot concentrations

Cuvette samples of equal concentration were made with Nan 550, Nan 488B and Nan 488C QDs in epoxy and in solution. Results showed that the Nan 488C QDs produced the highest emission intensity at this concentration in both solid and solution (see figure 4.11).
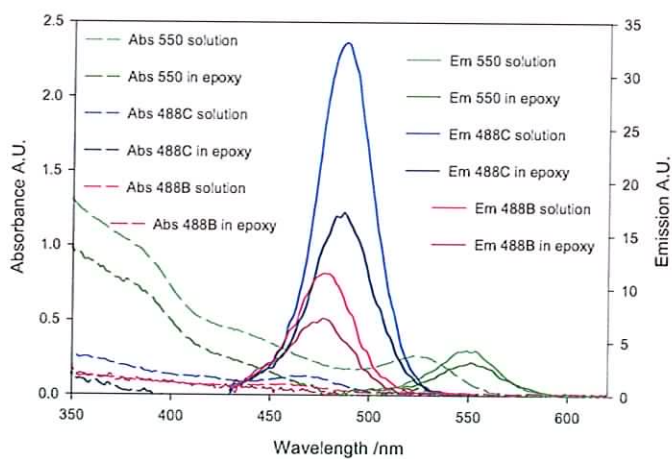
Figure 4.11: Absorbance and emission spectra of 0.02% (m/v) samples of Nan 550, Nan 488 B and Nan 488C QDs

Before casting the 488C QDs into the QDSCs, a concentration dependence study was carried out in solution. The resultant emission spectra can be seen in figure 4.12.
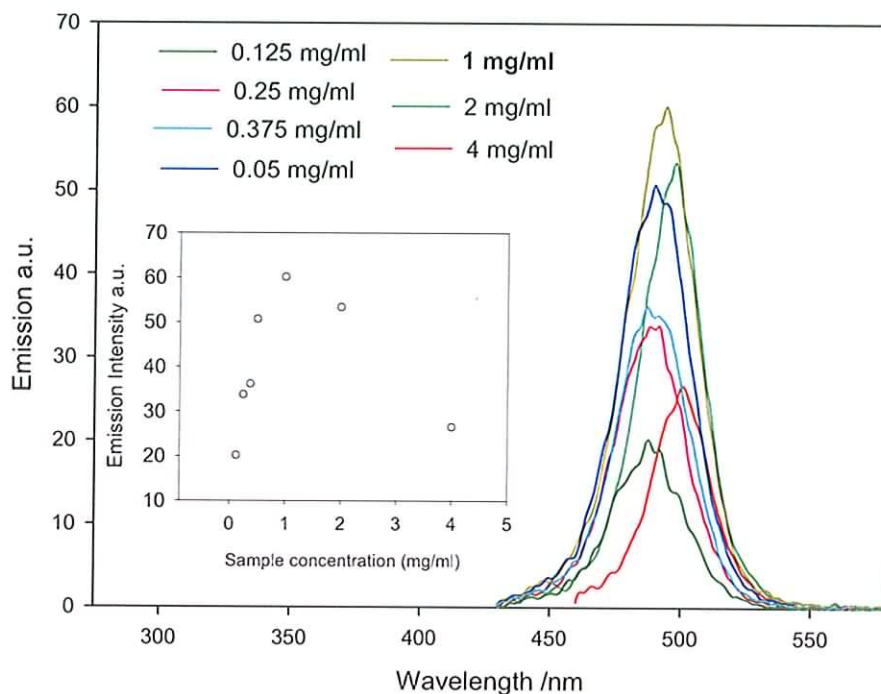
Figure 4.12: Emission spectra of different concentrations of Nan 488C QDs

The inlay in figure 4.12 shows the changes in emission intensity with increasing concentration. It shows that there was an increase in emission intensity as the concentration increased until a concentration of 1 mg/ml is reached. At this point there was a decrease in intensity and a red-shift of the emission peak. As explained in the previous chapter (section 3.2.4), this indicated that re-absorption of emitted light was occurring due to the high concentration of QDs. Based on the concentration dependence study it was decided to fabricate QDSCs of each of the measured concentrations excluding the highest concentration of 4 mg/ml since it caused a decrease in emission intensity. The aim was to

find an optimum QD concentration for this QD type in QDSCs of dimensions of 4 x 4 x 0.3 cm. Table 4.2 shows QDSCs produced with Nan488C QDs in 4 x 4 x 0.3 cm moulds, where corresponding cuvette samples were produced for each concentration.

Table 4.2: Details and photographs of QDSC 4 samples

Sample Number	QD Conc. % (m/v)	Photograph	Sample Number	QD conc. %(m/v)	Photograph
4.1	0		4.5	0.05	
4.2	0.012		4.6	0.10	
4.3	0.025		4.7	0.20	
4.4	0.037				
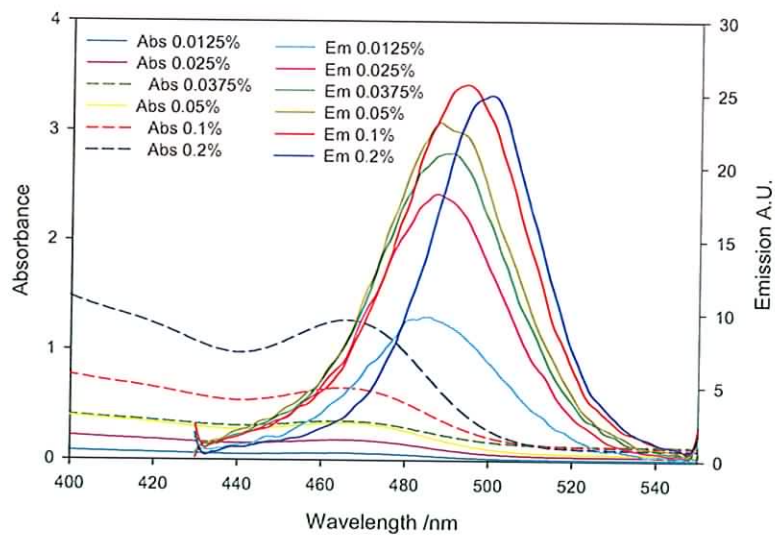
Figure 4.13: Absorbance and emission of QDSC 4 cuvette samples

Absorption and emission spectra of the QDSC 4 cuvette samples are shown in figure 4.13. There was a decrease in emission intensity of approximately 60% compared to the solution samples of the same concentrations shown in figure 4.12. The QD composite samples displayed the same pattern in emission intensity i.e. rising intensity with increasing concentration until 0.2% (m/v)was reached, at which point there was a decrease in intensity and a red-shift of the emission peak. This indicated that the QDs were exhibiting similar behavior in solid as in solution, although at a lower efficiency. Electrical measurements were taken using the setup described in section 4.2.2 of this chapter.

I-V curves for each of the QDSC 4 samples are shown in figure 4.14 and the power curves are plotted in figure 4.15. The epoxy only sample (sample 4.1) is used as a reference sample in each case.
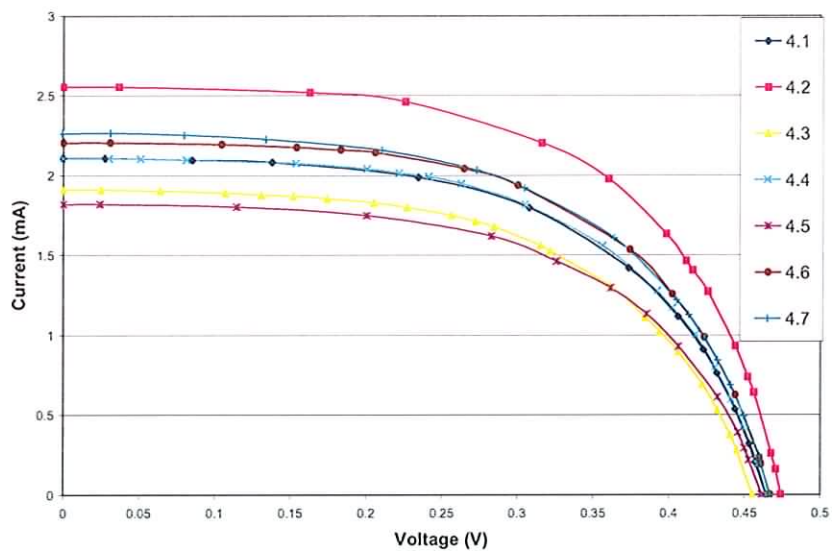
Figure 4.14: I-V curves for QDSC 4 samples
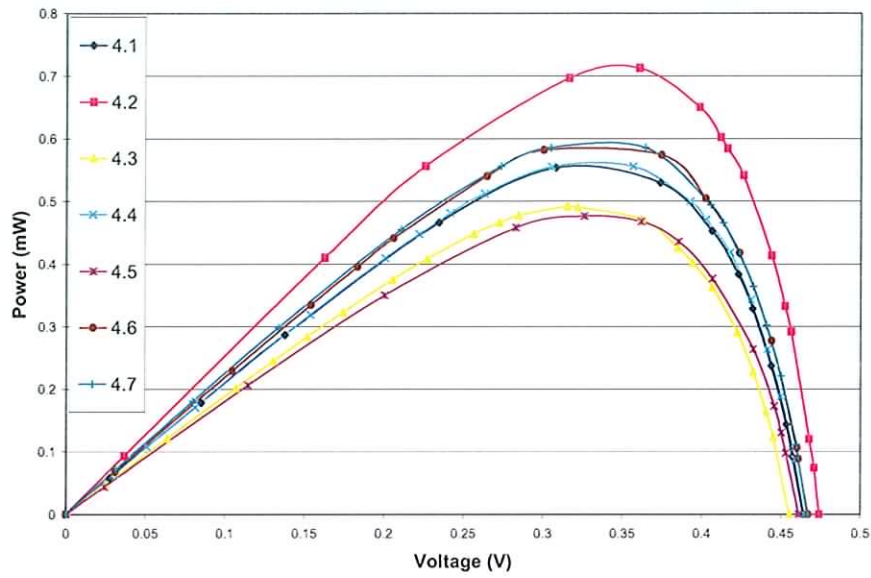
Figure 4.15: Power curves for QDSC 4 samples

Table 4.3: Results of electrical characterisation of QDSC 4 samples

Sample Number	QD conc. % (m/v)	P_{max} (mW)	Power per unit area (mW/cm^2)	Conc. Factor
PV cell	-	6.15	5.125	-
4.1	0	0.553	0.034	0.089
4.2	**0.012**	**0.713**	**0.045**	**0.116**
4.3	0.025	0.492	0.030	0.079
4.4	0.037	0.555	0.035	0.090
4.5	0.050	0.476	0.030	0.077
4.6	0.100	0.582	0.036	0.095
4.7	0.200	0.585	0.036	0.095

The concentration factor of a QDSC system is the ratio of the power output of the PV cell measured under direct illumination to the power output of the PV cell measured at the QDSC edge. The results shown in table 4.3 indicate that QDSC 4.2 had the highest concentration factor (0.116) and the highest power maximum value of 0.713 mW, this is higher relative to the output of the reference sample (0.553mW). These results indicated that lower concentrations of QDs produced the highest electrical output. The increase in efficiency due to the presence of QDs in this case is minimal even at the optimum concentration. The bar chart in figure 4.16 presents the power maximum values including error bars with values of +/-11 %.
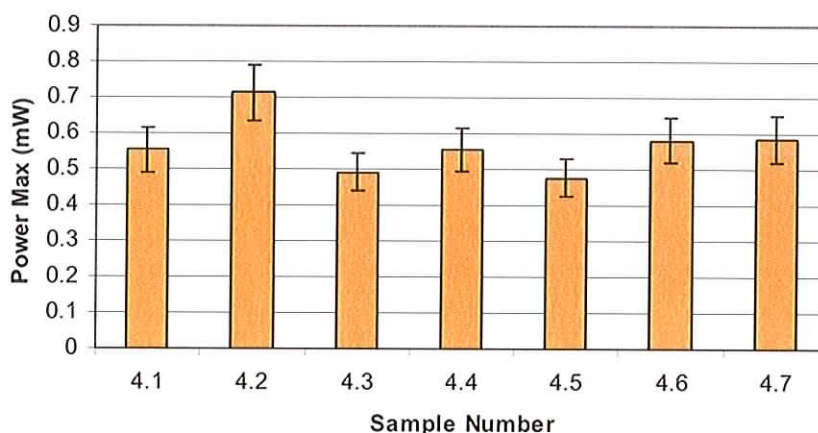
Figure 4.16: Power maximum values for QDSC 4 measured

Figure 4.16 shows that the power output of all QDSCs except QDSC 4.2 are within the error range. In addition, the trend seen in the emission spectra of the solution and cuvette samples was not observed in the power output of the QDSC plates. This may be due to the longer path length the light had to travel through the QDSC plate than in the cuvette. In a QDSC, successive reflection and emission events increase the chances of re-absorption

occurring. The low concentration factors of the QDSC plates could be due to limited utilisation of the spectral range of the incident radiation (*Rowan et al 2006a*).

In order to further investigate the effect of QD concentrations, the QDSC 4 samples were characterised using the 457 nm line of an argon ion laser. Electrical measurements were first taken in ambient light and then taken under laser illumination. The results are shown in figure 4.17.
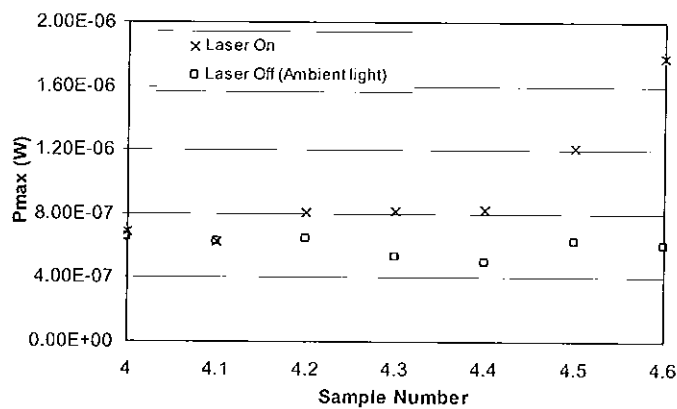
Figure 4.17: Power maximum points for QDSC 4 samples with laser off (blue square) and laser on (red crosses)

As expected, QDSC 4.1 (epoxy only) showed no increase in power output when excited with the laser as it did not contain any QDs. QDSC 4.2 showed a minimal increase, possibly due to the low concentration of QDs and samples 4.3 to 4.7 all showed a significant increase in power output when excited with the 457 nm laser line, the effect increasing with higher QD concentrations. This confirmed that the QDs were active within the concentrators when suitably excited and it indicated that higher QD concentrations produce higher power outputs.

126

Optical efficiency (η_{opt}) values (equation 4.1) were calculated for each sample using short circuit current values (*Kennedy et al 2007*). The calculated values were compared to those predicted by the ray trace model using three different QY values for the Nan488C QDs. The ray trace model developed at Dublin Institute of technology predicts optical efficiencies of QDSCs using Monte Carlo ray trace modelling. The model calculates the amount of incident rays that will reach the PV edge of a QDSC system by taking into account the various loss mechanisms, from this information the efficiency of QDSCs can be calculated. Various parameters can be altered to observe the effect on system efficiency, for example, the quantum yield of the QDs, refractive index of the matrix material, size and shape of the system and the configuration and type of reflective materials. The results of the QY study are shown in figure 4.18.
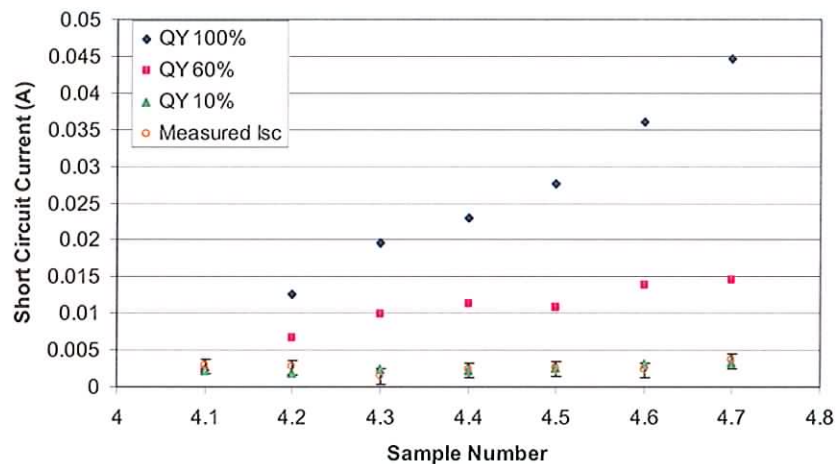
Figure 4.18: Measured and predicted I_{sc} values for QDSC 4 with three different QY values (*Kennedy et al 2007*)

In the modelled results, a QY of 10% gives the closest match to the measured values. This work gives us a good estimation of the QY of Nan488C QDs. This low QY value provides an explanation for the low concentration factors achieved by the QDSC 4 samples.

Due to the flaking of the mirrored acrylic and absorption of light by the top acrylic sheet in the first mould design, it was decided that in future the QD plate should be removed from the mould. This was achieved by attaching the mould sheets temporarily using silicone seal. Once the QD mixture was cured, the plate could be easily removed from the mould.

4.3.5 Characterisation of nine rectangular QDSCs and one triangular QDSC containing a range of concentrations of Evi 540 QDs

Evi540B QDs were purchased from Evident Technologies, the manufacturers quoted a QY between 30-50%. They were chosen due to their longer emission wavelength and higher quoted QY. Their emission peak was closer to the peak efficiency of a PV cell therefore they absorb a larger percent of the solar spectrum due to their broad excitation spectrum. Before casting the QDs into QDSC moulds, a concentration dependence study was completed to give an indication of the range of QDSC concentrations to be fabricated. Eight solutions were made containing QD concentrations ranging from 0.005% up to 0.385%. The absorbance and emission spectra are shown in figure 4.19.
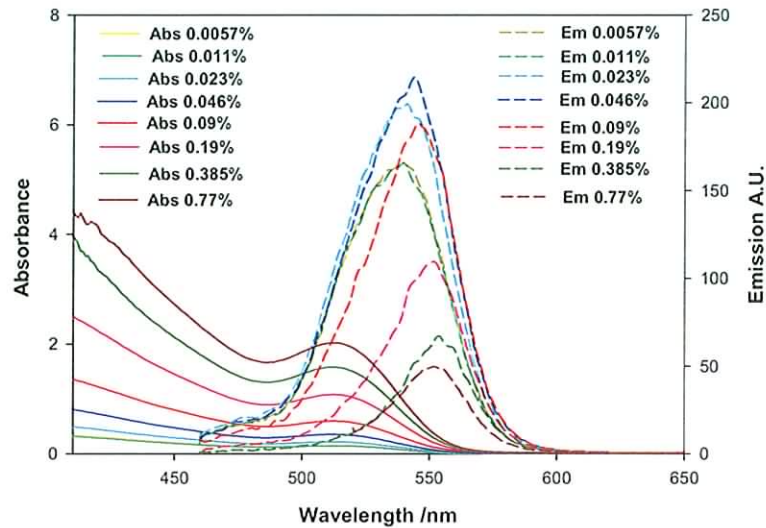
Figure 4.19: Absorbance and emission spectra of different concentrations of Evi 540B QDs in toluene solution

It can be seen that the emission intensity of the samples increased with increasing concentration until a peak was reached at 0.046%. After this the emission intensity decreased as the concentration rose. The rising absorbance that is seen caused re-absorption of emitted light and therefore a red-shift and reduction in the emission spectrum. Nine 4 x 4 x 0.3 cm QDSCs were fabricated containing this range of concentrations, a 0.046% right-angled triangular QDSC was also made. Following an initial set of I-V measurements that showed improved output with increased QD concentration, a 0.770% sample was added to the set. Each QDSC was made with both side and back air gaps and a white diffuse reflector was used as the rear reflector, the reasons for this mirror configuration are given in chapter 5. Details of each QDSC can be seen in table 4.4.

Table 4.4: Details and photographs of QDSC 5 samples

Sample Number	QD conc. Mass-Vol %	Photograph	Sample Number	QD conc. Mass-Vol %	Photograph
5.1	0		5.6	0.090	
5.2	0.005		5.7	0.190	
5.3	0.011		5.8	0.385	
5.4	0.023		5.9	0.770	
5.5	0.046		5.10	0.046	

The surface area of each QDSC varied slightly due to the formation of air bubbles at the exposed upper surface during curing. They were caused by shrinkage of the epoxy resin and were removed by grinding of the QDSC plate to a point below the air bubble. The performance of the plates was analysed in terms of power per cm^2 to eliminate the effect caused by size variation. The I-V and power curves are shown in figures 4.20 and 4.21.
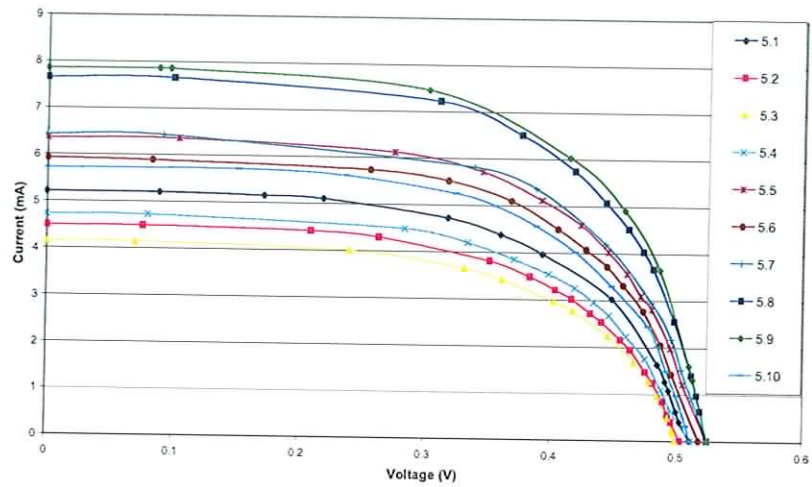
Figure 4.20: I-V curves for QDSC 5 samples
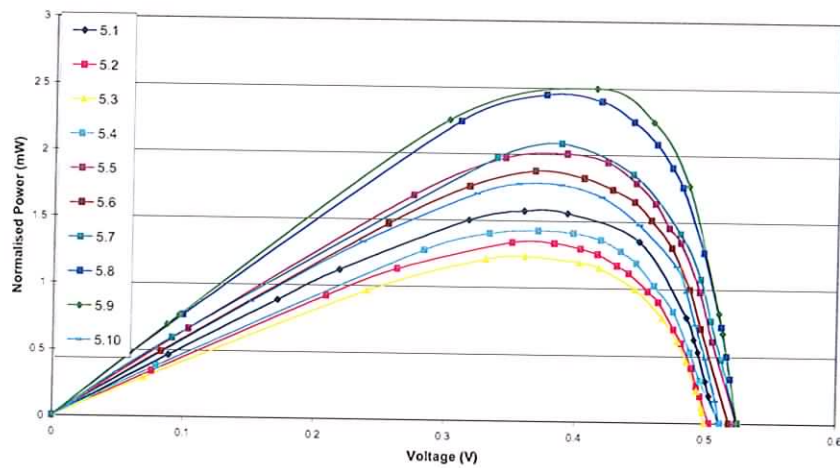
Figure 4.21: Power curves for QDSC 5 samples

Figures 4.20 and 4.21 show how the three lowest concentrations did not perform better than the reference sample (5.1). All QDSCs show an increase in output with increasing concentration except for QDSC 5.5, which performs almost as well as QDSC 5.7. The QDSC with the highest output is sample 5.9 containing the highest concentration of QDs (*Rowan et al 2006b*). The power maximum values, power/cm^2 and concentration factors are shown in table 4.5.

Table 4.5: Results of electrical characterisation of QDSC 5 samples

Sample Number	QD conc. % (m/v)	P_{max} (mW)	Power Density (mW/cm²)	Conc. Factor
PV cell	-	5.86	4.88	-
5.1	0	1.58	0.132	0.27
5.2	0.005	1.34	0.093	0.23
5.3	0.011	1.23	0.087	0.21
5.4	0.023	1.44	0.102	0.25
5.5	0.046	2.01	0.144	0.34
5.6	0.090	1.88	0.134	0.32
5.7	0.190	2.07	0.148	0.35
5.8	0.385	2.46	0.181	0.42
5.9	0.770	2.49	0.173	0.42
5.10	0.046	1.77	0.412	0.30

It is interesting to note the performance of the triangular QDSC (5.10) containing 0.046% QDs. It has an area less than one third the size of the rectangular QDSCs and therefore contained the equivalent amount of QDs as a 0.015% square QDSC. Since it produced a higher output than QDSCs 5.3 and 5.4 (0.011% and 0.023%), it can be deduced that it performed better than a rectangular QDSC containing 0.015% QDs. This implies that triangular geometries could be superior to rectangular QDSCs. This is supported by the power/cm² values, the triangular QDSC (5.10) has a value of 0.412 mW/cm², this is more than double the highest achieved by the rectangular QDSCs (0.173 mW/cm² for QDSC 5.9). In triangular systems the number of sides is reduced therefore reflection losses at the side mirrors are minimised. This geometry was investigated further and the results are shown in the next chapter. Figure 4.22 shows the power maximum values of each QDSC.

132
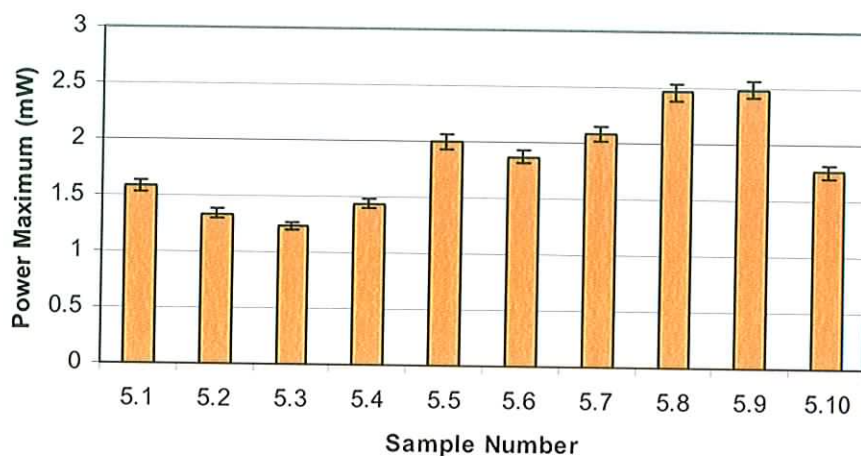
Figure 4.22: Power maximum values of QDSC 5 samples

The general trend indicates that there is an overall rise in efficiency as QD concentration increases (from sample 5.2 up to sample 5.9). QDSCs containing higher QD concentrations showed visible clusters of QD material (see figure 4.23). The absorption spectra of the plates are shown in figure 4.24.

(a)   (b)
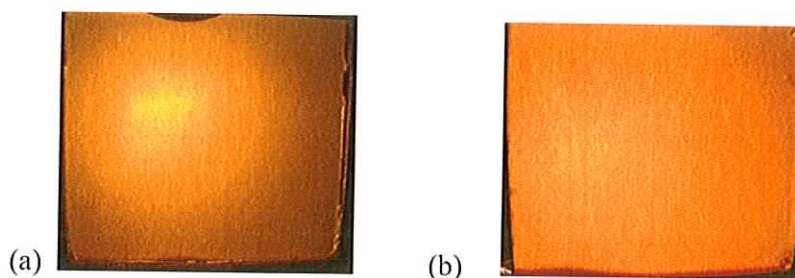
Figure 4.23: QD clusters (a) QDSC 5.7 and (b) QDSC 5.8

133
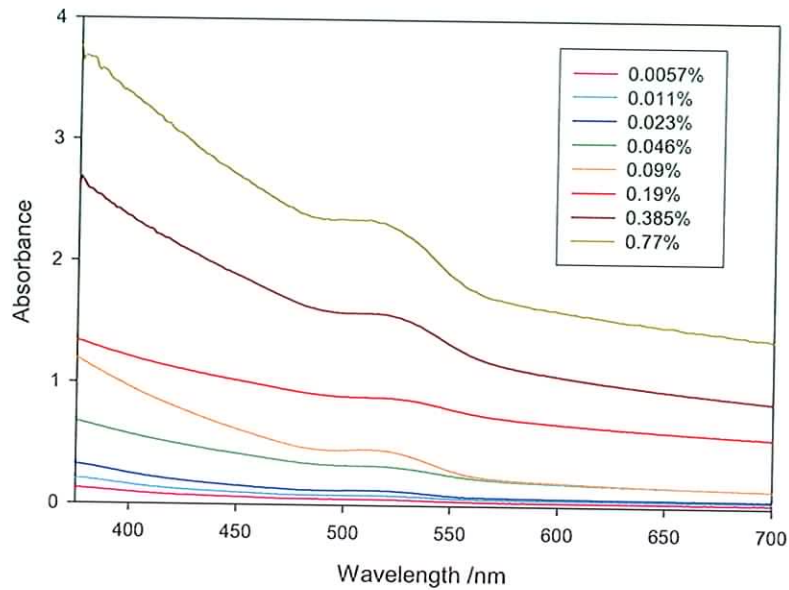
Figure 4.24: Absorbance spectra of QDSC 5 plates

It is clear from figure 4.24 that as the QD concentration increases, there is an increasing wavelength dependant background absorbance. This type of background is characteristic of scattered light and indicates that clusters of QD material are dispersing incident radiation. Therefore scattered light is making a contribution to the efficiency of the QDSCs of higher QD concentration.

4.4 Conclusions

In this chapter the refinement of QDSC fabrication and characterisation techniques were described. Oven curing was found to cause cloudiness in the epoxy resin, so oven curing was omitted from future samples. It was decided to remove the plates from their moulds

due to flaking of the reflective material and to reduce absorption of incident light by the mould plates.

The highest efficiency of the QDSC 4 samples was achieved by the QDSC containing the lowest concentration of QDs, it had a concentration factor of 0.116. The ray trace model provided an indication of the QY of the Nan488C QDs in the QDSC 4 plates. A QY value with an upper limit of 10% explains the low concentration factors achieved.

A higher power output than the PV cell facing the light source was not achieved i.e. there was no concentration factor above 1. The highest concentration factors in QDSC 5 were obtained with the higher concentrations of Evi540B QDs (0.05% (m/v) and 0.1% (m/v)). The concentration factor was 0.42 for both samples.

The highest power density (mW/cm^2) was achieved by the triangular QDSC in QDSC 5. It also produced a higher output than a rectangular QDSC containing an equal mass of QDs would have. This prompted a further investigation into triangular geometries. This is discussed in chapter five along with circular geometries and other aspects of QDSC design.

References:

ASTM E 892, Table2, American Society for Testing and Materials www.astm.org

Friedman, P.S., (1981), Luminescent Solar Concentrators, *Optical Engineering*, Vol.20, No.6, pp. 887-892.

Heidler, K., (1981), Efficiency and concentration ratio measurements of fluorescent solar concentrators using a xenon measurement system, *Applied Optics* Vol. 20, No. 5, pp. 773-777.

Heidler, K., Goetzberger, A., Wittwer, V., (1982), Fluorescent planar concentrator (FPC) Monte-Carlo Computer model limit efficiency and latest experimental results, *Proceedings of Photovoltaic Solar Energy Conference; Proceedings of the Fourth International Conference, Stresa, Italy, May 10-14, pp. 682-686*

IEA (2006) www.iea-pvps.org/pv/glossary.htm#STC

Kennedy, M., Rowan, B., McCormack, S.J., Doran, J., Norton, B.,(2007) Modelling of a Quantum Dot Solar Concentrator and comparison with fabricated devices, *Proceedings of 3rd Photovoltaic Science Application and Technology (PVSAT) Conference and Exhibition 28 – 30 March, Durham University, Durham.*

Kondepudi, R., Srinivasan, S., (1990), Performance evaluation of a luminescent solar concentrator with a liquid polymer matrix, *Indian journal of pure and applied physics*, Vol. 28, pp. 334-337.

Mansour, A.F., Salem, A.L., El-Sayed, N.M., Bassyouni, A.H., (1998), Spectroscopy, Photostability and Optical efficiency of luminescent solar concentrators, *Applied Solar Energy*, Vol. 34, No.3, pp. 55-62

Partain, L.D., (1995), *Solar cells and their applications*, Wiley Interscience.

Reisfeld, R., Shamrakov, D., Jorgensen, C., (1994) Photostable solar concentrators based on fluorescent glass films, Solar energy materials and solar cells, Vol. 33, pp. 417-427.

Roncali, J., Garnier, F., (1984) Photon-transport properties of luminescent solar concentrators:analysis and optimization, *Applied Optics*, Vol. 23, No.16, pp. 2809-2817.

Rowan, B. C., Gallagher, S. J., Doran, J. D., Norton, B., (2006 a), Performance Evaluation of Small-Scale Quantum Dot Solar Concentrators with different Quantum Dot densities, *Proceedings of the 2ⁿᵈ International Renewable Energy in Maritime Climates Conference, Dublin, Ireland, April, pp. 279-284.*

Rowan, B. C., Gallagher, S. J., Doran, J. D., Norton, B., (2006 b), Indoor characterisation of small-scale quantum dot solar concentrators of various geometries and QD

concentrations, *Proceedings of the 21st European Photovoltaic Solar Energy Conference and Exhibition, Sept 2006, Dresden, Germany, CD-ROM.*

Salem, A.I., Mansour, A.F., El-Sayed, N.M., Bassyouni, A.H., (2000), Outdoor testing and solar simulation for oxazine 750 laser dye luminescent solar concentrator, *Renewable Energy*, Vol. 20, pp. 95-107.

Sholin, V., Olson, J.D., Carter, S.A., (2007), Semiconducting polymers and quantum dots in luminescent solar concentrators for solar energy harvesting. *Journal of Applied Physics*, Vol. 101, pp. 123114-1- 123114-9.

Wittwer, V., Heidler, K., Zastrow, A., Goetzberger, A., (1981), Theory of Fluorescent Planar concentrators and experimental results, *Journal of luminescence*, Vol. 24/25, pp. 873-876.

Wittwer, V.,Stahl, W., Goetzberger, A., (1984), Fluorescent Planar concentrators, *Solar Energy Materials*, Vol. 11, pp. 187-197.

Zastrow, A., Wilson, H.R., Heidler, K., Wittwer, V., Goetzberger, A., (1984), Improvement of efficiency and stability of fluorescent planar concentrators (FPCs). First results from a 1m2 test collector system, Proceedings of the Fifth International Conference, Athens, Greece, October 17-21, pp. 202-207.

138

Chapter 5

New Directions for Quantum Dot Solar

Concentrator Development

5.0 Introduction

This chapter explores various aspects of system design and their effect on system losses with the aim of minimizing their effects. The factors affecting QDSC efficiency that were investigated in this chapter are outlined below:

o **Reflective Materials**

Critical cone losses account for approximately 25.5% of incident light being lost in a system with a refractive index of 1.5 *(Goetzberger and Wittwer 1979)*. Specular reflection off the back mirror in a QDSC system could account for a large percentage of this loss. This effect could be minimised by using a diffuse reflector to reflect light isotropically thereby increasing the possibility of the light striking the plate-air boundary at an angle outside the critical cone. This theory is investigated in section 5.1.

o **Reflection from PV cell**

In order to minimise reflection from the air-semiconductor interface it was necessary to use a material with a similar refractive index to couple the light efficiently onto the PV cell. Silicon oil was identified as a suitable material for optical matching. A comparative study shows that the use of silicon oil doubled the electrical efficiency in most cases, this is shown in section 5.2.

o **QDSC Geometry**

The aim in QDSC design is to construct a system that produces the highest possible power output while keeping material costs low. One way of altering costs and efficiencies is through utilizing different QDSC geometries. Initial QDSC systems were quadratic in shape but the optimum configuration could involve alternative geometries. Smaller geometries have the potential to minimise system costs and the pathlength of light to the PV edge.

A range of different sized QDSC geometries were fabricated and electrically characterized. The results were compared to those from a ray trace model (section 5.3). In addition to varying plate geometry, plates of different thickness were compared.

o **Utilisation of the solar spectrum**

It is desirable to have a QDSC system with a broad absorption spectrum to utilize as much of the solar spectrum as possible. One of the advantages QDs have over fluorescent dyes is

their broad absorption spectrum. Near Infrared (NIR) QDs are investigated due to their broad absorption and long emission wavelengths. Following this, mixing QDs with different absorption features together in a single solution is investigated.

5.1 Comparison of reflective materials (QDSC 6)

Two rectangular QDSC plates were fabricated for a comparison of different reflective materials and to investigate the potential benefits of side air gaps. An air gap provides another refractive index boundary for total internal reflection to occur thereby increasing the amount of light trapped inside the plate.

Two 4 x 3.5 x 0.3 cm QDSCs, both containing 0.0125% (m/v) concentration of Nan488C QDS were made, QDSC 6.1 and 6.2 are presented in figure 5.1.

(a)   (b)
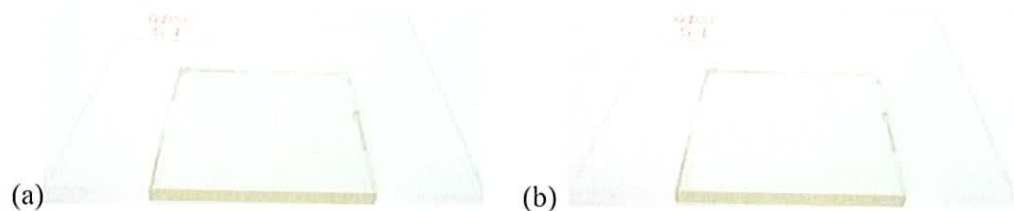
Figure 5.1: (a) QDSC 6.1 without side air gaps (b) QDSC 6.2with side air gaps

QDSC 6.1 was cast into a mould with reflective material attached around the moulds inner edges. The QD mixture then cured against the reflective material leaving no air gap between the QD plate and the edge mirrors. QDSC 6.2 was cast into a mould without reflective material attached and the QD plate was fully removed from the mould once cured. The plate was then positioned inside the mould plate with reflective material attached, providing edge mirrors with an air gap present. The electrical output of each

system was compared. Since neither of the QDSCs had back mirrors attached it was possible to compare a number of different reflective materials. The materials investigated are shown in table 5.1.

Table 5.1: Reflective materials investigated with QDSC 6.1 and 6.2

Number	Reflective Material
R1	Mirrored Acrylic
R2	Deposited Aluminium
R3	Reflective foil
R4	White diffuse Reflector
R5	Black Absorber
R6	Aluminium foil
R7	Matt Aluminium foil

R2 (deposited aluminium) was evaporated onto a sheet of acrylic using a 305 Edwards Evaporator, the other materials were available commercially. Each of the materials were measured with QDSC 6.1 and QDSC 6.2, by securing the material behind the QD plate and taking I-V measurements. Figure 5.2 shows the power maximum values for each measurement.
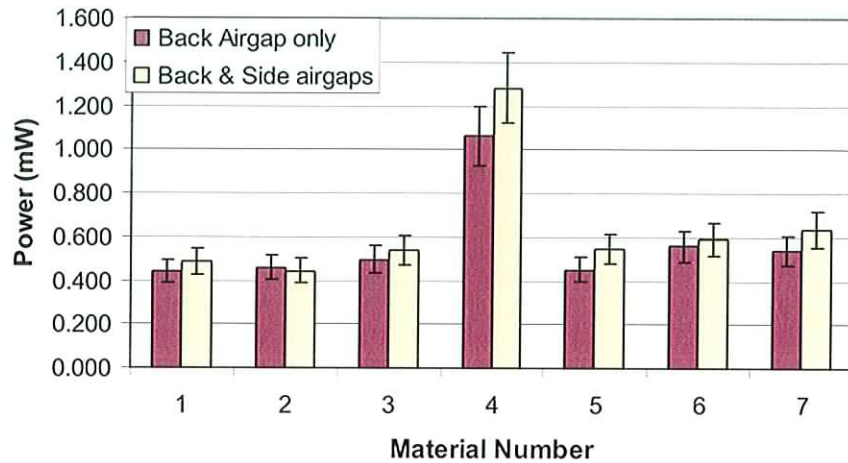
Figure 5.2: Power maximum values for QDSC 6.1 and QDSC 6.2 measured with different back reflectors

It is clear in figure 5.2 that the white diffuse reflector provided the optimum power output (*Rowan et al 2006*), by approximately a factor of 2, both with and without side air gaps. Diffuse reflectors have been seen to cause significant improvements in the efficiency of LSCs in the past (*Keil 1970, Filloux et al 1983, Lifante et al 1983, Roncali and Garnier 1984 (a), Mugnier et al 1987*). This improvement is due to two mechanisms; firstly, light that is lost through the critical cone can be recovered and secondly, reflected rays with wide angles of incidence will be refracted into the plate at an angle close to the critical angle for total internal reflection and can therefore reach the PV cell directly *(Roncali and Garnier 1984a).*

It is interesting to note the performance of the black absorber (R5) whereby its power output is comparable to the other reflective materials. This indicates that the direct reflectors could be sending a large percentage of incident light straight back out of the escape cone leading to a trapping efficiency similar to that of a black absorbing material.

143

With regards to the side air gaps, it cannot be said within experimental error that they invariably offer an advantage in each case. Although, for R4, R5 and R7 the side air gaps do result in a higher power output.

5.2 Optical Matching with silicon oil

In order to give an indication of the effect of using silicon oil for optical matching, I-V measurements for the QDSC 7 samples of different geometries (described in section 5.3) were carried out with and without silicon oil. The power maximum values for each sample are shown in figure 5.3.
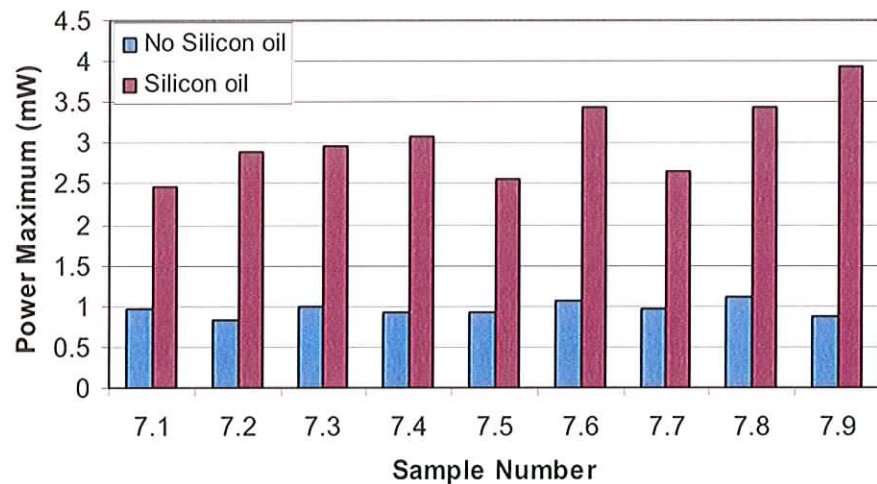
Figure 5.3: Power maximum values for QDSC 7 sample with and without silicon oil

It is clear that the optical matching had a significant effect on the electrical output of the QDSC systems. On average the power maximum value was 3.2 times higher when the silicon oil was used. This indicated that reflection from the PV cell surface caused a

144

considerable loss when there was no medium to couple light from the plate to the PV cell. Based on these findings, silicon oil was used in all measurements from QDSC 7 onwards.

5.3 Investigation of various geometries (QDSC7)

To investigate the effect of shape and size on concentrator efficiency, four different sized quadratic, two triangular and three circular QDSCs of various diameters were fabricated. Each one was cast with a 0.082% (m/v) concentration of Evi600B QDs. The absorption and emission characteristics plotted with the spectral response of a typical silicon PV cell is shown in figure 5.4.
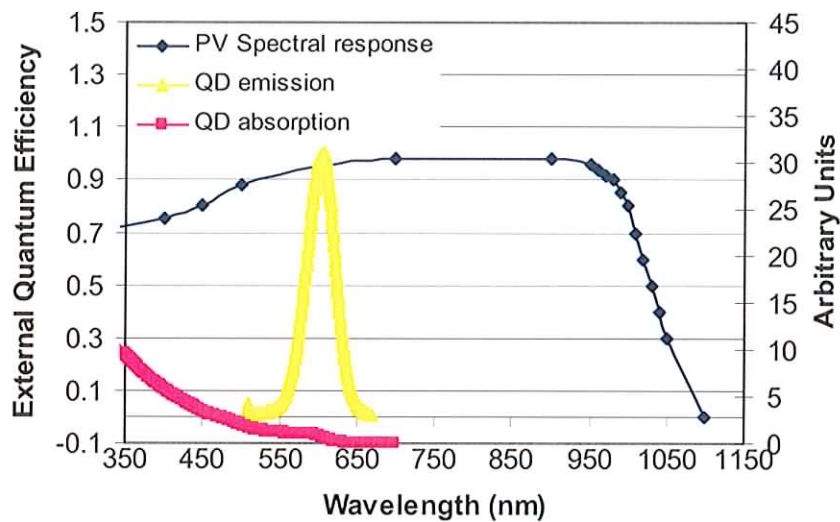
Figure 5.4: Absorbance and emission of Evi600B QDs and the spectral response of a typical PV cell

The emission wavelength of these QDs was 600 nm, a longer wavelength than the QDs used in the previous batch of QDSCs and therefore closer to the peak efficiency of a typical

145

silicon PV cell. They were used to further investigate the advantages of using larger QDs with longer emission wavelengths. Details and photographs of the QDSCs produced are shown in table 5.2.

Table 5.2: Details and Photographs of QDSC 7 samples

Sample Number	Shape	Photograph	Sample Number	Shape	Photograph
7.1	Square		7.6	Isoceles Triangle	
7.2	Square		7.7	Semicircle	
7.3	Rectangle		7.8	Circle D= 6 cm	
7.4	Rectangle		7.9	Circle D= 8 cm	
7.5	Right-angled triangle				

The samples were cast in three separate batches due to the large volume of QD/epoxy mixture required. Two squares of equal size were cast in separate batches to examine the reproducibility of QDSC samples and the large circle was cast individually due to its large volume. A variation in sample characteristics is evident from the absorbance spectra of the plates as seen in figure 5.5. While the same procedure was used each time, it is evident that each batch produced samples with slightly different absorption characteristics, although it is largely due to variations in scattering effects rather than QD characteristics.

146
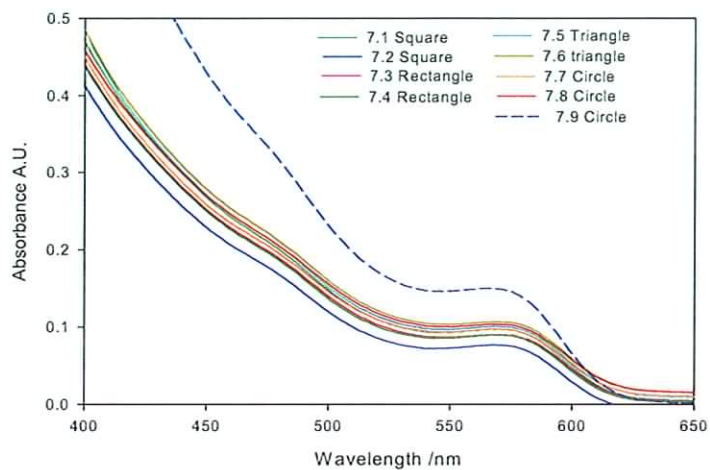
Figure 5.5: Absorbance spectra of QDSC 7 QDSC plates

Electrical characterisation was carried out using a PV cell with 10.5% efficiency. A rectangular sample without QDs was used as a reference, and it is represented by the red dotted line in figure 5.6.
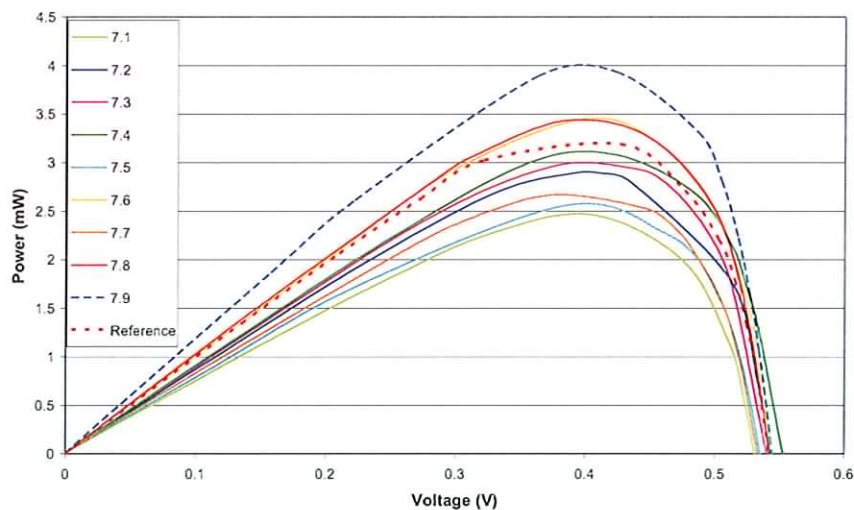
Figure 5.6: Power curves for QDSC 7

The power curves show that only three samples, 7.6, 7.8 and 7.9 exceeded the output of the reference sample. Figure 5.7 shows the power maximum values for each sample with error bars included.
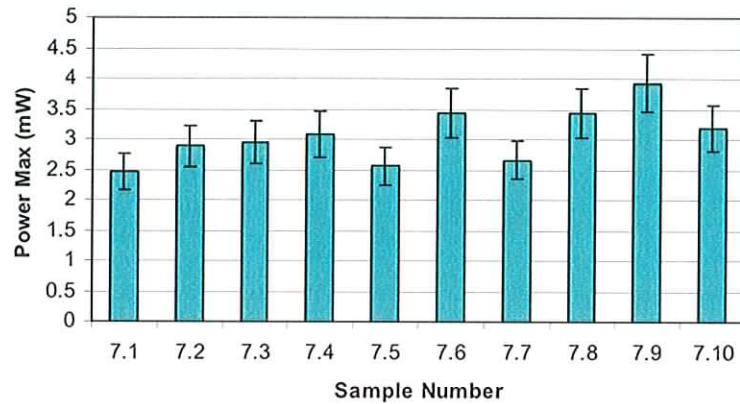
Figure 5.7: Power maximum values for QDSC 7 samples

Within the error margins (+/- 12.5%), it appeared that there was minor disparity in efficiency between the samples. Due to the broad range of sample sizes it was important to consider the power/cm^2 for each sample as shown in Table 5.3.

Table 5.3: Power maximum, Area, Power/cm^2 and Concentration factors for QDSC7 samples

Sample Number	Shape	Power max (mW)	Area (cm^2)	Power/cm^2	Concentration Factor
PV cell	-	12.60	1.2	10.5	-
7.1	Square 1	2.46	14.43	0.17	0.20
7.2	Square 2	2.89	14.04	0.21	0.23
7.3	Rectangle1	2.95	11.31	0.26	0.23
7.4	Rectangle 2	3.08	7.99	0.39	0.24
7.5	Triangle 1	2.56	3.9	**0.66**	0.20
7.6	Triangle 2	3.43	6.24	0.55	0.27
7.7	Circle Diameter 4cm	2.66	6.28	0.42	0.21
7.8	Circle Diameter 6cm	3.43	25.58	0.13	0.27
7.9	Circle Diameter 8cm	**3.93**	48	0.08	**0.31**
Ref	Square Epoxy	3.19	12.09	0.26	0.25

In terms of power per unit area, considerable variations occurred between the samples. The large circular plate (7.9) had the lowest value (0.08mW/cm^2) and the right-angled triangle, (7.5) had the highest value (0.66 mW/cm^2) followed by the isosceles triangle (7.6) (0.55 mW/cm^2)(*Rowan et al 2007a/2007b*). It can be concluded that in terms of production costs and output per unit area, triangular QDSCs were the most efficient. The measured concentration factors of the quadratic, triangular and circular samples are compared with those predicted by the ray trace model in figures 5.8, 5.9 and 5.10 respectively.
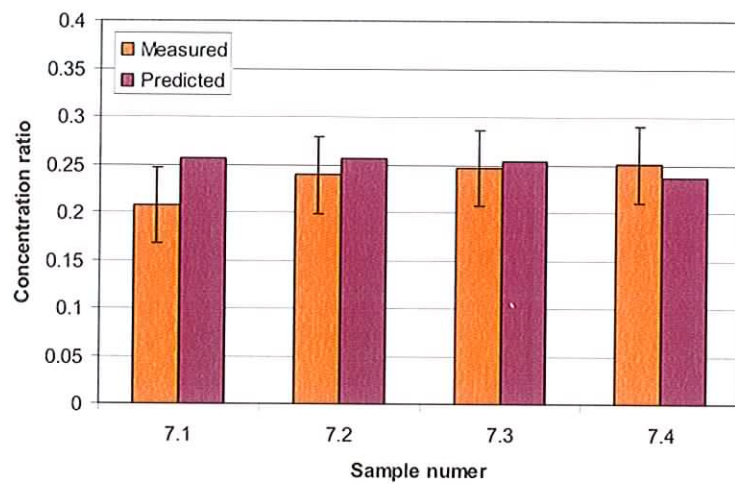
Figure 5.8: Measured and predicted concentration ratios for four quadratic QDSC 7 samples, where 7.1 and 7.2 are 4 x 3.5 cm, 7.3 is 4 x 3 cm and 7.4 is 4 x 2 cm (*Kennedy et al 2007*)

For the quadratic QDSCs of varying length, the ray trace model predicted a small decrease in concentration ratio with decreasing sample length due to less light being absorbed by the plate, but the magnitude of the decrease predicted is within experimental uncertainties.

149

It appears that there is minimal advantage in increasing sample length in quadratic samples, considering that sample 7.4 is almost half the size of samples 7.1 and 7.2 and the concentration factors are very similar. In quadratic samples, increases in length involve light travelling from further distances to the PV cell, allowing light to be lost due to re-absorption as it traverses the QDSC plate. The measured and predicted concentration ratios for the triangular samples are shown in figure 5.9.
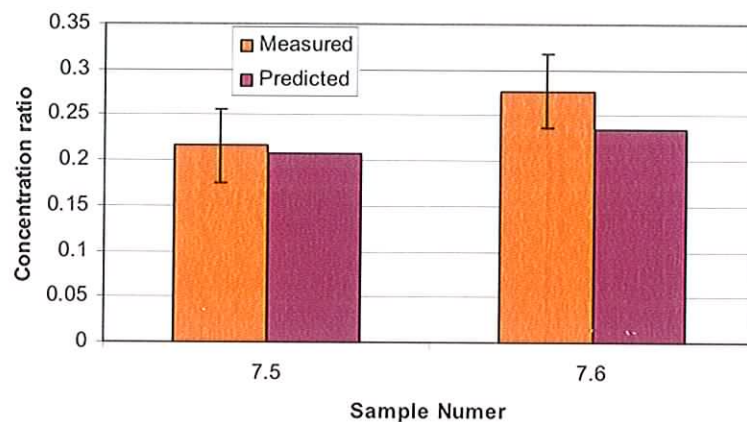
Figure 5.9: Measured and predicted concentration ratios for two triangular QDSC 7 samples, where 7.5 = rectangular triangle and 7.6= isosceles triangle

Sample 7.6 is longer and has a greater area than sample 7.5. The model predicts a higher concentration ratio for the larger triangle and this is in agreement with the measured results within a small margin of error, as shown in figure 5.9. Increasing the area of triangular samples appears to be beneficial. Unlike quadratic samples, when triangular plates are increased in size, a large amount of the light absorbed by the sample is close to the PV cell, this keeps re-absorption losses low. The measured and predicted concentration ratios for the circular samples are shown in figure 5.10.

150
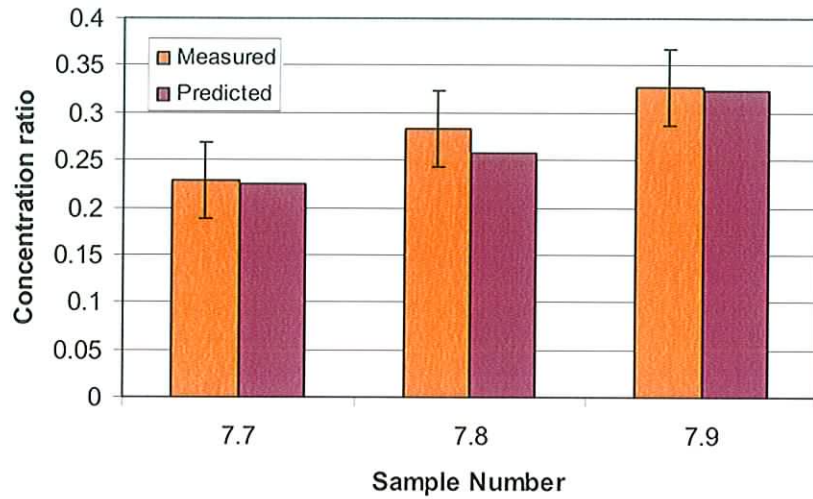
Figure 5.10: Measured and predicted concentration ratios for three circular QDSC 7 samples, where 7.7=Circle d = 4 cm, 7.8= Circle d= 6 cm, 7.9= Circle d= 8 cm

Higher concentration ratios were predicted with increasing circle diameter and this is supported by the measured results. As with the triangular samples, large circular samples maintain a large sample area close to the PV cell, keeping re-absorption and matrix absorption losses relatively low.

Overall there was good agreement between the measured and predicted data. The largest circular device produced the highest concentration ratio (0.31) and power maximum (3.93 mW).

5.4 Variation of Plate Thickness (QDSC 8)

Geometric Gain is defined as the ratio of the surface area of a QDSC plate to the area of the PV edge (see equation 4.2). It can be increased by increasing the surface area of a plate or by decreasing the area of the PV edge. The ray trace model predicts, for plates of varying thickness containing equal QD concentrations that increases in concentration factors of 19% could be achieved by decreasing plate thickness from 0.3 cm to 0.2 cm, as shown in figure 5.11.
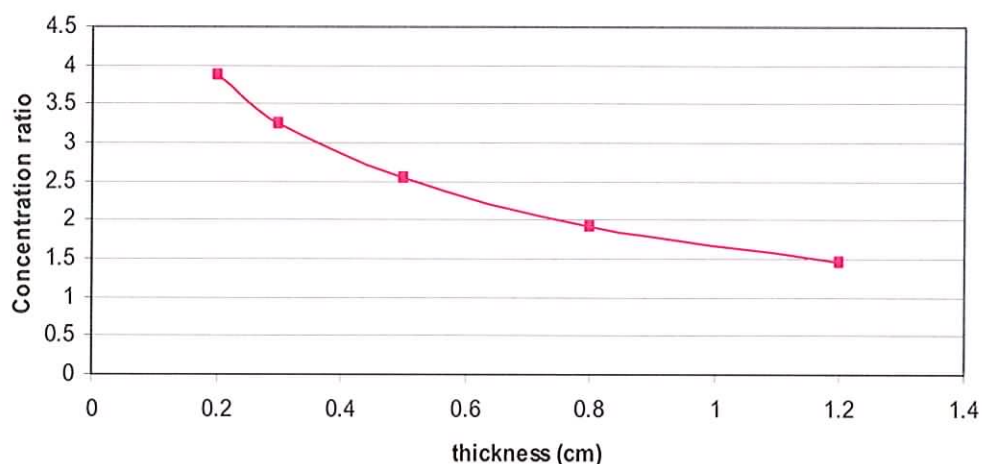
Figure 5.11: Predicted concentration ratios for plates of varying thickness

Three triangular QDSCs of varying thickness were fabricated containing equal QD concentrations. Plates of 0.30 cm, 0.20 cm and 0.15 cm thickness were produced containing 0.05% (m/v) of Nan 488B. Nan488B QDs had been established to be the most efficient QDs available at this time, as outlined in section 3.2.2. Two epoxy plates, 0.3 cm and 0.15

152

cm thick were also measured as reference samples. Details and photographs of each sample are shown in table 5.4.

Table 5.4: Details and photographs of QDSC 8 samples

Sample Number	Plate thickness (cm)	QD conc. % (m/v)	Geometric Gain	Photograph
8.1	0.30	0.05	3.25	
8.2	0.20	0.05	4.80	
8.3	0.15	0.05	6.50	
8.4	0.30	0	3.25	
8.5	0.15	0	6.50	

Each sample was electrically characterised using a 0.30 cm PV cell with 6.5% efficiency and silicon oil for optical matching. The 0.15 cm and 0.20 cm plates were positioned in the center of the PV cell during measurements. Figure 5.12 shows the power curves for the three QDSC plates and figure 5.13 shows the power curves for the two reference samples.
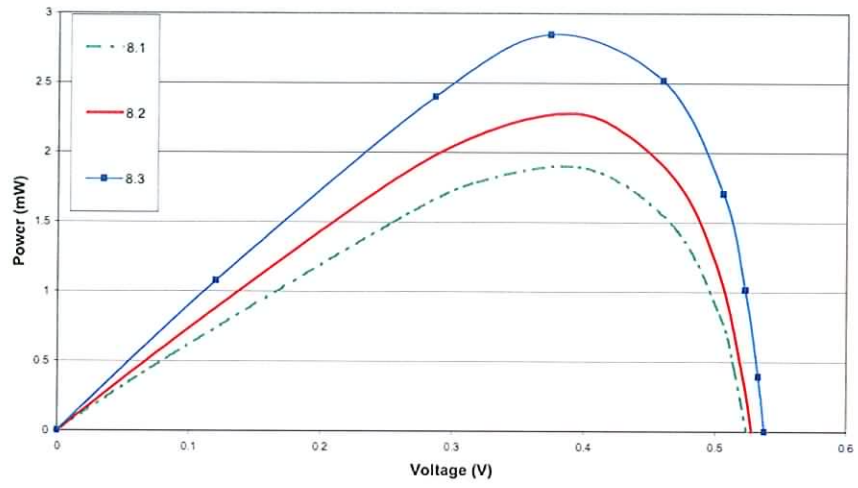
Figure 5.12: Power curves for QDSC 8 samples containing Nan488B QDs
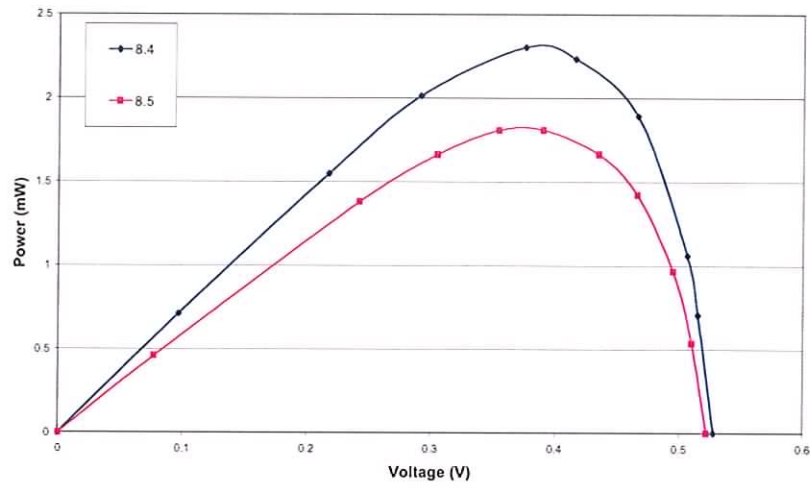
Figure 5.13: Power curves for QDSC 8.4 and 8.5 epoxy samples

As is clear from figure 5.12, the electrical output increased with decreasing plate thickness for the QDSC samples and the same trend can be seen with the epoxy reference samples in figure 5.13. The details and results are shown in table 5.5.

Table 5.5: Results of electrical characterisation of QDSC 8 samples

Sample Number	QD conc. %	Plate thickness (cm)	Geometric Gain	Power Maximum (mW)	Concentration Factor
PV cell	-	0.30	-	8.7	-
8.1	0.05	0.30	3.25	1.8	0.22
8.2	0.05	0.20	4.80	2.3	0.26
8.3	0.05	0.15	6.50	2.8	0.33
8.4	0	0.30	3.25	1.8	0.21
8.5	0	0.15	6.50	2.3	0.26

An 18% increase in concentration factor was achieved with a QDSC plate thickness of 0.20 cm (8.2) compared to 0.30 cm (8.1), which is very close to the 19% predicted by the ray trace model. There was a 50% increase in concentration factor with a QDSC plate thickness of 0.15 cm (8.3) compared to 0.30 cm (8.1). This effect may be caused by a reduction in re-absorption losses throughout the plate thickness. The use of a 0.30 cm PV cell to characterise the thinner plates would have resulted in a loss due to areas of the cell not being utilised. If PV cells of the same thickness as each plate were used for each thickness, a further improvement would be expected. An increase in concentration factor resulting from reduced plate thickness has been previously observed (*Roncali and Garnier 1984b*). The effect was significant and has positive implications towards cost of production of devices.

5.5 Investigation of Near Infrared QDs (QDSC9)

Near Infrared (NIR) QDs offer the advantage of having a broad absorption spectrum allowing increased utilization of the solar spectrum. In addition to this, a process known as multiple exciton generation (MEG) has been observed in Lead Selenide (PbSe) QDs. When

photons that are at two to three times the band gap are absorbed by a QD, they can lead to the production of multiple electron-hole pairs, resulting in QY values well above 100% (up to 300%)(*Schaller and Kilmov 2004, Hanna et al 2005*).

To investigate the performance of NIR QDs in QDSC devices Lead Sulphide (PbS) QDs (Evi900) were purchased with an emission wavelength of 900 nm. This corresponds to the area of peak spectral response of a typical silicon PV cell (see figure 5.4). A 633 nm laser line was used to excite the QDs and a S.A. Labram 1B Raman Spectrometer was used to measure the emission spectrum, as illustrated in figure 5.14.
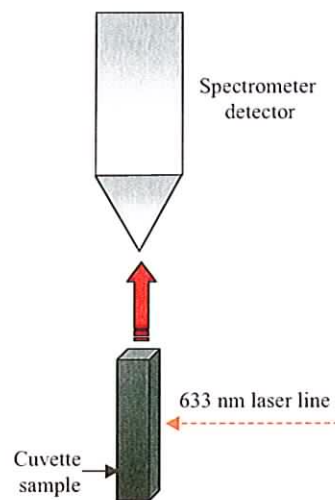
Figure 5.14: Emission measurement of Evi900 QDs using Raman Spectrometer

Figure 5.15 shows the absorbance of the Evi900 QDs in solution and the emission spectra both in solution and after incorporation into epoxy resin. It is clear that resin encapsulation caused a significant blueshift of the emission peak. Due to a change in experimental setup for emission measurements it was not possible to compare with previous QD emission.
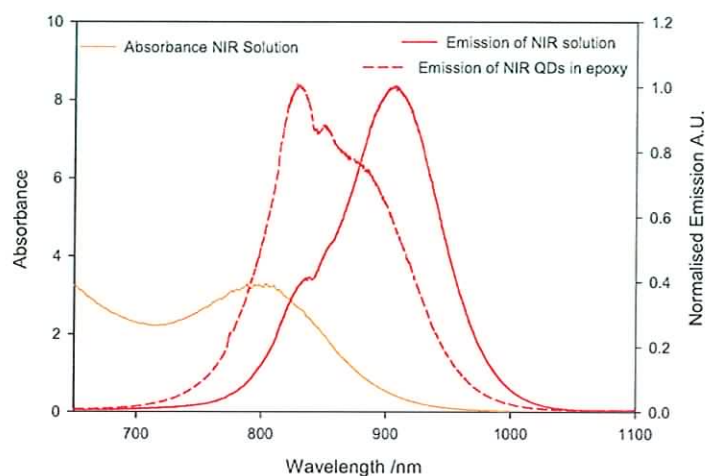
Figure 5.15: Absorption and emission spectra of Evi900 QDs

Seven 4 x 4 x 0.3 cm QDSC were fabricated, containing a range of concentrations of Evi900 QDs. Details of the QDSC plates produced are given in table 5.6.

Table 5.6: Details and photographs of QDSC 9 samples

Sample Number	QD conc. % (m/v)	Photograph	Sample Number	QD conc. % (m/v)	Photograph
9.1	0		9.5	0.0060	
9.2	0.0007		9.6	0.0125	
9.3	0.0015		9.7	0.0250	
9.4	0.0030		9.8	0.5000	

157

Electrical characterisation was carried out using a PV cell with 10.1% efficiency and the set-up described in section 4.2.2. The behavior of the samples under illumination was unusual, rapid variations in current readings from the ammeter occurred and made I-V measurement difficult. This effect increased with higher QD concentrations and was thought to be due to heating of the PV cell. Analysis of this effect was carried out by observing the changes in current over time while monitoring the temperature changes of the PV cell. Each sample was monitored for 20 minutes with short circuit current (I_{sc}) and temperature readings taken every 20 seconds. The results are shown in figure 5.16.
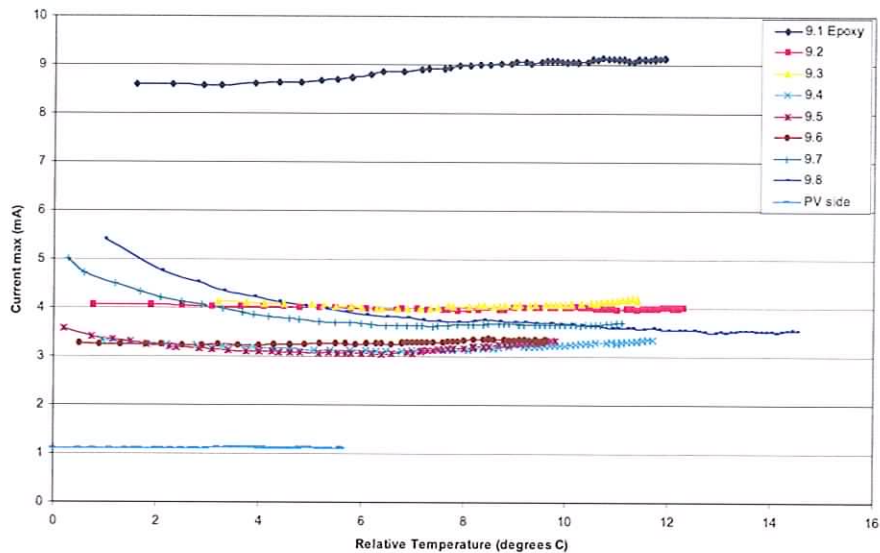
Figure 5.16: Temperature and Short circuit current (I_{sc}) readings for QDSC 9

It can be seen in figure 5.16 that there is no drop in the I_{sc} values of the epoxy reference sample (9.1) and for the two QDSCs containing the lower concentrations of Evi900 QDs (9.2 and 9.3). Following this, with increased QD concentration there is a clear drop in I_{sc} values within the first minute. This effect is intensified for the two samples containing the

highest concentrations of QDs. Samples 9.7 and 9.8 both start with I_{sc} values of 4.65mA and 5.51 mA, higher than samples 9.1 and 9.2 but both quickly fall to lower values of 3.91 mA and 3.94 mA when they have reached 2.1 °C and 6.1 °C respectively. QDSC 9.8 reaches the highest temperature of 14.5 °C, due to increased absorption by the QDs causing an increase in plate temperature. This measurement was carried out on a QDSC containing 0.025% (m/v) Evi540b QDs and current changes were not observed. Similar behavior has been reported for infrared laser dyes, decreasing QY with increasing temperature was observed while dyes with shorter emission wavelengths did not behave this way (*Zastrow et al 1981*).

Electrical measurements were taken for each QDSC after waiting for the current values to stabilise sufficiently. The power curves for each QDSC 9 sample are shown in figure 5.17 and the results are shown in table 5.7.
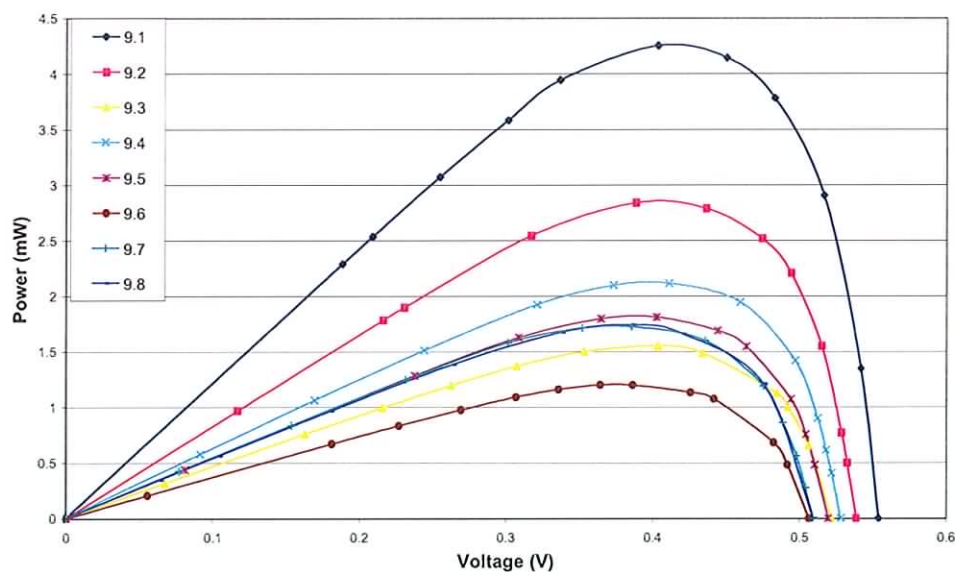
Figure 5.17: Power curves for QDSC 9 samples

Table 5.7: Power maximum, Power Density and concentration factors for QDSC 9

Sample Number	QD Conc. Mass-Volume%	Power Maximum (mW)	Power Density (mW/cm^2)	Concentration Factor
PV cell	-	12.5	10.42	-
9.1	0	4.25	0.32	0.34
9.2	0.0007	2.84	0.21	0.23
9.3	0.0015	1.55	0.12	0.12
9.4	0.0030	2.11	0.16	0.17
9.5	0.0060	1.81	0.14	0.14
9.6	0.0125	1.2	0.09	0.10
9.7	0.0250	1.72	0.13	0.14
9.8	0.0500	1.74	0.13	0.14

There is no clear trend in the results, making it difficult to draw a conclusion on the concentration dependence of the NIR QDs. It is clear from the results that none of the Evi900 QDSCs produced a higher power output than the reference sample. This indicated that the QY of the QDs was extremely low and therefore not suitable for this application. This is the same problem that existed for luminescent dyes; red and near infrared dyes displayed decreasing efficiency with increasing emission wavelength (*Zastrow et al 1981*). In the future, ideal QDSC devices will require NIR QDs due to their broad spectral absorption and the possibility of MEG but until higher QY values are achieved, their use in QDSCs is not feasible.

5.6 Mixing of Quantum Dots

The aim of this study was to investigate the possibility of expanding the absorption and emission spectra of QDs by mixing different types together. The two QD types used were Evi540 and Evi600, solutions of equal concentrations (0.16mg/ml) were measured in each case. The absorption, excitation and emission spectra of Evi540 are shown in figures 5.18.

The emission spectra that resulted from excitation at 450 nm and 545 nm are shown. It is clear that excitation wavelength does not affect the intensity or wavelength of the emission peak.
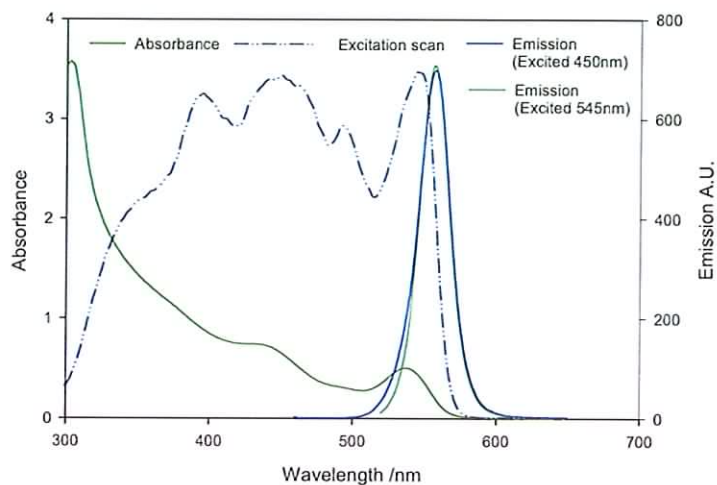
Figure 5.18: Absorbance, excitation and emission of 0.16 mg/ml solution of Evi540QDs
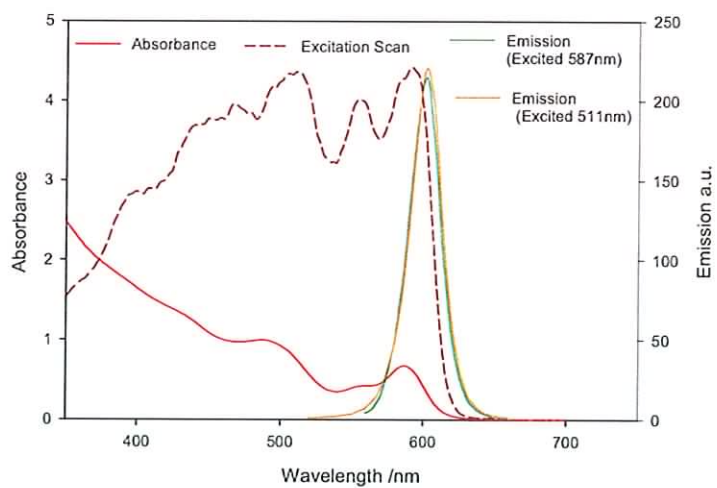
Figure 5.19: Absorbance, excitation and emission of 0.16 mg/ml solution of Evi600QDs

161

The absorbance, excitation and emission spectra of the Evi600 QDs are shown in figure 5.19. The solution was excited at two different wavelengths 587 nm and 511 nm, the resultant emission intensity is similar for both measurements.

A 0.16 mg/ml solution was prepared using equal amounts of Evi540 and Evi600 QDs. Upon mixing both QD types there were two possible outcomes. One is that the emission of the Evi540 QDs would provide increased excitation for the Evi600 QDs. The other is that the emission of the Evi540 QDs will be re-absorbed and lost due to imperfect QY of the Evi600 QDs. The absorbance, excitation and emission spectra are shown in figure 5.20.
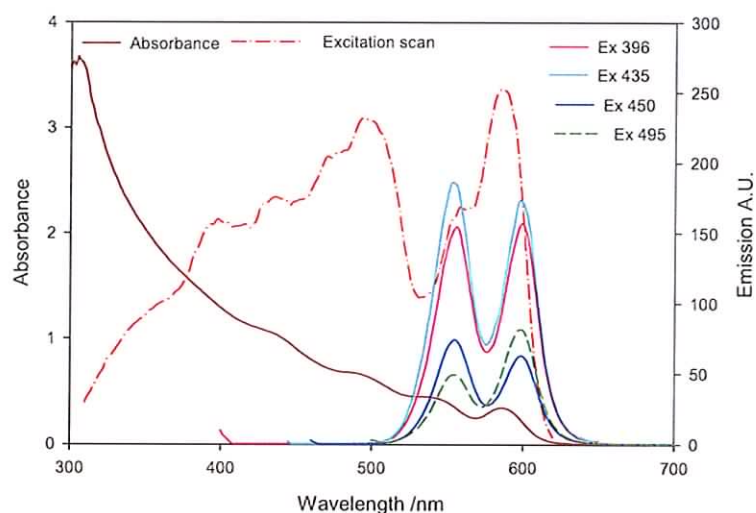
Figure 5.20: Absorbance, excitation and emission spectra of 0.16 mg/ml solution of Evi540 and Evi600 mixture

The QD mixture was excited at a number of wavelengths as shown in figure 5.20. The optimum emission intensity was achieved when the solution was exited at 435 nm. Excitation at shorter wavelengths resulted in higher emission intensity because both QDs were excited simultaneously. To establish whether mixing of the QDs resulted in increased

emission intensity, the integrated emission of the individual QDs was compared to that of the mixture. A value comprised of half of each of the emission intensities achieved by the individual solutions is included to determine if a loss due to re-absorption had occurred. The integrated emission values are shown in figure 5.21.
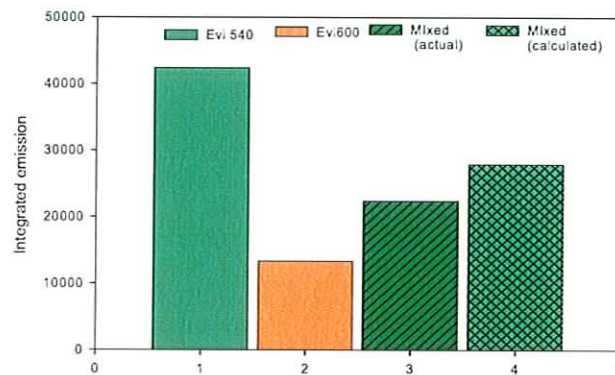
Figure 5.21: Integrated emission values for Evi540 (1), Evi600 (2), the QD mixture (3) and a calculated value for the QD mixture (4)

The integrated emission values indicate that re-absorption has occurred since the measured integrated emission is less than the calculated value. This is due to the Evi600 QDs having a lower QY than the Evi540 QDs as shown by their integrated emission values. The decrease in emission intensity could be acceptable if there was a sufficient increase in absorption, the absorption spectra are shown in figure 5.22.
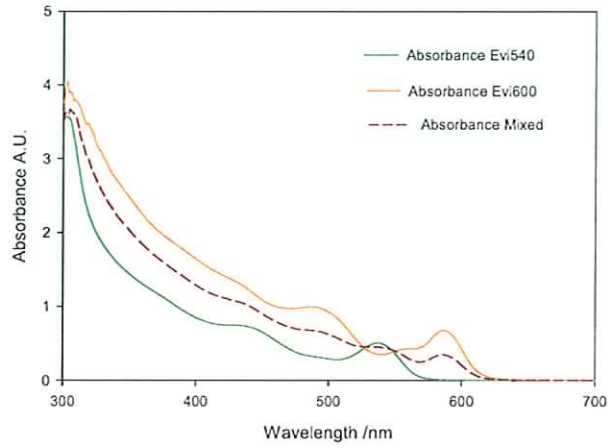
Figure 5.22: Absorption spectra of Evi540, Evi600 and the QD mixture.

From the absorption spectra it appears that there is no increase in absorbance when the QDs are mixed when compared to the absorbance of the Evi600 QD. To evaluate the amount of the solar spectrum that is absorbed by each sample the integrated values of the product of the absorbance values and the Air Mass (AM) 1.5 (*ASTM 2007*) solar spectrum intensity are shown in figure 5.23.
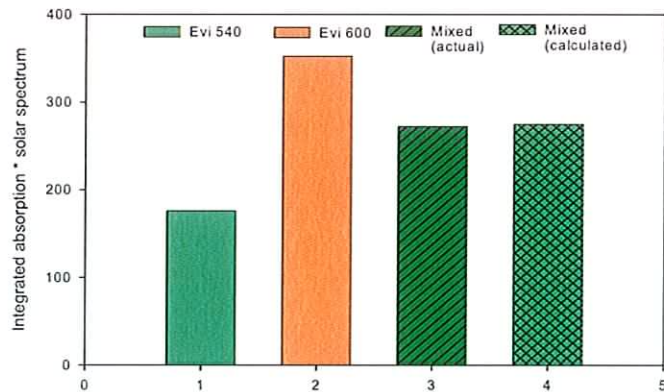
Figure 5.23: Integrated values for product of absorbance and AM1.5 solar spectrum

164

The results show good agreement between the calculated and measured absorbance values for the QD mixture indicating that no loss has occurred due to mixing the QDs. In terms of absorbance of the solar spectrum, the orange QDs alone absorb the highest amount, there does not appear to be advantage in mixing QDs in terms of absorbance or emission.

5.7 Conclusions

A comparison of reflective materials showed a white diffuse reflector increased electrical output by at least a factor of two. This increase is due to both recovery of light lost through the critical cone and reflecting light at wide angles to improve total internal reflection. This result is supported by previous work (*Roncali and Garnier 1984, Filloux et al 1983*).

The use of silicon oil between the QDSC edge and the PV cell was found to increase the electrical output by a factor of 3.2 on average. This indicates the amount of light that is trapped by total internal reflection at plastic to air interfaces and reflected off the PV cell.

An investigation into QDSC geometries was carried out comparing four different sized quadratic, two triangular and three circular systems. The highest concentration factor was produced by the large circular device (0.31), in agreement with the results predicted by the ray trace model (*Kennedy et al 2007b*). In terms of output per unit area, the right-angled triangle had the highest value (0.66 mW/cm^2) and the large circular device had the smallest values (0.08 mW/cm^2). If production costs were low then the large circular systems would be feasible but with high cost production, right-angled triangles would be preferable. Right-angled triangles were previously identified as the optimum LSC geometry (*Goetzberger*

and Gruebel 1977, Roncali and Garnier 1984b) and another group calculated that circular systems were the ideal LSC geometry (*Sidrach de Cardona et al 1985*).

Three QDSCs of different plate thickness and equal QD concentration were fabricated and their electrical outputs were compared. An 18% increase in concentration factor was achieved with a plate thickness of 0.20 cm compared to 0.30 cm and a 50% increase was achieved with the 0.15 cm plate. This improvement is possibly due to a reduction in path length through the sample leading to a reduction in re-absorption effects.

The use of NIR QDs was explored due to their broad absorption spectrum that could utilize a larger range of the solar spectrum. They were also interesting due to reports of MEG and QYs up to 300% (*Schaller and Kilmov 2004, Hanna et al 2005*). Seven QDSCs containing a range of concentrations of Evi900 QDs were fabricated and tested. Under illumination, the current readings varied over time and appeared to drop with increasing temperature. Electrical measurements revealed that the NIR QDSCs did not produce higher outputs than the epoxy reference sample, indicating that the QY of these QDs was extremely low. These results coupled with the unusual behaviour under illumination suggest that commercial NIR QDs are not suitable for use in QDSCs at this time. Due to their broad absorption and their potential for MEG, development of these QDs should lead to improved efficiencies making them suitable for this application.

Finally, mixing of different QD types was investigated as a way to utilise more of the solar spectrum. Evi540 and Evi600 QDs were measured individually and then combined in one solution. The results showed that re-absorption of emitted light occurred and resulted in a lower emission intensity than was calculated. The absorption range did not improve after mixing the QDs, the Evi600 QDs alone absorbed more than the QD mixture. There appeared to be no advantage in mixing QDs with different absorption and emission

166

features together in one sample. The idea of layers or stacks of plates containing different

QD types could be a better way of utilizing more of the solar spectrum.

References:

ASTM (2007) G173-03e1 Standard Tables for Reference Solar Spectral Irradiances: Direct Normal and Hemispherical on 37° Tilted Surface, *ASTM International.*

Filloux, A., Mugnier, J., Bourson, J., Valeur, B., (1983), Fluorescent solar concentrators using liquid solutions, *Revue de Physique Appliquee* , Vol.18, no.5, pp. 273-279.

Goetzberger, A., Witter, V., (1979), Fluorescent planar collector-concentrator for solar energy conversion, *Festkorperprobleme*, Vol XIX, pp. 427-450.

Hanna, M.C., Ellingson, R.J., Beard, M., Yu, P., Micic, O.I., Nizik, A.J., (2005), Quantum Dot Solar Cells: High Efficiency through Multiple Exciton Generation, *Proceedings of 2004 DOE Solar Energy Technologies Program Review Meeting, 25-28 October 2004, Denver, Colorado.*

Keil, G., (1970) Design principles of fluorescence radiation converters, *Nuclear Instruments and methods*, Vol. 87, pp. 111-123.

Kennedy, M., Rowan, B., McCormack, S.J., Doran, J., Norton, B., (2007a) Modelling of a Quantum Dot Solar Concentrator and comparison with fabricated devices, *Proceedings of 3rd Photovoltaic Science Application and Technology (PVSAT) Conference and Exhibition 28 – 30 March 2007, Durham University, Durham, pp.123-126.*

Kennedy, M., McCormack, S.J., Doran, J., Norton, B., (2007b) Modelling the effect of device geometry on concentration ratios of quantum dot solar concentrators, *Proceedings of ISES Solar world congress 2007, Beijing, China, September 18-21st 2007.*

Lifante, G., Cusso, F., Meseguer, F., Jaque, F., (1983) Luminescent solar concentrators as bifacial captors, *Solar Cells*, Vol. 8, pp. 355-360.

Mugnier, J., Dordet, J., Pouget, J., Valeur, B., (1987) A photometric approach of fluorescent solar concentrators, Role of diffuse reflectors and spectral sensitivity of solar cells, *Revue de Physique appliqué*, Vol. 22, pp. 89-100.

Roncali, J., Garnier, F., (1984a) New Luminescent back reflectors for the improvement of the spectral response and efficiency of luminescent solar concentrators, *Solar Cells*, Vol. 13, pp. 133-143.

Roncali, J., Garnier, F., (1984b) Photon-transport properties of luminescent solar concentrators:analysis and optimization, *Applied Optics*, Vol. 23, No. 16, pp. 2809-2817

Rowan, B. C., Gallagher, S. J., Doran, J. D., Norton, B., (2006) Indoor characterisation of small-scale quantum dot solar concentrators of various geometries and QD concentrations, *Proceedings of the 21st European Photovoltaic Solar Energy Conference and Exhibition, Sept 2006, Dresden, Germany. CD-ROM.*

Rowan. B., McCormack, S. Doran, J., Norton, B., (2007a) Investigation of Various Geometries of Quantum Dot Solar Concentrator. *Proceedings of 3rd Photovoltaic Science Application and Technology (PVSAT). Conference and Exhibition. 28 – 30 March 2007, Durham University, Durham.*

Rowan, B., McCormack, S., Doran, J., Norton, B., (2007b) Quantum Dot Solar Concentrators: An investigation of various geometries, *Proceedings of Proceedings of SPIE Optics and Photonics Conference, San Diego, California, USA, August 26-30 2007, CD ROM.*

Sidrach de Cardona, M., Carrascosa, M., Meseguer, F., Cusso, F., Jaque, F., (1985) Edge effect on luminescent solar concentrators, *Solar Cells*, Vol. 15, pp. 225-230.

Schaller, R.D., Kilmov, V.I., (2004) High-efficiency carrier multiplication in PbSe nanocrystals:implications for solar energy conversion, *Physics Review Letters*, Vol. 92, pp. 186601.

Zastrow, A., Heidler, K., Sah, R.E., Wittwer, V., Goetzberger, A. (1981) On the conversion of solar radiation with fluorescent planar concentrators. *Proceedings of the 3rd International Photovoltaic Solar Energy Conference, Cannes, France October 27-31 1980 pp. 413-417.*

Chapter 6

Conclusions & Future Work

6.0 Quantum Dot Efficiencies

The manufacturers of the majority of the QDs did not provide quantum yield values. Evident technologies quoted 30-50% for all of their CdSe/ZnS QDs with batch-to-batch variability. It appears that reproducibility of QD efficiencies is a problem in the synthesis of QDs. Using the ray trace model, a QY of 10% provided the optimum agreement between measured and predicted results for the QDSCs containing a range of concentrations of Nan488C QDs. A similar measurement of the Evi600 QDs used in the QDSC 7 samples of various geometries indicted a QY of 14%. This information coupled with the appearance of the QD composites and the poor performance of the QDSCs indicates that the efficiency of the QDs used in this study was low. A recent study investigating the use of commercial QDs for use in LSCs concluded that QDs with high QYs and sufficiently small overlap of absorption and emission bands were not yet available (*Sholin et al 2007*).

QD development is ongoing and QY values of up to 85% have been achieved (*Xie et al 2004*). Once such high QY values are reproducible in bulk quantities and long-term stability is achieved, using QDs as replacements for dyes will become feasible. The

progress of QD development should be monitored through both commercial channels and through research institutes.

6.1 Matrix material

In chapter 2 an epoxy resin was clearly identified as the most suitable matrix material out of the seven materials investigated in this study. It had the lowest absorption coefficient, the least effect on QD emission intensity and it retained this stability longer than the other samples (*Gallagher et al 2006*). A study carried out by *Knight et al* 2004 with the aim of producing a stable fluorescence standard also found an epoxy resin to be suitable for QD encapsulation. They found that PMMA, a polymer often considered to be best suited to this application resulted in severe damage to QD efficiency (*Knight et al 2004*). Other work using a pre-polymerisation technique with PMMA and QDs resulted in blue shifts of the QD spectra providing further evidence that PMMA is unsuitable for this application (*Pang et al 2005*). Much research is being carried out in this area because successful encapsulation of QDs into polymer matrices is crucial to their development in the field of opto-electronics.

Lee et al found that the incorporation of QDs into polylaurylmethacrylate (PLMA) matrices in the presence of TOPO had little effect on the QY, reductions in QY ranged from 16.7 to 20% (*Lee et al 2000*). In another study, the use of a polymer from the perfluorocyclobutane (PFCB) family was used due to its low optical loss over a broad range of wavelengths, low polymerisation temperature and thermal stability. It was found to have minimal effect on the optical properties of the QDs, there was no shift or decrease in emission observed

(*Olsson et al 2004*). Future studies in this area could benefit from further investigation into the suitable matrix materials to minimise the effect of QD encapsulation on QD efficiency.

6.2 Quantum Dot Composite Stability

Core-shell QDs are expected to be stable due to passivation of the QD core providing increased resistance to photochemical degradation (*Alivisatos 1997*). A 70% decrease in emission intensity was observed for the QDs in toluene solution after 23 weeks as seen in section 3.3.3. The stability study of QD composites in section 3.3.4 highlighted the effect that light exposure has on samples emission intensity over time (*Gallagher et al 2005*). Recent work has indicated that the use of polymer solutions instead of pure solvents such as toluene lead to an increase in QY and extended stability under continuous illumination due to static passivation of the surface defects of the QDs by the polymer molecules (*Biju et al 2007*). Developments in QD production have resulted in the fabrication of multishell QDs, where the shell composition is gradually changed from CdS to ZnS. The reduced strain of lattice mismatches prevents the formation of defect sites thereby increasing the QY. Multishell QDs have exhibited superior photochemical and colloidal stability (*Xie et al 2004*).

It appears that commercially available CdSe/ZnS QDs do not yet exhibit sufficient stability for use in this application but reports indicate that progress is being made in achieving improved stability. In future work it would be worth investigating the performance of multishell QDs in composite form in terms of both efficiency and stability.

6.3 New Directions for QDSC Development

An investigation into the optimum reflective material clearly showed that a white diffuse reflector produced the highest electrical output. Laboratory tissues were used to provide the white diffuse reflector, this material would not be suitable for use in an outdoor or commercial device. Layers of titanium dioxide reflective paint (*Heidler 1982*) or diffuse white paint sprays would be suitable for outdoor use.

It was shown that in most cases air gaps increased the amount of light trapped inside a QDSC plate. The air gaps provided an extra plastic to air interface at which more light could be trapped by total internal reflection. For outdoor testing of future systems it will be necessary to produce devices with integrated diffuse reflectors with air gaps included.

Four quadratic, two triangular and three circular QDSC devices were fabricated containing 0.082% (m/v) of Evi600B QDs. In terms of power output there was minor disparity between samples of varying geometry, although the highest concentration factor was achieved by the circular system. Circular geometries with the whole perimeter as a collecting surface have previously been identified as the optimum LSC design (*Reisfeld and Jorgensen 1982, Sidrach de Cardona et al 1985*). It could be possible to investigate the advantages of collecting from the whole circle perimeter using flexible PV material. Efficiencies of up to 12.8% have been achieved using flexible polymers to produce PV cells (*Tiwari et al 1999*). Since circular systems are not suitable for covering large planar surfaces due to the interstices between devices, hexagons have been suggested as an alternative to circular devices (*Reisfeld and Jorgensen 1982*). A comparison of circular and

hexagonal devices would be an interesting prospective study. The use of bifacial cells between two or more systems would also be worth investigating once high efficiencies have been achieved with single devices (*Reisfeld and Jorgensen 1982*).

Decreasing plate thickness was found to increase concentration factors by up to 50% indicating that future device fabrication should focus on thinner devices. A comparison using size matched PV cells should be carried out, although it is difficult to obtain PV cells less than 0.3 cm (*Meyer 2007*). The use of thinner plates allows for investigation into stacking of QDSC plates (*Goetzberger and Wittwer 1981*) containing different QD types. Two 0.15 cm plates or three 0.1 cm plates could be stacked together and characterised using a 0.3 cm PV cell. Light that is not absorbed by the upper plate would be transmitted to the lower plate and absorbed by a QD with a longer emission wavelength. By stacking a number of thin plates to a single PV cell, the absorption range of the system would be expanded. Goetzberger and Wittwer originally suggested stacked systems using PV cells with different band gaps to correspond to the emission wavelength of each plate (*Goetzberger and Wittwer 1982*). Stacked systems have been found to produce up to 16% increase in electrical output compared to individual plates (*Farrell et al 2006*). Future work should further investigate stacking of QDSC plates as the use of NIR QDs was found to be unsuccessful at increasing the utilisation of the solar spectrum due to low QY, as shown in sections 5.5. In section 5.6, the mixing of different QD types in a single solution was investigated as a means to increase the absorption range. Our results showed that there was no increase in the absorption range or in emission intensity. Broadening of the absorption spectrum of QDSCs systems is of great importance, it has been estimated using a ray trace model that approximately 44% of incident light is not absorbed due to the limited absorption range of QDs (*Kennedy et al 2007b*).

6.5 The Optimum QDSC Design

Based on the results of the experimental work carried out on QDSC systems throughout this study, an optimised QDSC system would be comprised of:

o Matrix material: Epoxy resin based on its low absorption coefficient, minimal effect on QD emission (22.5% reduction in intensity) and sample stability (~6 months).

o Fabrication method: Vacuum over to remove air bubbles, no oven curing (as shown in sections 3.3.1 and 4.3.1).

o Reflective material: white diffuse reflector with air gaps (section 5.1)

o PV cell optically matched using silicon oil or adhesive

o Plate thickness: 0.15 cm (section 5.4)

o Geometry: Large circular device with 8 cm diameter

Optimum optical efficiency and concentration factor values, achievable using the above components can be estimated using the electrical results obtained from the QDSCs characterised throughout this study. Table 6.1 shows the optical efficiencies (η_{opt}) (see equation 4.1) of the QDSCs that showed the highest concentration factors.

Table 6.1: Concentration factors and optical efficiency values of most efficient QDSCs

Sample Number	Geometry	QD type	QD conc. % (m/v)	Conc. Factor	η_{opt} (%)
5.5	Square	Evi540b	0.046	0.34	2.94
5.6	Square	Evi540b	0.090	0.32	2.75
5.7	Square	Evi540b	0.190	0.35	3.03
5.8	Square	Evi540b	0.385	0.42	3.7
5.9	Square	Evi540b	0.770	0.42	3.54
5.10	Triangle	Evi540b	0.046	0.30	8.43
7.5	Triangle	Evi600b	0.082	0.30	5.67
7.9	Circle (d=8cm)	Evi600b	0.082	0.31	1.46
8.3	Triangle	Nan488b	0.050	0.33	4.55

QDSC 5.10 produced the highest optical efficiency of 8.43% followed by QDSC 7.5 (5.67%). These values compare favourably with optical efficiencies achieved to date (1.8-18%).

The optical efficiency achieved experimentally is significantly higher than that achieved by Sholin et al (0.3% for CdSe/ZnS in a liquid concentrator) *(Sholin et al 2007)*, providing a positive outlook for the development of QDSCs using the techniques developed throughout this study.

This study has developed QDSCs and investigated their feasibility, results have highlighted the need for high efficiency QDs with a large stokes shift and improved stability. It has also been shown that it is necessary to broaden the absorption range of QDSC systems to

optimise utilisation of the solar spectrum. Developments in QD synthesis are proceeding rapidly, generating scope for further QDSC development.

References:

Alivisatos, A.P., (1997), Nanocrystals: building blocks for modern materials design, *Endeavour*, Vol. 21, No. 2, pp. 56-60.

Biju, V., Kanemoto, R., Matsumoto, Y., Ishii, S., Nakanishi, S., Itoh, T., Baba, Y., Mitsuru, I., (2007), Photoinduced Photoluminescence variations of CdSe Quantum Dots in polymer solutions, *Journal of Physical Chemistry*, Vol. 111, No. 22, pp. 7924 –7932.

Farrell, D.J., Chatten, A.J., Buchtemann, A., Barnham, K.W.J., (2006), Fabrication, characterisation & modelling of quantum dot solar concentrator stacks, *Proceedings of Photovoltaic Energy Conversion Conference Record of the 2006 IEEE 4th World Conference May 2006*, pp. 217-220.

Gallagher, S. J., Rowan, B. C., Doran, J. D., Norton, B., (2005), Examination of optimum carrier materials and quantum dots for a Quantum Dot Solar Concentrator using spectroscopic techniques, *Proceedings of SPIE Optics and Photonics Conference, San Diego, California, USA*.

Gallagher, S. J., Rowan, B. C., Doran, J. D., Norton, B., (2006) Quantum Dot Solar Concentrator: Device characterisation using spectroscopic techniques, *Solar Energy*, Vol. 81, pp. 540-547.

Goetzberger, A., Wittwer, V., (1981), Fluorescent planar collector-concentrators: a review, *Solar Cells*, Vol. 4, pp. 3-23.

Heidler, K., Goetzberger, A., Wittwer, V., (1982), Fluorescent planar concentrator (FPC) Monte-Carlo Computer model limit efficiency and latest experimental results, *Proceedings of Photovoltaic the Fourth International Solar Energy Conference, Stresa, Italy, May 10-14* ,*pp. 682-686.*

Knight, A.,Gaunt, J., Davidson, T., Chechik, V., Windsor, S., (2004), Evaluation of the Suitability of Quantum Dots as Fluorescence Standards, *NPL Report DQL-AS 007.*

Kennedy, M., Rowan, B., McCormack, S.J., Doran, J., Norton, B., (2007a), Modelling of a Quantum Dot Solar Concentrator and comparison with fabricated devices, *Proceedings of 3rd Photovoltaic Science Application and Technology (PVSAT) Conference and Exhibition 28 – 30 March 2007, Durham University, Durham, pp. 123-126.*

Kennedy, M., McCormack, S.J., Doran, J., Norton, B., (2007b), Ray-trace Modelling of Quantum Dot Solar Concentrators and Comparison with Fabricated Devices, *Proceedings of 3rd Photovoltaic Science Application and Technology (PVSAT) Conference and Exhibition 28 – 30 March 2007, Durham University, Durham, pp. 27-30.*

Lee, J., Sundar, V.C., Heine, J.R., Bawendi, M.G., Jensen, K.F., (2000), Full Colour Emission from II-VI Semiconductor Quantum Dot-Polymer composites, *Advanced Materials*, Vol. 12, No. 15, pp.1102-1105.

Loh, E., Scalapino, D.J., (1986), Luminescent solar concentrators: effects of shape on efficiency, *Applied Optics*, Vol. 25, No.12, pp. 1901-1907.

Meyer, T., (2007), Personal communication .

Olsson, Y.K., Chen, G., Rapaport, R., Fuchs, D.T., Sundar, V.C., Steckel, J.S., Bawendi, M.G., Aharoni, A., Banin, U., (2004), Fabrication and optical properties of polymeric waveguides containing nanocrystallline quantum dots, *Applied Physics Letters*, Vol. 85, No.19, pp. 4469-4471.

Pang, L.,Shen, Y., Tetz, K., Fainman, Y., (2005), PMMA quantum dots composites fabricated via use of pre-polymerisation, *Optics Express*, Vol. 13, No. 1, pp. 44-49.

Reisfeld, R., Jorgensen, C.K., (1982), Luminescent solar concentrators for energy conversion, *Struture and bonding*, Vol.49, pp.1-36.

Sholin, V., Olson, J.D., Carter, S.A., (2007), Semiconducting polymers and quantum dots in luminescent solar concentrators for solar energy harvesting, *Journal of Applied Physics*, Vol. 101, pp. 123114-1- 123114-9.

Sidrach de Cardona, M., Carrascosa, M., Meseguer, F., Cusso, F., Jaque, F., (1985), Edge effect on luminescent solar concentrators, *Solar Cells*, Vol. 15, pp. 225-230.

Tiwari, A.N., Krejci, M/. Haug, F.-J., Zogg, H.,(1999), 12.8% Efficiency Cu(In, Ga)Se[2] solar cell on a flexible polymer sheet, *Progress in photovoltaics*, Vol. 7, No. 5, pp. 393-397.

Xie, R., Kolb, U., Li, J., Basche, T., Mews, A., (2004), Synthesis and characteristaion of highly luminescent CdSe-Core CdS/Zn 0.5Cd0.5S/ZnS multishell nanocrystals, *Journal of the American Chemical Society*, Vol.127, No. 20, pp. 7480-7488.